POLITECNICO DI MILANO

DEPARTMENT OF ELECTRONICS, INFORMATION AND BIOENGINEERING (DEIB)

DOCTORAL PROGRAMME IN ELECTRICAL ENGINEERING

ELECTROMAGNETIC COEXISTENCE ISSUES BETWEEN POWER AND DATA LINES IN POWER LINE COMMUNICATION SYSTEMS USED IN SMART GRIDS

Doctoral Dissertation of:

Abduselam Hamid Beshir

Supervisor:

Prof. Flavia GRASSI, Prof. Petre-Marian NICOLAE

Tutor:

Prof. Sergio Amedeo PIGNARI

The Chair of the Doctoral Program:

Prof. Marco MUSSETTA

Year 2022 –35th cycle

Acknowledgments

First, I would like to express my sincere gratitude towards my main supervisor Prof. Flavia Grassi for her advice and guidance. It is once a lifetime opportunity to work with her and I really appreciate her attitude, guidance, and support. She has constantly encouraged and supported me from the beginning of the project to the end. Her observations and comments helped me to establish the overall direction of the research and to move forward with investigation in depth.

Next, I would like to take this opportunity to thank my co-supervisor Prof.dr.eng. Petre Marian Nicolae for his support and guidance, especially during the secondment period at the University of Craiova. I would like to thank the supervisory board members in ETOPIA project; Prof. dr. Frank Leferink, Prof. dr. Heyno Garbe, Prof. dr. Robert Smolenski and Prof. dr. David Thomas. I would like to thank also Mr. Jan Beerens, the ETOPIA project coordinator, for his help in managing the timetables to finish the project on time.

Then, I would like to thank the Polimi EMC group members: Prof. Sergio A.Pignari, Prof.Giordano Spadachini, Dr. Xinglong Lui, Dr. Xiaokang Wu and Lu Wan, for their help and cooperation throughout my research period. I would like to take this opportunity also to thank Prof. Paolo S. Crovetti for his help and guidance in many parts of my research. Besides, I would like to thank all the administrative staffs at Politechnico di Milano.

Finally, I would like to thank all my family members who supported me throughout the PhD period. More specifically, I would like to thank my aunt, Leyla Sherif, my father-in-law Eng. Mahmoud Teyib and my mother-in-law Amina Sherif.

Abstract

Power Line Communication (PLC) technologies are used in many applications and offer the advantage of utilizing existing power cables for both power and data transmission, thus minimizing cost and complexity. Nevertheless, PLC technology requires further investigation to solve possible co-existence issues due to the noise coming from power electronics converters. This thesis presents an activity carried out to study the interference between coexisting power converters and nearby communication systems such as PLC. Therefore, the thesis first discusses the modelling of noise sources mainly power electronics converters. In this regard, both white-box and black-box modelling techniques are investigated in detail considering their application in predicting electromagnetic interference (EMI) emissions in complex networks such as the Low Voltage (LV) distribution network. More specifically, the white-box modelling approach is implemented to study conducted emission (CE) propagation from the LV network to the main grid with the help of PSpice MATLAB co-simulation, where different noise sources are modelled in PSpice considering parasitic elements and MATLAB Simulink is used to implement control schemes for synchronization. The effects of the shunt capacitors, circuit breakers, transmission lines and power factor of the loads on the CE propagation of the LV network to the main grid are discussed in detail.

However, black-box modelling is applied to a three-phase inverter, by implementing an alternative procedure to identify the parameters describing the active part of the model. Besides, two limitations of black-box modelling are investigated. The first regards the need for the system to satisfy the linear and time-invariant (LTI) assumption. The influence of this assumption on prediction accuracy is analyzed with reference to the zero, positive and negative sequence decomposition. It is shown that predictions for the positive/negative sequence are highly influenced by this assumption, unlike those for the zero sequence. The second limitation is related to the possible variation of the mains impedance, which is not satisfactorily stabilized at low frequency, that is outside the operating frequency range of standard line impedance stabilization networks.

The thesis also discusses both the simulation and experimental activities towards finding alternative ways of reducing the CE of power converters by using Random Pulse Width Modulation (RPWM) scheme. The analysis is carried out by using PSpice-Simulink co-simulation in order to achieve effective modelling of the converter on the one hand (PSpice), and easy implementation of the modulation scheme on the other hand (Simulink). Both simulation and experimental results entailed that RPWM resulted better attenuation of the noise of power converters compared to the conventional Pulse Width Modulation Scheme (PWM).

Besides, this thesis reports the activity carried out to evaluate the interference between randomly modulated power converters and PLC systems. To this end, both software simulations and experimental tests have been carried out with the final goal of understanding the conditions under which RPWM schemes can be considered as an effective alternative to conventional PWM in applications involving PLC systems. In details, the effects of different RPWM parameters such as switching frequency, spreading factor and random number update rate on the G3-PLC are investigated. In addition, different RPWM schemes such as Random Frequency Modulation (RFM) and Random Pulse Position Modulation (RPPM) are compared in terms of performance so to highlight which RPWM is best suited to assure coexistence with PLC systems. The impact of RPWM on the communication channel is evaluated in terms of Frame Error Rate, Channel Capacity and Channel Capacity Loss metrics. Experimental results confirmed that randomly modulated converters with switching frequencies near

the G3-PLC bandwidth can cause more significant disturbance and coexistence issues than switching frequencies out of this range. Results also show that the spreading factor and the random number update rate of RPWM have a direct effect on the communication channel. Moreover, a trade-off between EMI reduction and coexistence issues is observed, i.e., RFM, which is very effective for EMI reduction, is found to be very disruptive for G3-PLC compared to alternative random modulation techniques like RPPM.

Eventually, the thesis presents an experimental activity aimed at modelling the G3-PLC modems by a black-box modelling approach. Modelling G3-PLC modems is an essential task to investigate electromagnetic compatibility (EMC) issues related to the coexistence of the PLC signal with the high-frequency noise affecting low voltage networks, mainly due to the presence of power converters and non-linear loads. Since detailed information on the modem internal architecture is usually not available to the end-user, this work investigates the possibility to develop behavioral (black-box) models of G3-PLC modems, whose parameters can be estimated starting from measurements carried out at the modem output ports. To this end, suitable test benches are set up, and used for model-parameter extraction as well as for validation purposes. It is proven by experiments that an equivalent representation involving non-ideal voltage sources (i.e., in terms of extended Thevenin/Norton equivalent circuits) is no longer feasible for the transmitting modem, since the presence of a closed-loop control system invalidates the linearity assumption. Hence, while the receiving modem is still modelled through an impedance matrix (since it behaves as a linear device), an alternative representation is proposed for the transmitting modem, which resorts to the use of two ideal voltage sources in accordance with the substitution theorem. Experimental results prove that the proposed modelling strategy leads to satisfactory prediction of the currents propagating on the PLC system in the frequency interval of interest. Hence, it could be used in combination with high-frequency models of the other components in the network to investigate EMC and coexistence of the PLC signal with the high-frequency noise generated by power converters.

Contents

List of Tables

List of Figures

List of Abbreviations

AC	alternating current
ADC	analog-to-digital conversion
AMI	Automatic Meter Infrastructure
AMR	Automatic Meter Reading
ARIB	Association of Radio Industries and Businesses
BPL	broadband over power lines
CE	conducted emission
CENELEC	European Committee for Electrotechnical Standardization
CISPR	Comité International Spécial des Perturbations Radioélectriques
CM	common mode
DC	direct current
DG	distributed generations
DM	differential mode
DSL	digital subscriber line
DUT	device under test
EMC	electromagnetic compatibility
EMI	electromagnetic interference
EPRI	Electric Power Research Institute
ESL	equivalent series inductor
ESR	equivalent series resistor
EV	electric vehicles
FCC	Federal Communications Commission
FER	frame error rate
FFT	fast Fourier transform
FM	frequency modulation
IEEE	Institute of Electrical and Electronics Engineers
IGBT	insulated-gate bipolar transistor
ITU	International Telecommunication Union
LISN	line impedance stabilization network
LTI	linear and time-invariant
LV	Low Voltage
MV	Medium Voltage
NB	narrow band
PDSL	power-line digital subscriber line
PFC	power factor correction capacitor
PLC	Power Line Communication
PLL	Phase-locked loop
PLN	power line networking
PLT	power line telecom
PRIME	Power Line Intelligent Metering Evolution Alliance
PSD	Power Spectral Density
PSK	Phase Shift Key

PV	photovoltaic
PWM	Pulse Width Modulation Scheme
QPSK	quadrature phase-shift keying
RDCM	random duty-cycle modulation
RF	radio frequency
RFM	random frequency modulation
RNUR	random number update rate
RPPM	random pulse position modulation
RPWM	random pulse width modulation
SG	smart grid
SiC	silicon carbide
SPWM	Sinusoidal Pulse Width Modulation
UNB	Ultra Narrowband
VNA	Vector Network Analyzer
WSS	wide-sense stationary

CHAPTER 1

Introduction

1.1. The Power Line Communication technology

The term Power Line Communication (PLC) is known with a various name like as power line carrier, power-line digital subscriber line (PDSL), power line telecom (PLT), power line networking (PLN), mains communication, and broadband over power lines (BPL), is the communication technology which utilizes the existing power cables for both power and data transmission [1]. Therefore, the main power system networks such as transmission and distribution networks can be used besides the delivery of DC or 50/60 Hz AC power, as a means of communication medium for both low and high-speed data transfer. Since, PLC does not require any installation of new wires which as a result, would significantly reduce the deployment costs and can enable communication with hard-to-reach nodes where the RF wireless signal suffers from high levels of attenuation like in the underground structures or the buildings with obstructions and metal walls, or simply wherever the wireless signal is undesirable due to the Electromagnetic Interference (EMI) issues in places like hospitals, PLC is now getting much attention in numerous areas of applications. Of course, PLC is not a new concept, and it has been used as a communication system by power utilities for command-and-control applications over high and medium voltage lines between remote stations in the late 19th century [2].

Having the advantages of using existing power cables for data transmission, PLC is now getting much attention in different applications. For example, broadband internet access can be offered by PLC over the distribution network that feeds houses and buildings [3,4]. Of course, there are other communication systems which compete with PLC such as digital subscriber line (DSL) [5], optical fiber [6] and Wi-Fi [7]. However, the exploitation of the power delivery structure, which is widespread worldwide, more than the common twisted pair cables or the optical fibers, represents a strength point for the PLC technology. Indeed, high speed in-home connectivity was also desirable, allowing the home gateway to provide uninterrupted flow of heterogeneous traffic between the outdoor and the indoor networks, hence among the service provider and the end user, as a typical DSL internet connection. Wi-Fi has fostered such a paradigm and it has been largely researched, developed and marketed as stated. However, wireless technology may also experience complications, mostly due to unfavorable propagation conditions and limited radiated power for safety reasons that do not allow to grant full coverage at the promised speeds, e.g., in multiple floor dwellings with the presence of reinforced concrete floors [8]. Indeed, PLC protocols with advanced technologies are now becoming common for high-speed broadband internet access which can compete with DSL and Wi-Fi [9,10].

Besides the in-home broadband internet access applications, the use of PLC in Smart Grid (SG) is becoming very famous. Indeed, the SG represents one of the most appealing application contexts for PLC and, consequently, a lot of effort has been spent by the research community in this area [11,12]. In addition, the application of PLC in Electric Vehicles (EV) and Home and Industry automation are becoming other topics of interest [13-17].

Existing PLC technologies can be categorized depending on the bandwidth in: Ultra Narrowband PLC (UNB-PLC), Narrowband PLC (NB-PLC), and Broadband PLC (BPL). UNB-PLC refers to systems using a very narrow bandwidth for data transmission in the frequency range below 3 kHz and is limited to data rates of a few hundred bps [18]. NB-PLC refers to systems that work with medium data rates in frequency intervals between 3 and 500 kHz. This frequency range includes the European CENELEC bands, the US FCC band, the Chinese band, and the Japanese ARIB band. Finally, BPL encompasses a large variety of systems that aim at high data rates, operating in the frequency range from 1 MHz up to 250 MHz [19]. The most common PLC technologies are summarized in Table 1.1 including application areas.

Table 1.1: Summary of the most common PLC deployments.

Category	PLC Technology	Promoter	Standard	Band	Max.Data rate (kbps)
NB-PLC	OSGP	Echelon	IEC 14908.1	CENELEC A (35-91 kHz)	3.6
	Meters	ENEL	CLC TS 50568-4	CENELEC A (35-91 kHz)	9.6
	PRIME	PRIME Alliance	ITU-T G9904	CENELEC A, ARIB &FCC	Up to 1000
	G3-PLC	G3 Alliance	ITU-T G9903	CENELEC A, ARIB &FCC	34
BB-PLC	OPERA	IBERDROLA		2-18 MHz	10,000
	IEEE1901	IEEE		2-60 MHz	500,000
	ITU-T G.hn	ITU-T		2-100 MHz	2,000,000
	HomePlug AV	HomePlug		2-30 MHz	200,000
	IEEE1901.1-2008(SG PLC)	Huawei		< 12 MHz	10,000
	IEEEP1901.3 (IoTPLC)	Panasonic		< 100 MHz	Up to 1000,000

1.2. PLC Application in Smart Grid

Communication technologies play a significant role in the SG scenario, as they allow the interaction of consumers with energy management systems to ensure the optimal operation of the grid. Therefore, applications of PLC in SG's are mainly related to the electricity distribution and communication between consumers and the utility. Current examples of these applications are Automatic Meter Infrastructure (AMI) systems, EV charging systems, Telecontrol applications, Smart Cities, and DG systems [18,20]. For these applications of PLC in SGs, both NBPLC and BPL technologies are being used. In fact, most of the Automatic Meter Reading (AMR) deployments currently used exploit Narrow Band PLC (NB-PLC) technologies such as PRIME, G3-PLC, or IEEE 1901.2 for transmitting metering data [21,22]. Table 1.2 shows the frequency bands used by PLC in SG applications.

Table 1.2: Summary of available NB-PLC frequency bands for SG application in different regions of the world.

Region	Organization	Frequency band (kHz)
EU	CENELEC A	3-95
	CENELEC B	95-125
	CENELEC C	125-140
	CENELEC D	140-148.5
USA	FCC	10-490
CHINA	EPRI	3-500
JAPAN	ARIB	10-450

1.3. Main Challenges of PLC in SG applications

Even if the PLC system uses the existing power infrastructures for data transmissions, there are mainly two challenges which limit its application. The first one is associated with the transmission medium. Indeed, power supply networks are not suitable for data communication, since the two systems are designed for different objectives, e.g., in a power grid, it is very difficult to achieve the condition of matching with the terminal loads, which is a prerequisite for transmitting high-frequency signals without distortion, especially, in long distances and in high noise environment [23]. For instance, power transformers are typically quite poor at transferring frequencies much above 50 or 60 Hz. Besides, the limitation of the bandwidths allowed for PLC application in SG as summarized in Table 1.2 (international standards such as CENELEC in Europe and FCC in US limit the allowed frequency range for PLC less than 100 kHz or 500 kHz) restricts not to use the full potential of power lines for PLC. Given this limited frequency, alongside the high attenuation rate of power lines, it is not possible to obtain satisfying performance from even well-known PLC standards (such as PRIME, G3 and Meters & More etc.).

The second main challenge is associated with the presence of numerous noise sources in power grids mainly due to power electronics converters and nonlinear loads such as LED light dimmers, electric motors, and noise from switching power supplies. This impulse noise can seriously degrade the high frequency communication. So, at best, PLC will experience packet loss greater than most competing technologies, and data rates that aren't all that impressive anymore. Of course, there are also additional challenges or limitations of the PLC deployments such as low transmission speed, sensitivity to disturbance, nonlinear distortion and cross-modulation between channels, large size and the high price of capacitors and inductors used in the PLC system [24,25].

Therefore, PLC technology requires further investigation to solve existing limitations. The scope of this thesis is limited to the challenges associated with the impulsive noise from power electronics converters which create coexistence issues. Hence, the main goal of this thesis work is to study the EMI between power electronics converters and PLC systems in SG applications. The effects of other loads are not in the topic of interest.

The presence of power electronics converters in the AC mains represents a source of high frequency conducted noise, which may cause coexistence issues with the PLC signal. The supra-harmonics in the frequency range 2–150 kHz from power converters disturbs the NB-PLC being used in SG applications even if the NB-PLC technologies use robust modulation and error correction techniques [26,27]. Therefore, it is necessary to study the interference between power and data lines in applications where the two systems coexist.

To study the EMI between coexisting power converters and communication systems in complex networks such as in SG, it is tremendously important to derive first the EMI models of both power converters and communication systems. This will help to develop strategies to predict and suppress cross interference. Both power converters and communication systems can be modeled using “white-box” modelling approach where the detail information about circuit components including parasitic elements are available. But in practice it is very difficult to get each and every detail of network parts, and this kind of modelling is very challenging. Besides, modelling PLC system using white-box approach and integrating this model with power system networks for EMI analysis is very challenging due to the limitation of available software tools. An alternative way of modelling both the noise source and the communication system are to use “behavioral modelling” or “black-box modelling” approach, where the noise source can be modelled by looking at only the input output signals without the prior

knowledge of the components inside the device. This modelling scheme is less complex and provides an approximate model of the device for EMI analysis [28,29].

Besides the EMI modelling, it is necessary to find an alternative way of reducing the EMI of power converters than using the conventional EMI filters, especially in applications where size is a great concern. EMI filters are widely used for filtering out the EMI noise generated by power converters. However, when size is a great concern like aircraft and automobile applications, there should be another option to minimize conducted emissions (CE's). One of the practical solutions to suppress CE's is to work on the converter's modulation schemes, especially considering the availability of cyber-physical systems, which facilitating implementations and cooperation between different systems and controllers [30,31]. Pulse Width Modulation (PWM) is used for most converters. In conventional PWM schemes, the harmonics power is concentrated on the deterministic or known frequencies with a significant magnitude, which leads to mechanical vibration, noise, and EMI. One solution to this problem is to use random pulse width modulation (RPWM) schemes. By applying randomness on the conventional PWM scheme, the harmonic power will spread out so that no harmonic of significant magnitude exists, and peak harmonics at discrete frequency are significantly reduced. Differently from conventional modulation techniques, in RPWM, one or more parameters of the switching pulse, such as pulse position, switching frequency, or duty cycle, are varied randomly to spread the spectral peaks of the noise exiting the converter [32].

There are also doubts with regards to the advantages/disadvantages of different RPWM in power grids involving PLC systems, where spreading of the noise may result an increase in error in the communication systems. Indeed, recent studies showed that there is an interference between randomly modulated power converters and PLC systems [33-35]. Therefore, there is an urgent need to investigate the effects of random modulated converters on the coexisting PLC systems to understand the conditions under which RPWM can be considered as an effective alternative to conventional modulation schemes, because this topic is relatively new. This includes both simulation and experimental investigations.

Therefore, this thesis first covers the EMI modelling of noise sources (mainly power electronics converters) considering both white-box and black-box modelling approaches with their respective applications and possible limitations in the EMI analysis application. Then, the thesis focuses on alternative modulation schemes mainly RPWM to reduce the CE's of power converters, both in simulation and laboratory experiments, where different RPWM techniques will be compared with conventional PWM. Moreover, the coexistence between randomly modulated power converters and PLC systems will also be investigated both in simulation and experiment. Finally, this thesis covers an activity to find black-box model of G3-PLC systems which can be used in the EMI analysis of complex networks for future works.

1.4. Thesis objectives

The main objectives of this thesis work are:

- Model source of EMI, mainly power electronic converters using "***white-box***" modeling approach, where detail circuit parameters are available, and by using "***black-box***" modelling approach by looking at the input/output parameters, where the details of circuit components are not available. Then, use the EMI model of noise sources in the CE prediction of complex networks such as Low Voltage distribution networks and Photovoltaic based distributed generating units.
- Finding alternative ways of reducing the EMI of power converters using ***Random Pulse Width Modulation*** (spread spectrum) techniques.
- Model and study the coexistence issues between power converters and communication systems

in applications where the two systems coexist such as ***PLC system*** in SG applications.

- Find a suitable black-box model of G3-PLC system.

1.5. Thesis organization

This thesis is comprised of six chapters. The first chapter serves as an introduction to the thesis where common issues regarding the coexistence between the power and data lines were outlined.

Chapter 2 presents the EMI modelling of power electronics converters using both "white-box" and "black-box" modelling approach and their use in predicting EMI in a low voltage distribution network is outlined. Besides, the advantages of using different software virtually such as MATLAB-PSpice co-simulation in performing nearly practical EMI simulation is addressed.

Chapter 3 discusses the alternative ways of reducing EMI of power electronics converters using Random Pulse width Modulation (RPWM) scheme is discussed in detail. This chapter covers both simulation and laboratory experiment activities to study the benefit of using RPWM to reduce the CE of power converters.

Chapter 4 summarizes the coexistence issues between randomly modulated power converters and coexisting PLC systems. Both simulation tools and laboratory experimental results are reported in this chapter. Besides, the main parameters of RPWM which affect the coexistence more are outlined.

Chapter 5 presents the experimental test campaign to find black-box model of the G3-PLC modem, with the final goal of using the black-box model in the coexistence issue assessment of complex power system networks such as SG.

Chapter 6 reports the conclusion and future works of this thesis.

CHAPTER 2

Modelling of EMI sources

2.1. Modelling of EMI sources

In order to predict the EMI induced on the data lines, the noise source should be modelled as the first step. Different modelling techniques can be used to model the noise source mainly the power converters. When accurate data of the converter are available, the converter can be modelled through a white-box modelling approach. However, when the structure of the converter is not known, a black-box modelling approach is the preferable solution. The following sections outlines an activity to use both white-box and black-box modelling approaches for EMI analysis.

2.2. White-box modelling of power converter

White-box models are circuit models, including parameters representative for the functional behaviour of the converters as well as the control system. They are derived based on the available manufacturer data and circuit element specifications. However, most of the time it is very difficult to obtain the required information on the internal architecture and specifications of the converters from the manufacturers. This is especially true for those circuit components representative for parasitics, which can hardly be estimated even by measurement. This makes it very difficult to apply this modelling techniques for EMI prediction. For simple converters, the white-box model approach provides the most versatile solution for EMI prediction. However, such an approach becomes quite complex as the number of semiconductor devices increases and it may lead to convergence issues in simulation.

Modern simulation software like SPICE software helps to integrate the non-ideal model of circuit components such as resistors, inductors, capacitors and switching devices, (diodes, IGBTs and MOSFETs) so that nearly practical simulation can be performed. This improves the simulation model accuracy especially in EMI simulations where the main parasitic elements of the switching devices play significant role. For example, the SPICE model of wide band gab semiconductor devices such as SiC and GaN can be easily downloaded from their manufacturers and can be used in PSpice. However, sometimes the system under analysis can be very complex to model using only one software. Though PSpice is very powerful in modelling circuit elements with nearly practical representations, it is not convenient to apply different controllers i.e., it is very hard to implement RPWM using PSpice. Moreover, it is very hard to model power system networks like distribution networks with many inverter systems, due to synchronization difficulties. This can be improved by using PSpice SIMULINK co-simulation, where PSpice is used to model the circuit components considering parasitic elements, and SIMULIK is applied to implement control circuit such as synchronization and RPWM. By doing so the accurate modelling of power system networks can be achieved and the EMI analysis can be carried out easily.

In this regard, a collaboration activity between Polimi EMC group and Ricerca sul Sistema Energetico (RSEspa) was held to model and predict the EMI of a low voltage (LV) distribution network. The main objective of this collaboration work was to provide different EMI models (both time domain

and frequency domain) of the LV network, and to assess the effects of different components of the LV network such as photovoltaic (PV) panels, transmission lines, circuit breakers and power factor correction capacitors (PFC), on the propagation of CE to the main grid. Therefore, detail analysis was carried out considering time domain simulation (white-box modelling using PSpice Simulink co-simulation) and using frequency domain simulations (Ansys and MATLAB). In this section, only the simulation campaign towards the white-box modelling approach is presented (the frequency domain analysis is not presented here for brevity).

2.2.1. Description of the System under Analysis

The schematics of the Low Voltage (LV) network which is considered in this work is shown in Figure 2.1. There are three load branches (L_1, L_2, and L_3) connected to the busbar (S_0), which is supported by the transformer and Medium Voltage (MV) grid (branch L0). For some load branches, there are renewable energy PV systems, linear loads, and power factor correction (PFC) capacitors at

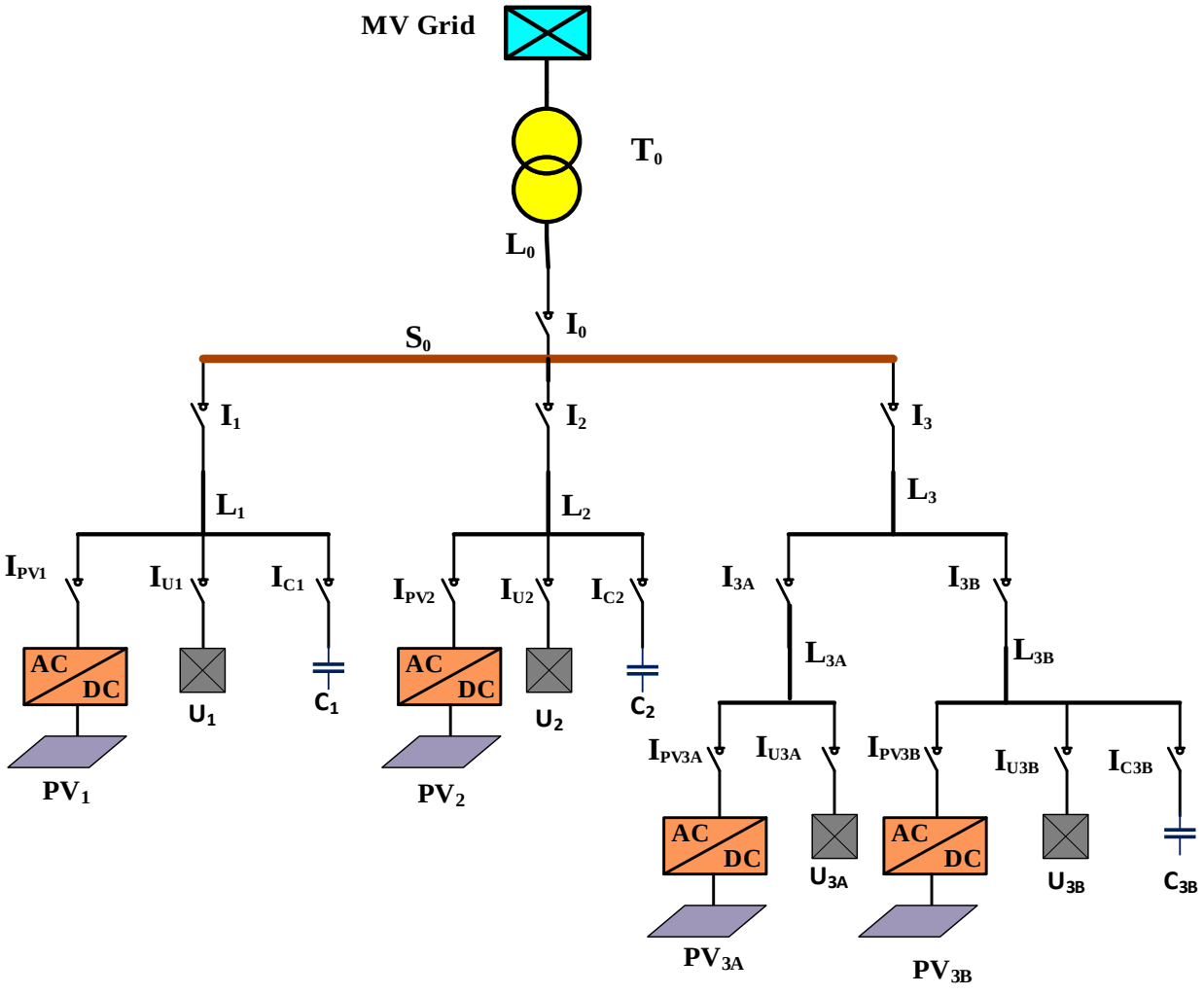

Figure 2.1: Schematics of the LV network which will be considered in this work.

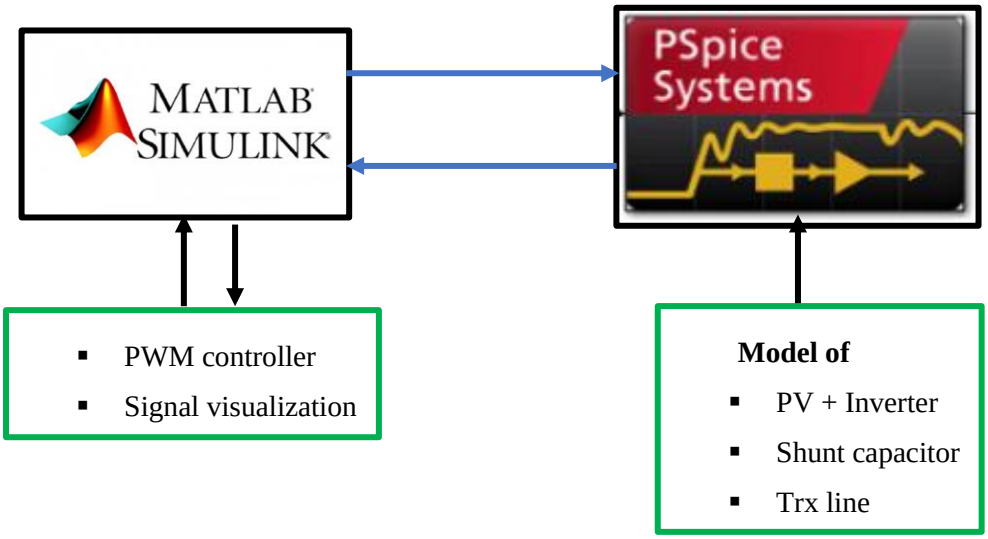

Figure 2.2: Schematics of the PSpice-Simulink co-simulation.

the terminal of each power transmission line. The shunt capacitor is used to improve the load power factor to a desired level. For branch L_3, there are two sub-branches (L_{3a} and L_{3b}). The profiles of the LV network components such as the loads, shunt capacitors, transmission lines, circuit breakers and the transformer are summarized in **Appendix A1**.

The LV network modeling and its EMI analysis are carried out by using PSpice-Simulink co-simulation to achieve effective modelling of the inverter, transmission line and shunt caps on the one hand (PSpice), and easy implementation of the modulation scheme to synchronize the PV inverter with AC grid on the other hand (Simulink) as shown in Figure 2.2. The non-linear characteristics of the inverter, transformer, load and shunt caps as well as their parasitic elements will be considered by the PSpice model. PSpice is preferable to model a converter, since it allows performing realistic simulations based on actual specification and datasheet of components like IGBTs, diodes, inductors, and capacitors. However, Simulink offers more freedom on signal visualization compared to PSpice software and easier to implement the control system (i.e., the PWM signals). The time domain simulations are post processed and converted to frequency domain using FFT.

2.2.2. Modelling of the Distribution Network

2.2.2.1. Photovoltaic system

Without loss of generality, a three-phase inverter connecting a PV panel, along with an LCL filter, is modeled as the PV system. The principal drawing of this system is illustrated in Figure 2.3. The complete circuit model of this system, including functional parts and parasitic components, will be implemented in SPICE and used in the time-domain simulation approach. The solar panel Photo watt Technologies (Isère, France) PW 1650-24 V, whose parasitic parameters are adopted from [36], is used to construct the PV array for the system. In this work, the PV array contains 32 PV panels in series to provide the proper DC power supply. The circuit model of the PV panel including the parasitic elements is highlighted in Figure 2.4 (a). Besides, the three-phase inverter augmented with parasitic elements considered in this work is shown in Figure 2.4 (b) [37] (parasitic elements are summarized in **Appendix A1**). The inverter switches at 5 kHz switching frequency with conventional Sinusoidal Pulse Width Modulation (SPWM). Moreover, an LCL filter (see Figure 2.5) is designed according to the IEEE std. 519/2014 and P1547-2003 requirements [38] and by following the procedures in [39].

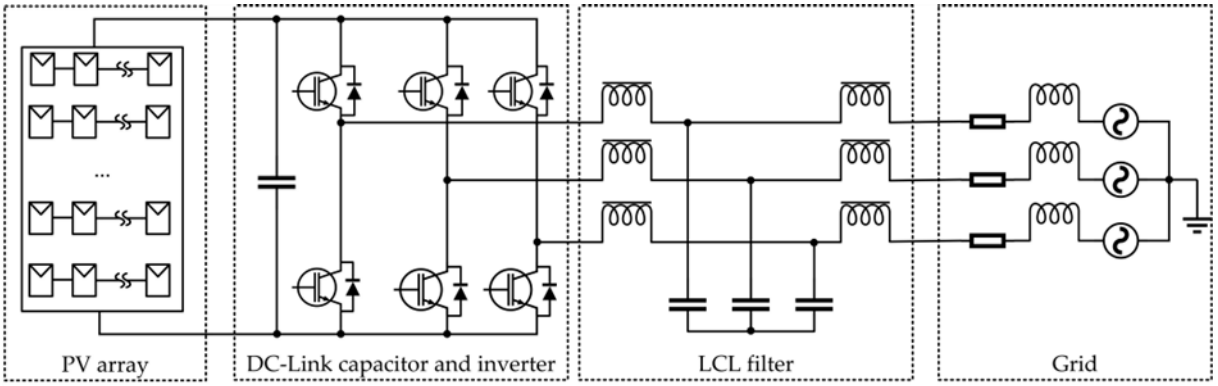

Figure 2.3: Principle drawing of a grid-connected three-phase inverter system.

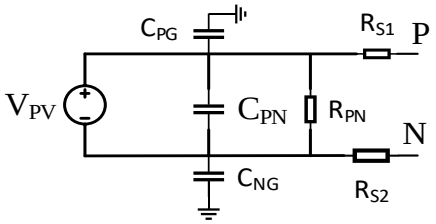

(a)

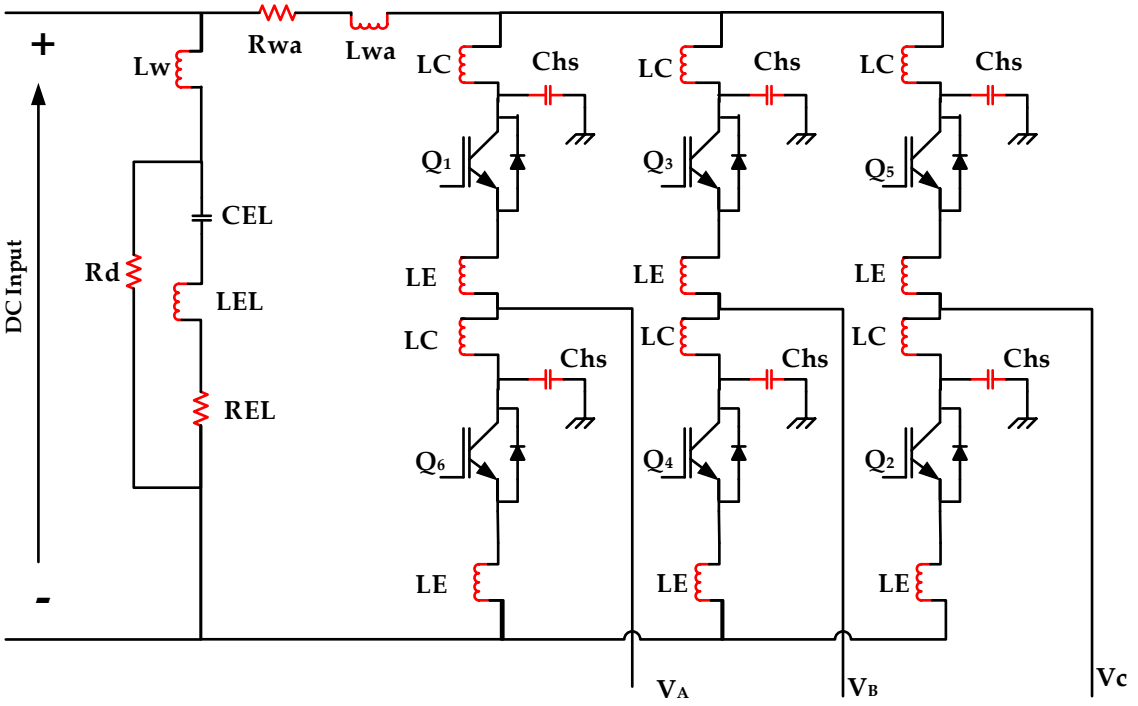

(b)

Figure 2.4: Circuit representation of (a) PV panel; and (b) three phase inverter, where parasitic elements are outlined in red.

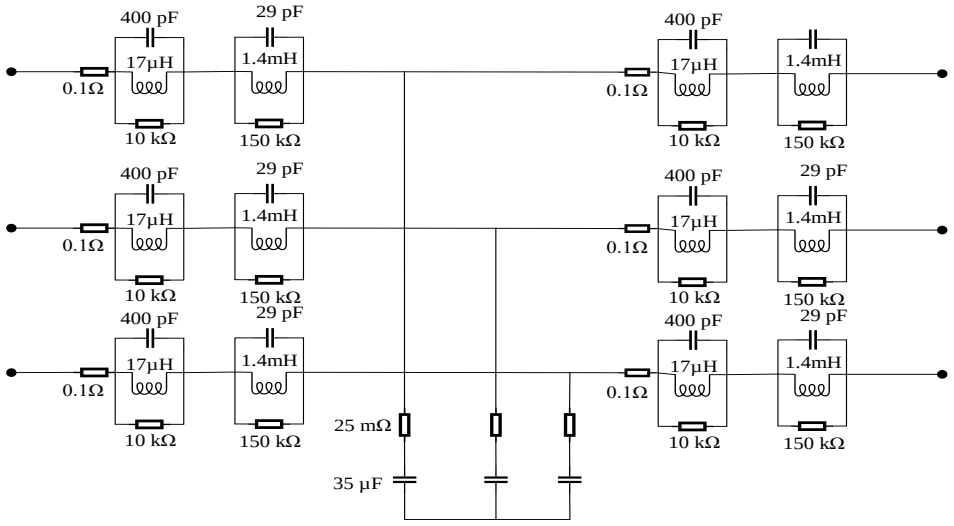

Figure 2.5: Circuit model of the LCL filter.

2.2.2.2. Linear Loads and Power Factor Correction Capacitors

From the nominal operating condition of the linear loads in **Appendix A1**, the equivalent RL circuits can be obtained as shown in Table 2.1. In the simulation, these RL-circuit representations are used for time-domain and frequency-domain simulations.

Table 2.1: Parameters of the equivalent RL circuits of linear loads

Load	R (Ω)	L (mH)
U1	2	5
U2	1.8	3.5
U3A	4.3	6.7
U3B	5.1	12

The function of PFC capacitors is to improve the power factor of linear load to the required values (0.9 in this case). It is worth mentioning that the connection of PFC capacitors is very important in the EMC point of view. For instance, the grounded star connection type provides a path to the ground, which is absent in the delta connection. Besides, the non-ideal behavior of the PFC capacitors at high frequency due to the equivalent series inductor (ESL) and equivalent series resistor (ESR), may cause significant issues for the propagation of the CE.

2.2.2.3. LV Power Transmission Lines and Busbar

The power transmission lines, and busbar are important ingredients for the analysis of CE's propagation. For instance, different placement of cables can cause different per-unit-length (p.u.l) parameters, which affect the characteristic impedance of the cable. Besides, cable lengths determine the total chain parameters, which eventually reflect on the propagation of the CE's. The p.u.l parameter of each branch line has been determined by using Ansys software. Since the RLGC parameters are frequency-dependent, the values are extracted at the frequency of 1 MHz (the CE analysis is up to 1 MHz). Moreover, the cables are represented by a cascaded lumped circuit model to avoid convergence issues in PSpice. For instance, for the cables with 70 or 80 meters, the cascaded cable length is chosen as 10 meters, since the length of each cascaded section should be much smaller (10 times) than the wavelength of the maximum frequency of interest (in this case the section length should be chosen less than one-tenth of the wavelength at 1 MHz).

2.2.2.4. Circuit Breakers

The circuit breakers are modeled for three statuses: close, ideal open, and non-ideal open. For the close status, it is regarded as a perfect conductor, i.e., there is no voltage drop across the circuit breaker. For the ideal open status, it is considered as an open circuit, i.e., there is no current going through the circuit breakers. It is noted that the circuit breakers may not behave as the ideal open status in the real application [40], the non-ideal open status of the circuit breaker is modeled as a small capacitance C_i between the breaking terminals as shown in Figure 2.6. This capacitance plays a significant role in the CE analysis, especially at high frequency because the CEs may propagate through this capacitor even if the circuit breaker is switched off. Thus, it is necessary to study the effects of the non-ideal switched-off status when some branches are working in an island mode.

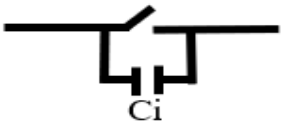

Figure 2.6: circuit model of the circuit breaker considering non ideal behavior.

2.2.2.5. Power Transformers

The transformer model suitable for this analysis is selected from the available white-box model [41]. The adopted transformer model (see Figure 2.7) utilized the intelligent optimization algorithm to obtain the equivalent circuit up to 1.2 MHz (including both functional and parasitic elements). It is worth mentioning that, in general, the model of the power transformer depends on its specifications, such as rated power, current, and internal structure. Even the same model type from the same manufacture can show slight differences in the characteristics. The equivalent circuit parameters of the selected transformer can be inferred from [41].

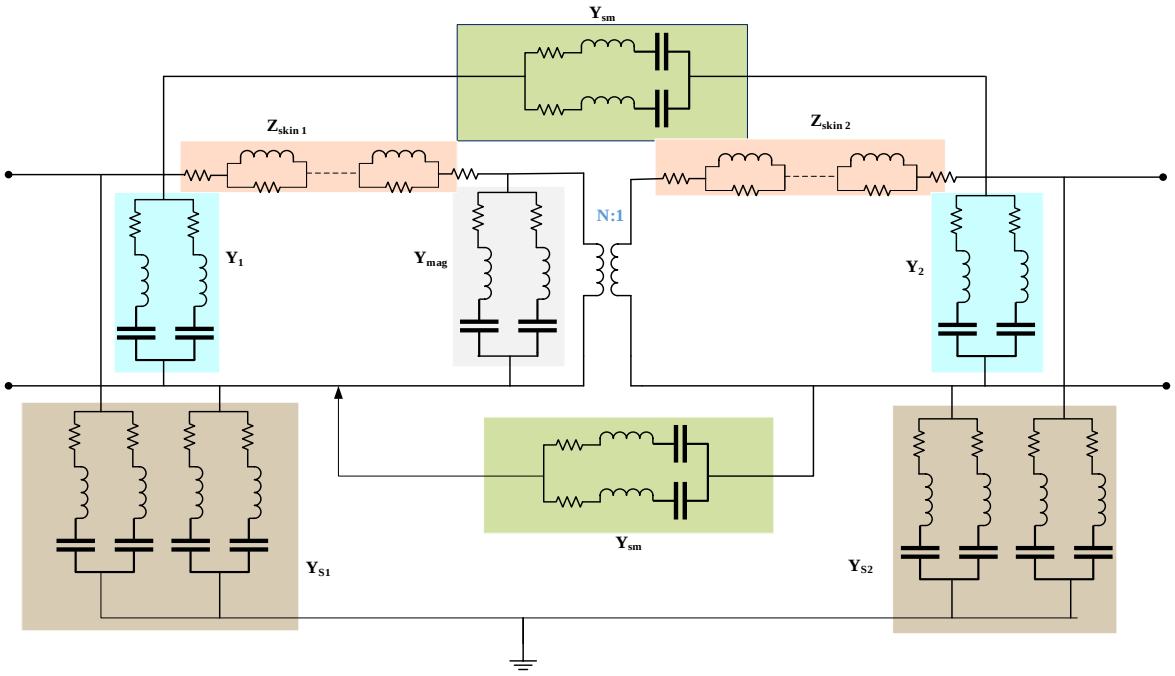

Figure 2.7: Transformer model considered in this work.

2.2.2.6. Equivalent Model of the MV Network

The MV network is approximated by equivalent R and L values referred to the HV side as a 0.12 Ω resistor in series with a 2.5 mH inductor for each phase.

2.2.3. Development of Simulation Tools for the Analysis of the Propagation of Disturbances

The LV network is modeled using PSpice SIMUINK co-simulation. Figure 2.8 shows the PSpice model of the LV network with all the parts discussed in sub-section 2.2.2. However, MATLAB Simulink is used to synchronize the PV panels with the main grid. Figure 2.9 shows the control circuit implemented in SIMULINK where the PSpice system block represents all the circuits modeled in PSpice. The phase-locked loop determines the grid frequency, and this frequency is used to control the PWM signals of the inverters so that the inverter and the grid are kept synchronized. Moreover, the PSpice system block allows to export any of the intended currents and voltages (in the time domain), and this is convenient to post-process using MATLAB.

Figure 2.10 (a) shows the LV grid and the PV panels phase-to-phase voltages before they are connected together. As it can be seen, the two voltages are synchronized at the steady state (the PV panels can be connected to the LV). Besides, Figure 2.10 (b) shows the currents drawn by the loads which are synchronized, and their magnitudes are also in line to the data provided in the **Appendix A1**. Therefore, the model can be used to predict CE to the Grid and is ready to be used for further analysis.

2.2.4. Result and Discussion

In this section, the obtained results from the simulation are discussed in detail. Since reporting all the analysis and results will make this report vague, only simulation results associated with one branch (L_1 with load and PFC) is presented where the other two branches (L_2 and L_3) are disconnected. Moreover, only the results concerning the effects of the PFC and circuit breaker on the propagation of CEs are presented for brevity. Therefore, the following three cases are presented. At the beginning, the effects of the connection of the PFC (star and delta connection), on the CE propagation to the AC grid is presented. Next, the influence of the parasitic elements of the PFC capacitor on the CE to the grid is discussed. Finally, the effects of the circuit breaker (when it is open) on the noise currents to the grid are investigated.

2.2.4.1. Effects of the connection of PFC capacitors

In this configuration, the purpose is to analyze the relationship between the power factor due to PFC capacitors connected in different configuration and the CE propagating to the AC grid. Hence, the real power (50 kW) is kept the same, and the reactive power is fixed to have the 0.9 power factor of the linear load by considering three arrangements, i.e., by using PFC capacitor connected in star (neutral point grounded), in delta and without any PFC connected.

Figure 2.11 (a) and Figure 2.11 (b) show the noise voltages and currents propagating to the busbar (S_0). It is shown that by adding the delta-connected PFC capacitor, both voltages and currents are not changed compared with the case in the absence of the shunt capacitor. On the other hand, if the PFC capacitors are in grounded star connection, the CE propagating to the AC grid can be reduced significantly since the grounded star connection provides a path to the ground. Therefore, connecting PFC capacitors in grounded star has a great advantage to reduce CE even if the required size of the capacitors are three times larger than delta connection to have the same power factor improvement. However, there is no significant difference on the noise propagating to the AC grid noticed when the PFC capacitor is connected in ungrounded star compared to delta connection as shown in Figure 2.12 (a) and Figure 2.12(b) since in this case the star connection does not provide grounding path to the

noise.

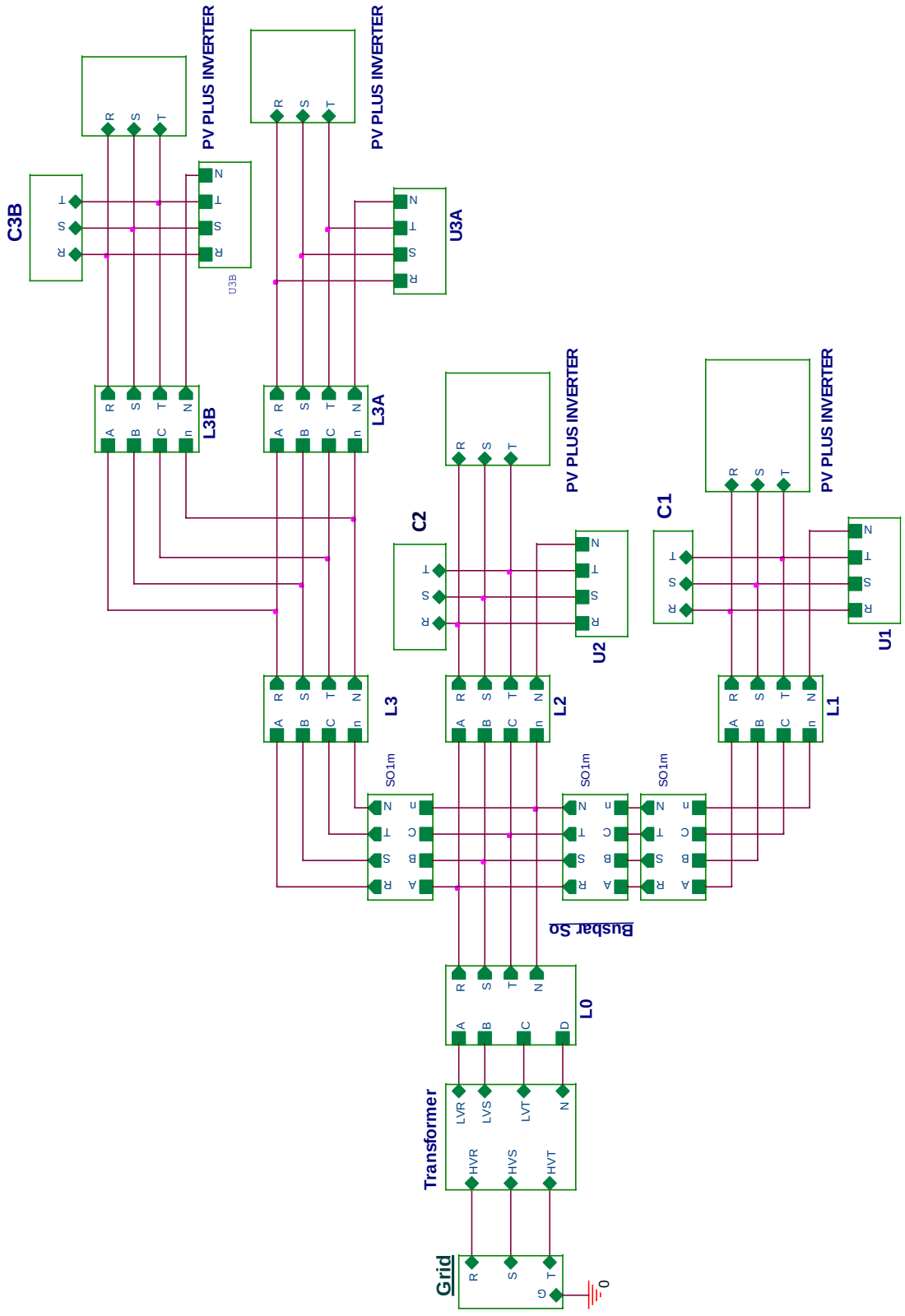

Figure 2.8: PSpice model of the LV electrical network.

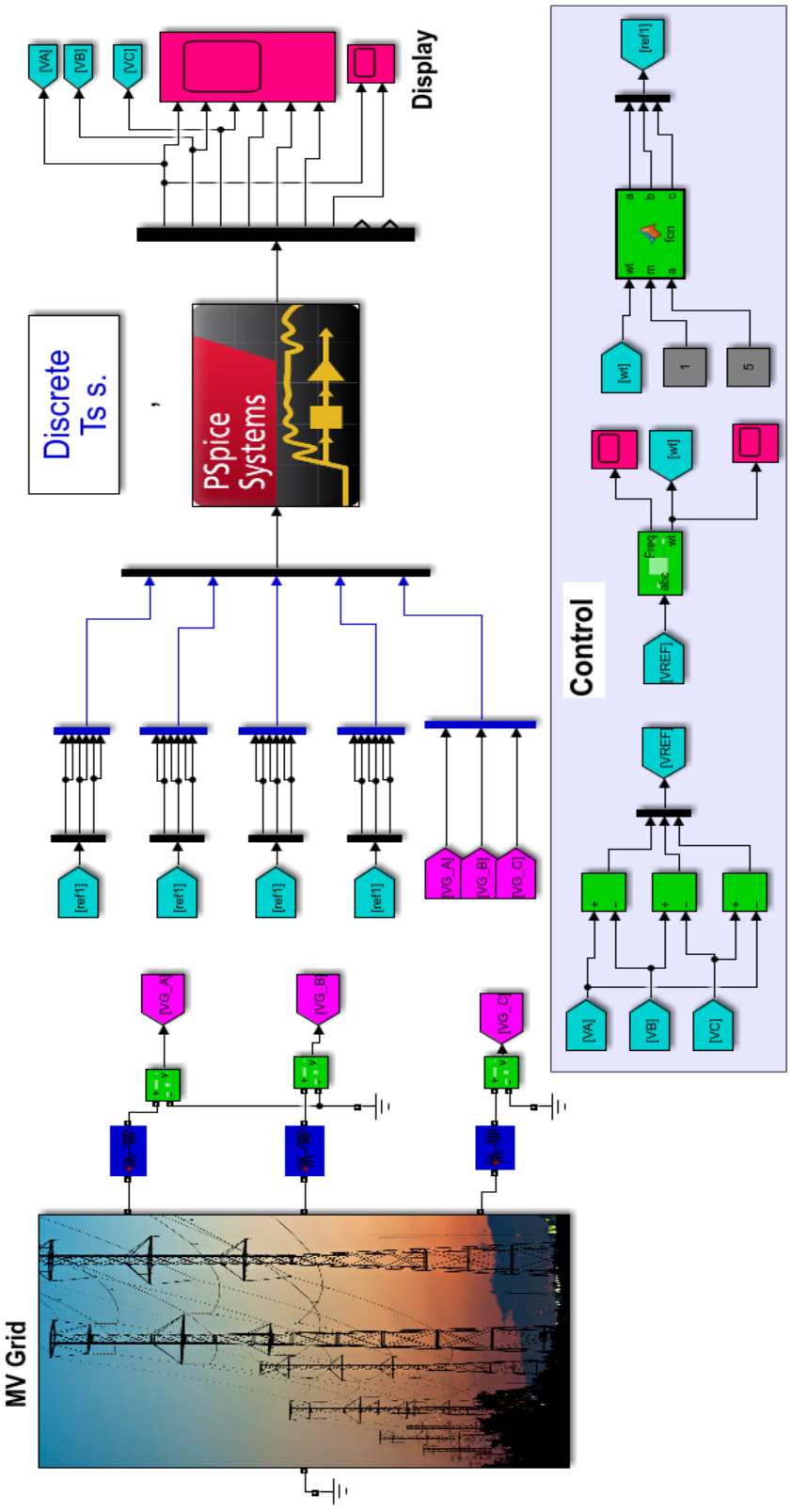

Figure 2.9: MATLAB-PSpice co-simulation setup implemented in SIMULINK.

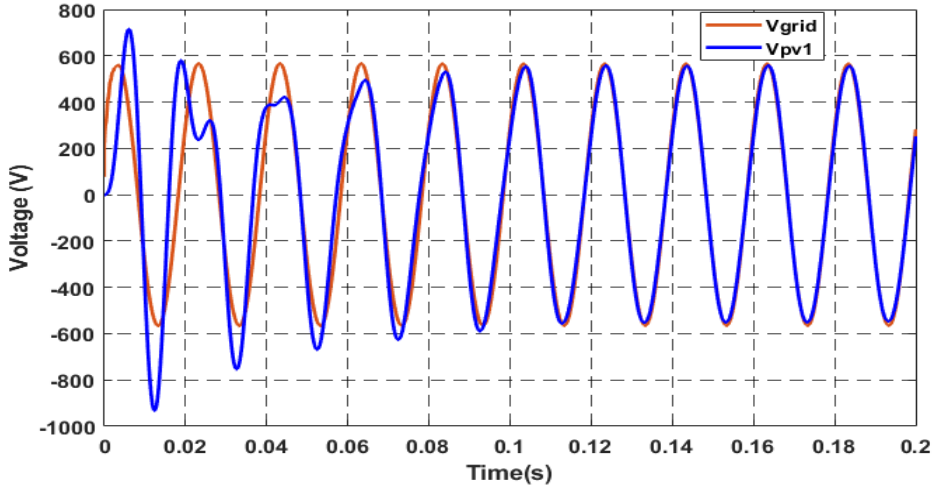

(a)

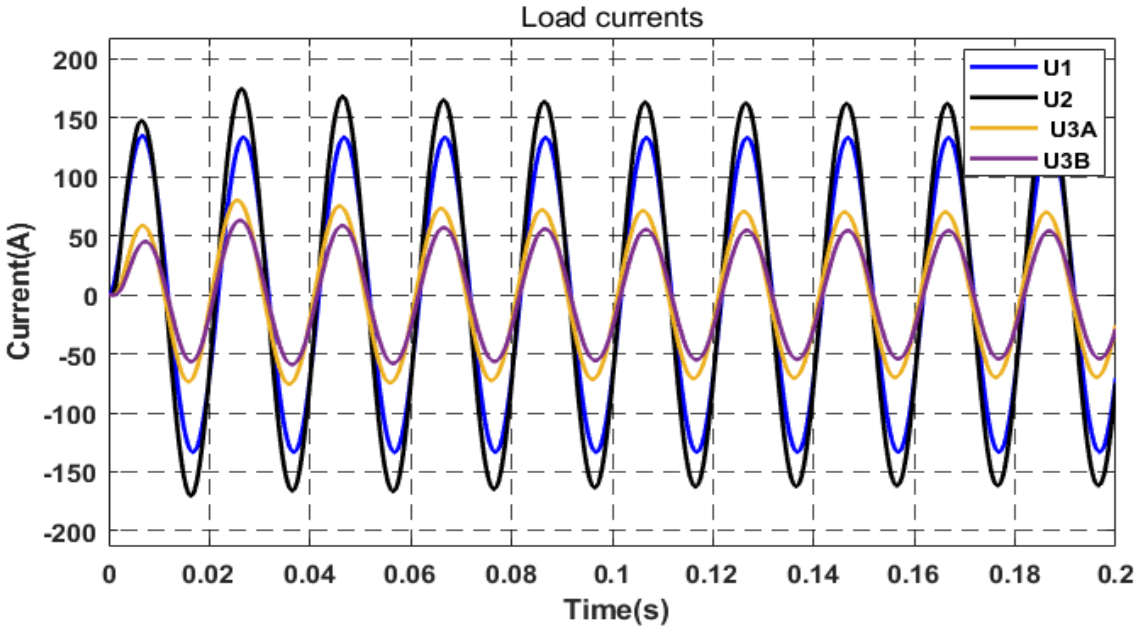

(b)

Figure 2.10: Voltages and currents at the LV network.

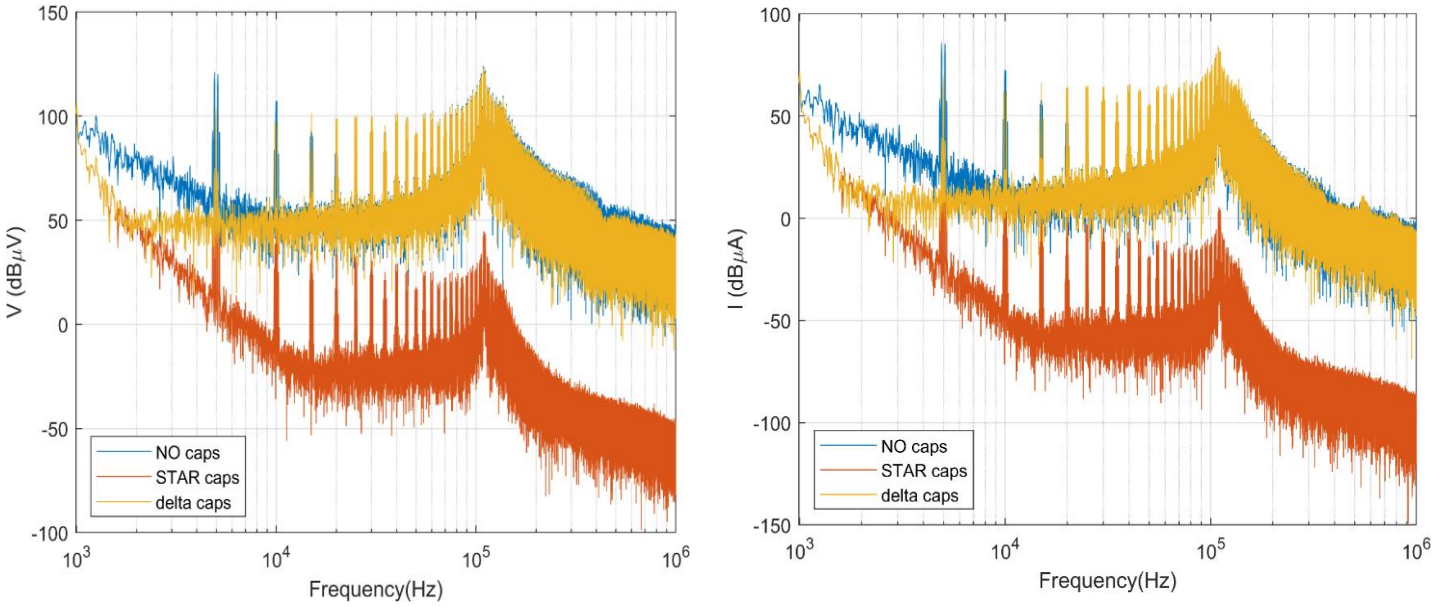

(a) (b)

Figure 2.11: Noise voltages and currents measured at the busbar with considering grounded star and delta connected PFC.

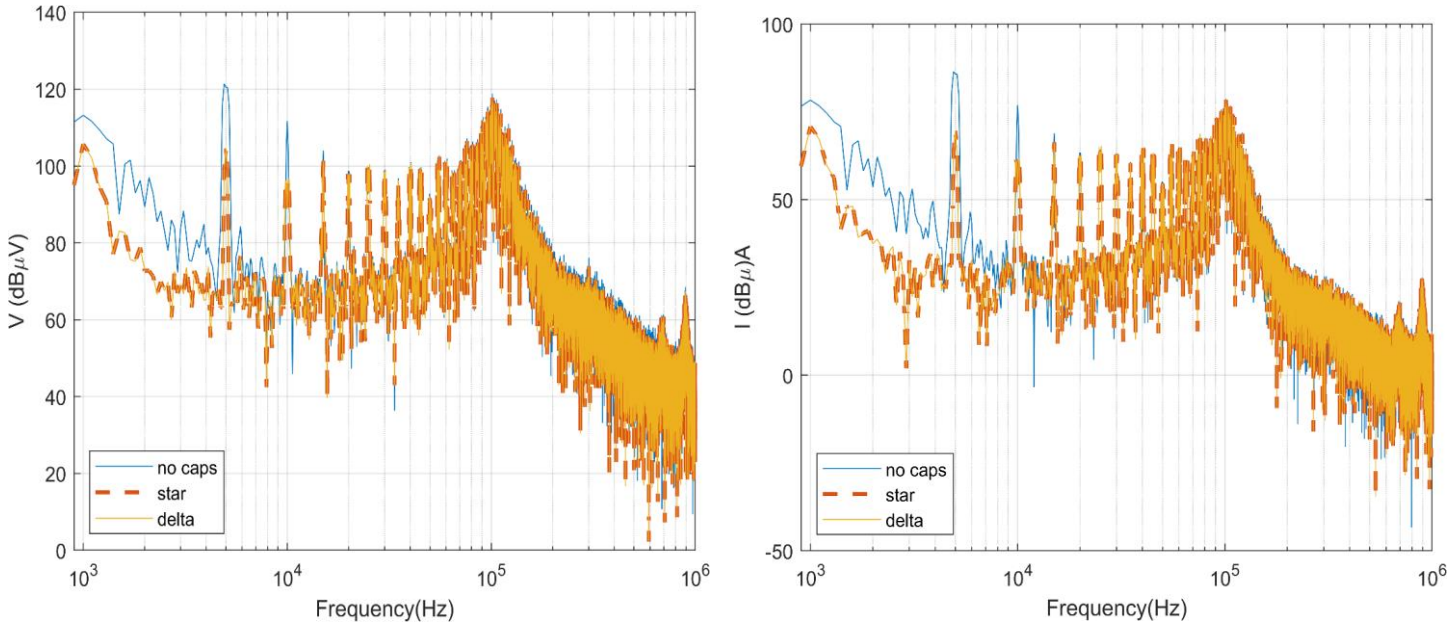

(a) (b)

Figure 2.12: Noise voltages and currents measured at the busbar with considering ungrounded star and delta connected PFC.

2.2.4.2. Effects of the Parasitics of PFC capacitor

In this sub-section, the effects of the non-ideal behavior of the PFC capacitor due to the parasitic components ESR and ESL is studied. The PFC capacitor (88.09 uF in delta connection and 264.27 uF in star connection) is connected to improve the power factor of the linear load from 0.8 to 0.9. The ESR of the PFC capacitor is set as 2 mΩ, and different values of ESL (fom 1 uF to 100 nF) is considered. The voltage at the busbar and the current propagating to the AC grid when the PFC capacitor is

connected in star are shown in Figure 2.13 (a) and Figure 2.13 (b) respectively. As it can be seen clearly, maximum and minimum noise propagation to the AC grid occurs when there is no PFC capacitor connected and when ideal PFC capacitor (without ESL) is connected respectively. The PFC capacitor helps besides improving the power factor, diverting the noise current by creating a very small impedance compared to the impedance of the grid. However, this is true only when the PFC capacitor is ideal. In general, the influence of CE reduction due to the PFC capacitor is weakened when the PFC capacitor is not ideal i.e., the CE's to the AC grid can be significantly increased if the star-connected PFC capacitor shows inductive behavior. This conclusion is supported by looking the impedance of the load with different working conditions as shown in Figure 2.13 (c). The impedance of the load is very low when there is an ideal PFC capacitor connected to it. However, it increases with an increase in the ESL of the PFC capacitor, since the capacitor have an inductive behavior and results more noise current to propagate to the grid.

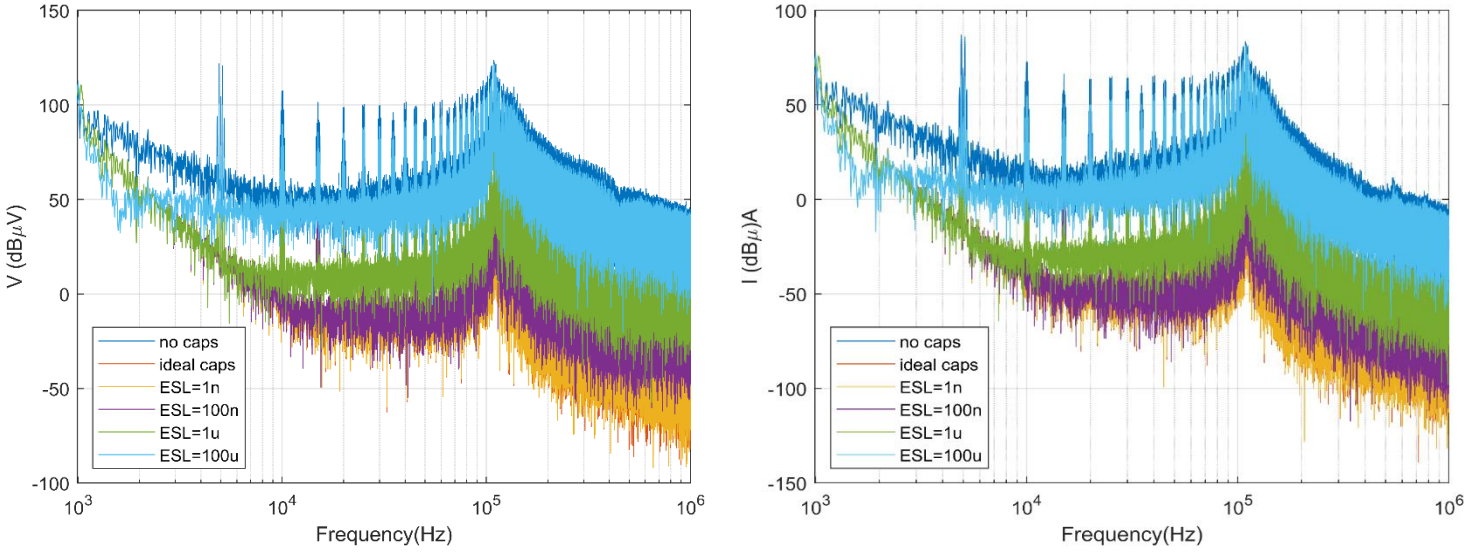

(a)

(b)

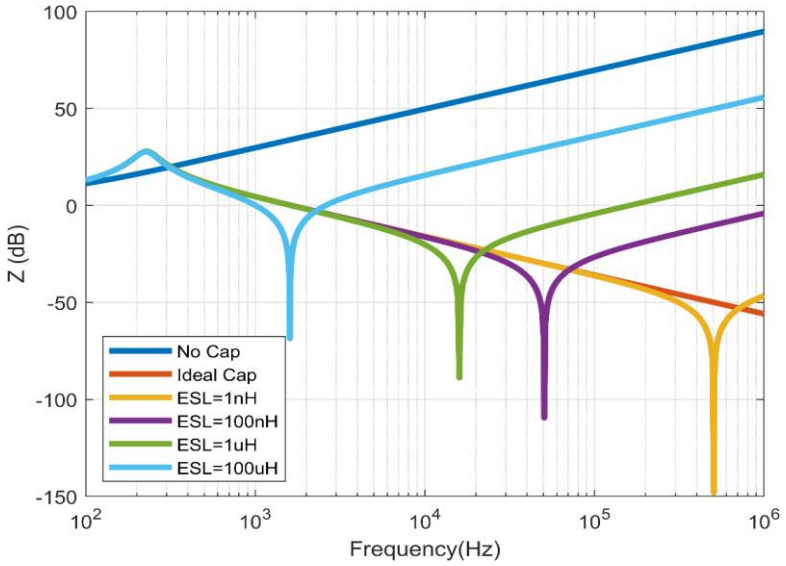

(c)

Figure 2.13: Noise voltages and currents propagated to the AC grid and Impedance of the shunt capacitor with considering different values of parasitics.

2.2.4.3. Effects of the load power factor on CE propagation

In this configuration, the purpose is to analyze the relationship between the power factor of linear load and the CE propagating to branch L_0 (by evaluating *Vbus_L0* and *Ibus_L0*). Thus, the setup keeps only branch L_0 and L_1 present, and the circuit breakers ideally disconnect branches L_2, L_{3a}, and L_{3b}. Besides, the PFC shunt capacitors in line L_1 are also removed. For branch L_1, the real power (50 kW) kept the same. The power factors are set from 0.2 to 1 by assigning different inductances of the linear load (see Table 2.2). The influence of the power factor on the current and voltage of branch L_0 is shown in Figure 2.14 (a) and Figure 2.14(b). As can be seen, poor power factor (below 1) caused significant noise current to propagate to the AC grid compared to the ideal power factor (pf=1). This phenomenon can be explained robustly regarding the input impedance (Z11) of the linear load seen by the PV-inverter where different power factor is considered. This can be seen in Figure 2.14 (c), where the impedance

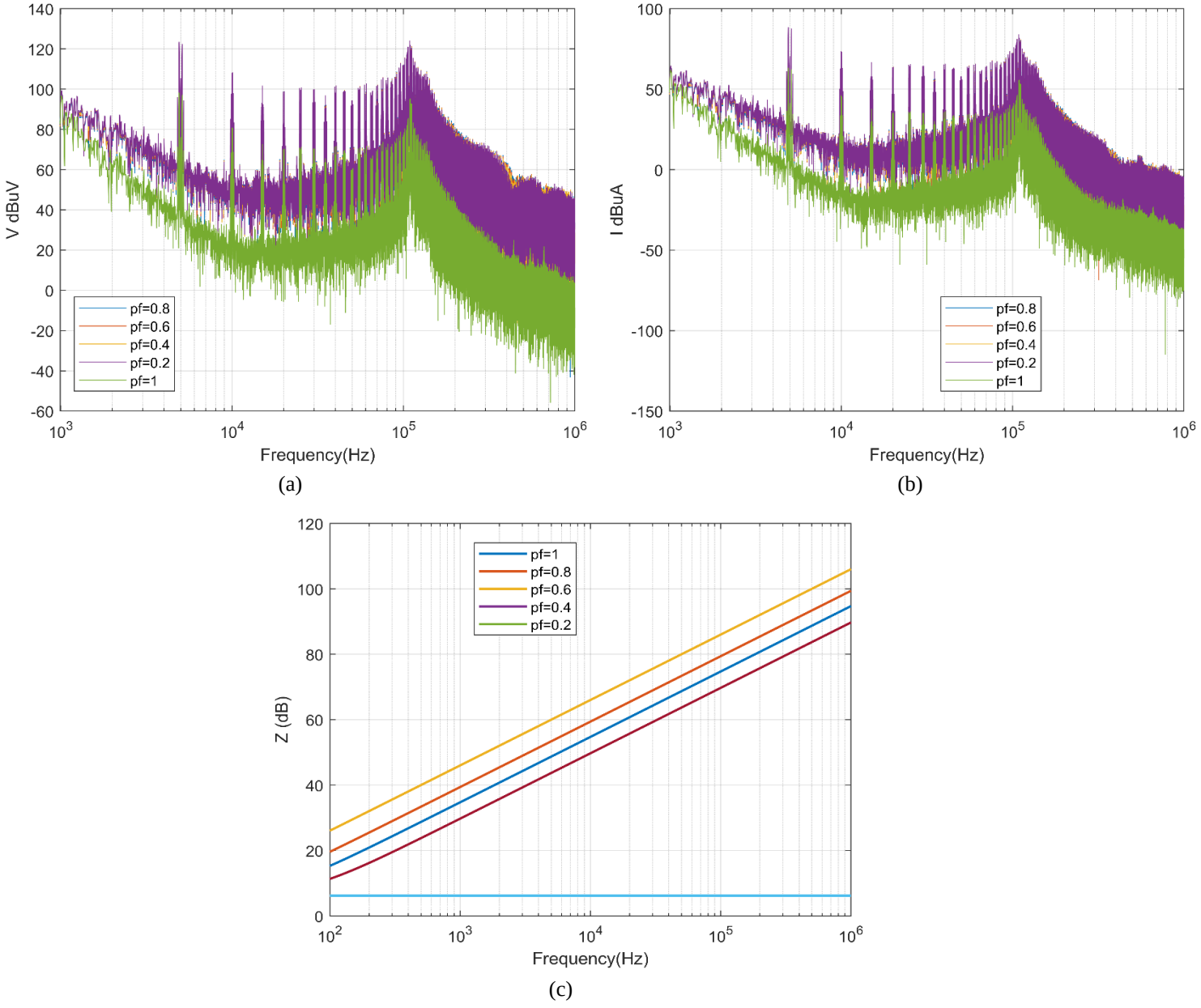

Figure 2.14: Noise voltages and currents measured at the busbar with considering different configuration of shunt capacitor.

of the linear load where power factor is less than one is significantly higher compared to unity load power factor. This indicates that more current propagats to L_0 rather than the linear load, no matter the deviations of the power factor compared to the unity power factor. Infact, the CE's propagating to L_0 when pf=1 are much lower than other power factor values.

Table 2.2: Parameters of the linear load of branch L1 with fixed real power (50 kW) and different power factor.

Power factor		0.2	0.4	0.6	0.8	1.0
Parameters	**R (ohm)**	2	2	2	2	2
	L (mH)	32	15	9	5	0

2.2.4.4. Effects of the parasitics of the circuit breaker on CE propagation

In this configuration, the purpose is to investigate the CE propagation when one branch is under the island mode. For example, the branch L_1 is chosen to work offline, with a non-ideal circuit breaker in open status. For this case, the parallel capacitor of the non-ideal circuit breaker is varied from 10 pF to 100 pF, and the CEs propagating in branch L_1 is plotted in Figure 2.15. As it can be seen, the current IL_1 from the CB_1 to the busbar is sensitive to the non-ideal behaviour of the CB1 in which considerable noise current propagates to the AC grid where higher value of parallel capacitor is chosen even if the CB_1 is in open position. Therefore, it is necessary to consider the parasitic capacitor of the CBs when performing EMI simulation.

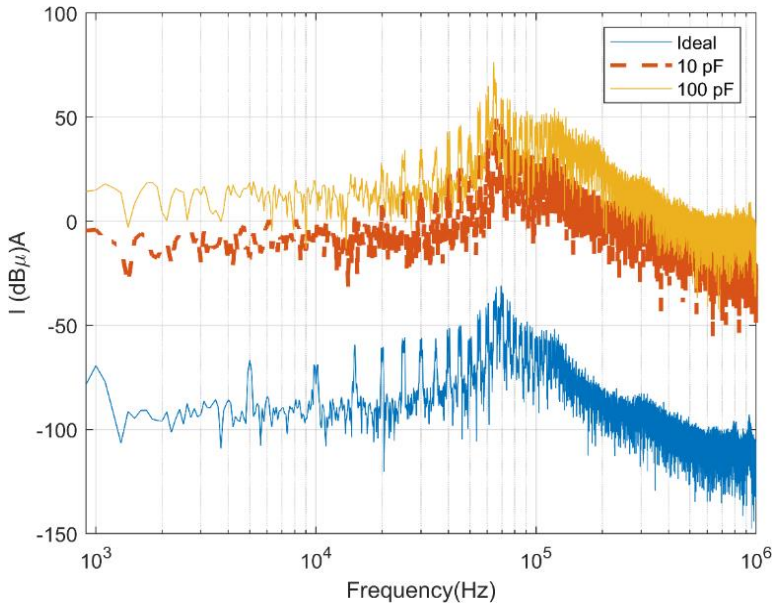

Figure 2.15: Noise currents measured at the busbar with considering different values of parasitic capacitance of the circuit breaker.

2.3. Modeling Noise Source Using Black Box Approach

This section presents an activity held to model Photovoltaic (PV) based three-phase inverter using black-box modelling approach for EMC analyses. The work was done in collaboration with RSE research group. The main objective in this work is to find a suitable black-box model of a three-phase inverter so that the model can be used to predict the CE in complex power system networks. Besides, it is a motivation to investigate the main constraints of modelling such a noise source using black-box modelling approach. The PV based three-phase inverter, along with an LCL (i.e., inductor-capacitor-inductor) filter connected to the grid discussed in Section 2.2 and shown in Figure 2.3, is considered in this part.

The theoretical assumption behind black-box modelling approach is that the device under analysis can be treated (at least approximately) as a linear and time-invariant (LTI) system. However, since switching modules exhibit an inherently time-variant and non-linear behavior, a thorough investigation aimed at identifying the conditions for applicability and possible limitations of black-box modelling is required. It is worth mentioning that from the viewpoint of black-box modelling, the LCL filter plays a fundamental role in masking the nonlinear and time-varying behavior of the inverter, thus making the LTI assumption generally satisfied.

For this purpose, the black-box modelling technique in [42], which was originally adopted for modelling DC-DC converters in a satellite power system, is extended in this work. The model aims to predict the CE peaks related to the switching frequency and its harmonics exiting the AC side of a three-phase inverter connected to a PV panel. For the proposed modelling procedure, accuracy, applicability, and possible limitations of black-box modelling are systematically investigated, by paying particular attention to the low-frequency part of the spectrum down to 2 kHz (since the switching frequency of the inverter here considered is 5 kHz). To this end, an explicit model of the whole system (i.e., a model involving the switching modules, the control system as well as parasitic components) is preliminarily implemented in SPICE (it stands for Simulation Program with Integrated Circuit Emphasis) and used as a virtual environment to emulate the steps of the proposed experimental procedure and to obtain a prediction of the generated CE to be used as a reference to validate the proposed modelling strategy.

The proposed black-box model representation of the inverter is shown in Figure 2.16. The inverter (together with PV panels and LCL filter) is represented by a Norton equivalent, i.e., a noise source current and a passive admittance [42]. As discussed before, the applicability and effectiveness of this strategy are limited to the modelling of linear and time-invariant devices only. Since power converters are intrinsically non-linear and time-variant networks, black-box modelling requires preliminary verification that the device can be treated, at least approximately, as an LTI system. In several works [43–45], such an assumption was assumed to be satisfied, since the converter under analysis was equipped with an EMI filter or decoupling capacitors /functional inductors, which can mask the inherently non-linear and time-varying behavior of the switching modules.

2.3.1. Black-Box Modelling Procedures

The procedure here exploited to identify black-box model parameters involves two different setups. The former is used to evaluate the entries of the admittance matrix (passive part of the model), the latter is to extract the frequency response of the noise (current) sources (the active part of the model).

2.3.1.1. Passive Part of the Black-Box Model

As the first step, the entries of the admittance matrix $\boldsymbol{Y}_{dut}$ are characterized through Vector Network Analyzer (VNA) measurement of the scattering parameters (S-parameter) at the output port of the LCL

filter, as shown in Figure 2.17. For measurement, the gate signals and the DC-link voltage supply should be disconnected from the inverter for safety reasons. To mimic VNA measurement conditions by the SPICE model, both the DC voltage sources, and the gate signals sources are replaced by short circuits. The obtained 3 by 3 S-parameter matrix ($\boldsymbol{S}_{dut}$) is then converted into the corresponding 3 by 3 admittance matrix $\boldsymbol{Y}_{dut}$ by post-processing of measurement data [46]. The S parameters can be easily measured using the procedure in [47] as shown in Figure 2.18.

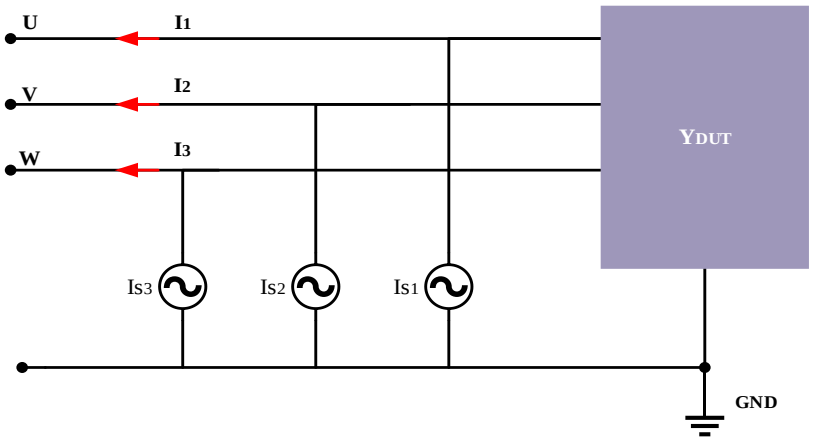

Figure 2.16: Black-box model of the three-phase inverter system.

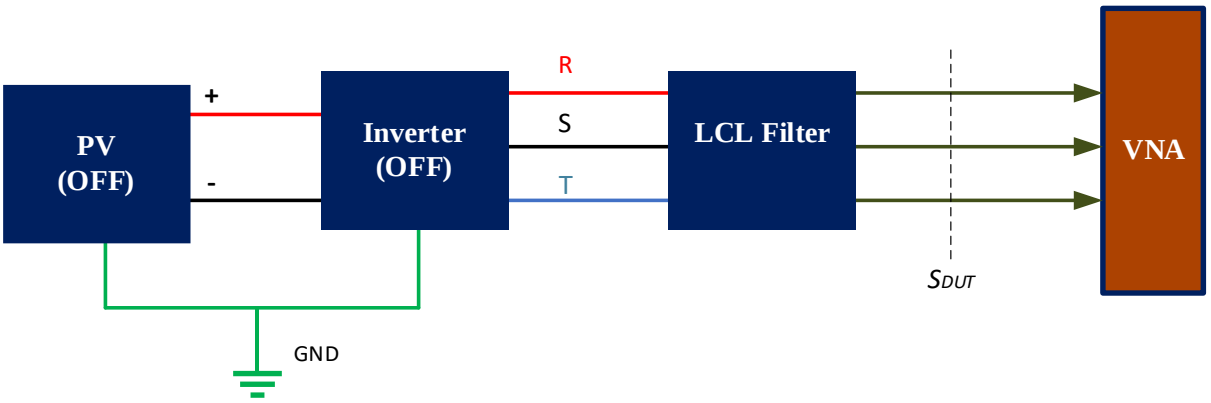

Figure 2.17: Measurement setup exploited to evaluate the entries of the admittance matrix (passive part of the black-box model).

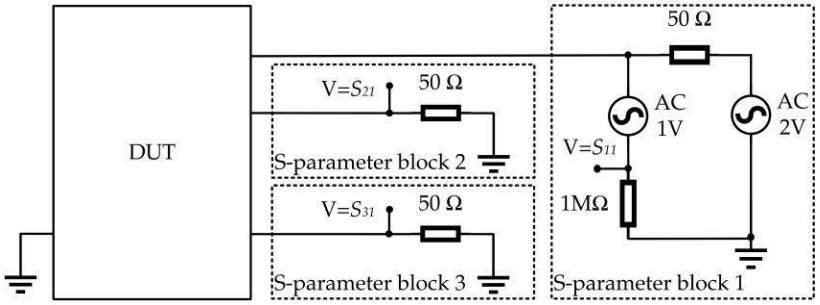

Figure 2.18: SPICE implementation of the measurement setup used to evaluate the passive part of the model: The three blocks connected at the DUT ports are used to emulate the three ports of a VNA.

2.3.1.2. Active Part of the Black-Box Model

To extract the current sources I_{s1}, I_{s2}, and I_{s3} (active part of the black-box model), the test setup in Figure 2.19 is exploited where the three phase LISN is deployed to measure the voltages V_4, V_5, and V_6 at the 50 Ω terminal. The currents I_4, I_5 and I_6 can be easily determined by dividing those voltages by 50 Ω. Then, the line voltages (V_1, V_2 and V_3) and currents (I_1, I_2 and I_3) can be determined using 6 by 6 ABCD matrix of the LISN using (2.1). Of course, the circuit discussed in Section 2.3.1.1 can be used to characterize the LISN as a 6-port network (the first three ports in the inverter side and the rest are on the LISN measurement port).

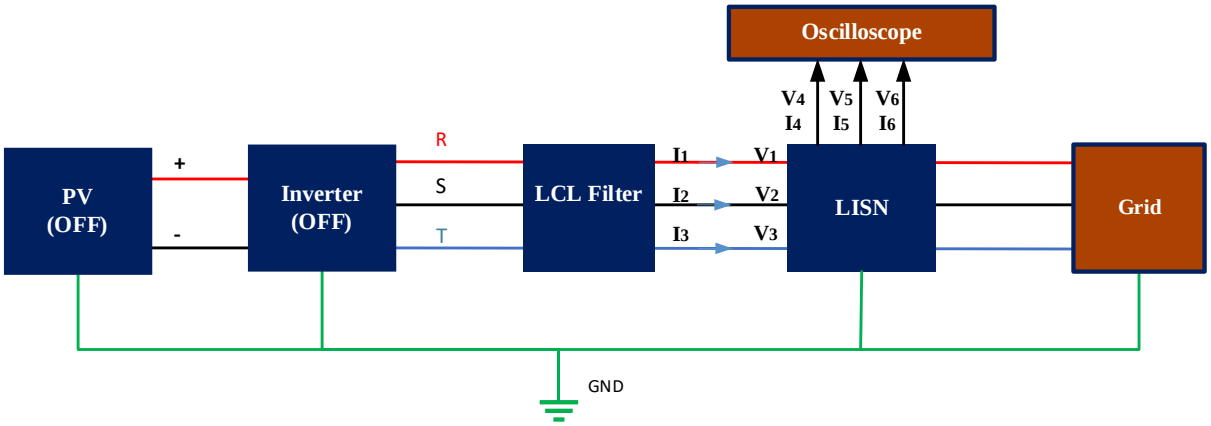

Figure 2.19: Measurement setup exploited to evaluate the active part of the black-box model, i.e., the three current sources I_{S1}, I_{S2} and I_{S3}

In SPICE, the aforesaid setup was implemented by connecting 50 Ω resistors at the LISN output ports to emulate the oscilloscope channels. Additionally, to preliminarily characterize the LISN in terms of six-port network, the blocks already introduced in Figure 2.18 are connected on both sides of the LISN, with the active block connected to one of the six ports at a time, to evaluate the entries of the 6 by 6 S-parameter matrix, $\mathbf{S}_{\mathrm{LISN}}$.

Once this matrix is known, voltages (V_1, V_2, V_3) and currents (I_1, I_2, I_3) at the *DUT* side of the LISN are computed as:

$$[\,V_1 \;\; V_2 \;\; V_3 \;\; I_1 \;\; I_2 \;\; I_3]^T = \boldsymbol{ABCD}_{LISN}\,[V_4 \;\; V_5 \;\; V_6 \;\; I_4 \;\; I_5 \;\; I_6 \;\;]^T \qquad (2.1)$$

where $ABCD_{LISN}$ is the 6 by 6 *ABCD* matrix of the LISN, obtained starting from the corresponding S-parameters matrix $\boldsymbol{S}_{LISN}$ [46]. Eventually, the noise currents in the black-box model are retrieved as:

$$[I_{S1} \quad I_{S2} \quad I_{S3}]^T = [\, I_1 \quad I_2 \quad I_3 \,]^T + Y_{DUT} \quad [V_1 \quad V_2 \quad V_3]^T \qquad (2.2)$$

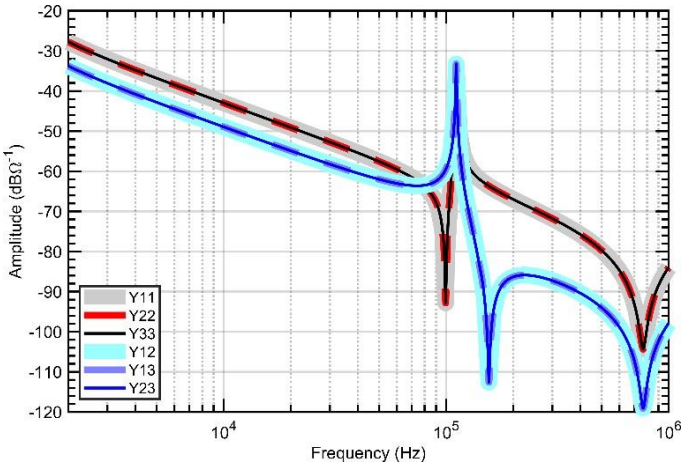

(**a**)

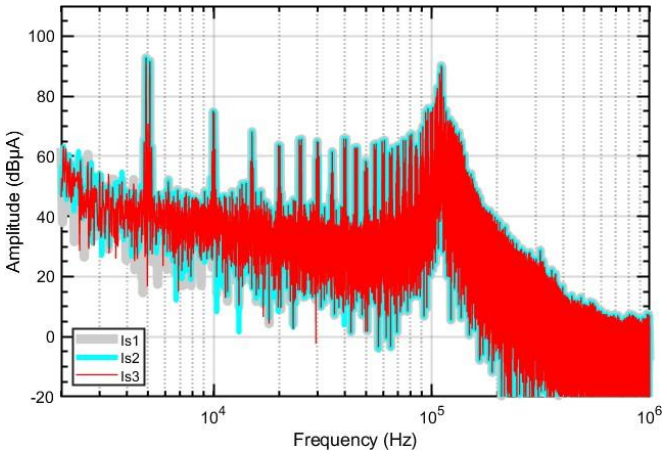

(**b**)

Figure 2.19: Extracted black-box model: (**a**) Selected six Y-parameter of DUT; (**b**) Three current sources.

The magnitude of the extracted black-box-model parameters, i.e., the entries of the Y matrix and the three current sources, is plotted in Figure 2.20. The first plot, Figure 2.20(a), shows the frequency response of *DUT* admittances and the three current sources are shown in Figure 2.20(b).

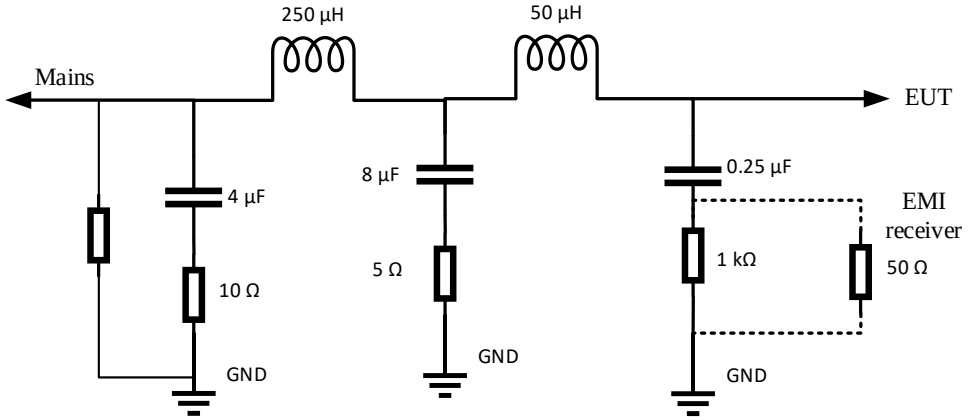

Figure 2.20: Schematics of the LISNs considered in this work: CISPR16-1-2.

It is worth mentioning that LISN effectiveness in stabilizing the impedance seen from the *DUT* outlets in the whole frequency interval of interest is fundamental for model- parameter extraction. Indeed, since the LISN is connected with the mains for CE measurement, its effectiveness in providing a stable impedance, despite possible variation of the mains impedance, determines the accuracy of the noise-source extraction. To this end, CISPR16 LISN shown in Figure 2.21 is considered to extract the active noise currents.

2.3.2. Setup for Model Validation

To effectively validate the accuracy of the obtained black-box model, the CE exiting the converter under loading conditions (sufficiently different from those exploited for model-parameter identification, Figure 2.19, are to be predicted and compared) versus those obtained by exploiting the explicit model of the converter (here used as reference quantities). To this end, an additional EMI filter, Figure 2.22(a), is included between the system and the LISN to appreciably modify the converter working conditions despite the presence of the LISN. The obtained measurement setup is shown in Figure 2.22(b).

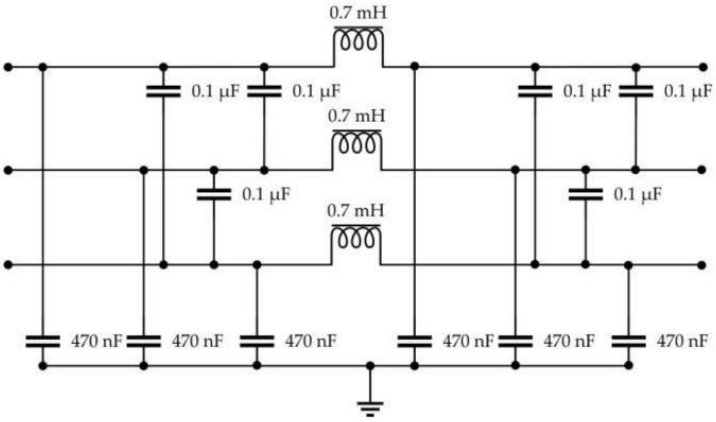

(a)

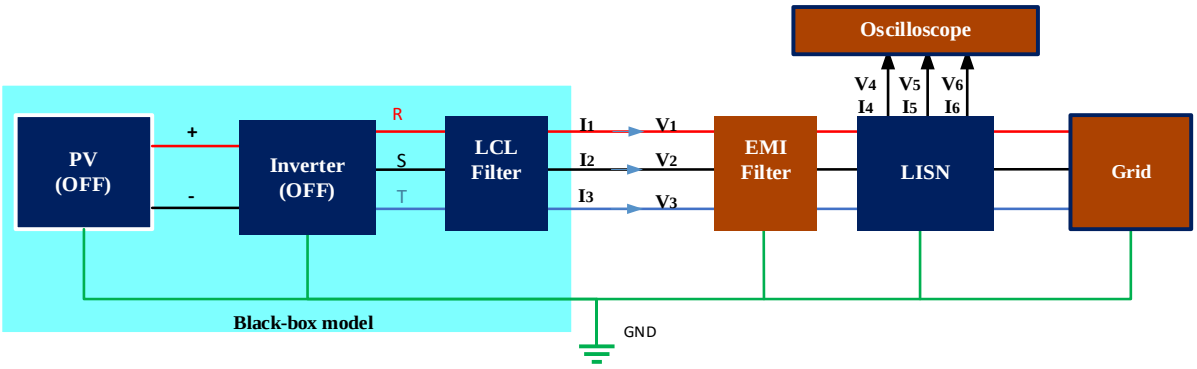

(b)

Figure 2.21: Validation of the black-box model: an additional EMI filter (**a**) is included in the measurement setup (**b**) to modify the working conditions of the converter.

2.3.3. Model Verification Result and Discussion

As the first step, the CEs exiting the inverter are evaluated in the presence and the absence of the EMI filter in terms of voltages measured at the output (i.e., at the receiver side) of a *LISN* compliant with CISPR16 specifications. Therefore, the CEs simulated in the absence of the EMI

filter are then used as input data to extract the black-box model of the inverter. Conversely, the CEs simulated in the presence of the filter are used to assess the effectiveness of the extracted black-box model in predicting the emissions exiting the inverter under analysis, in combination with a different set of working conditions.

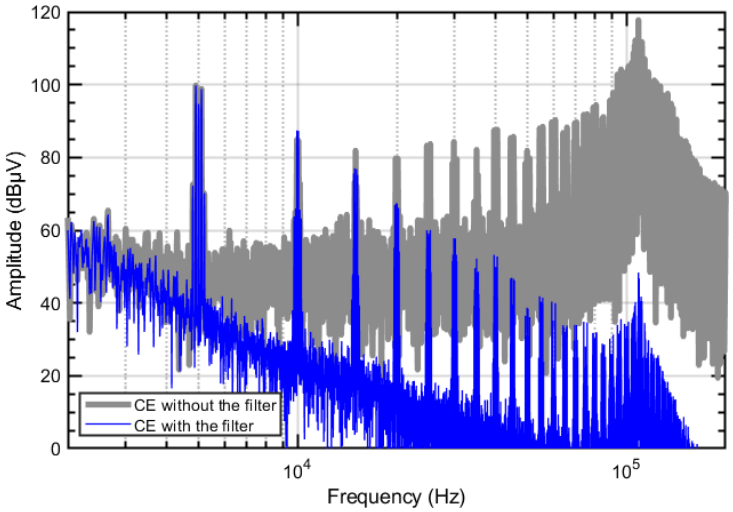

Figure 2.22: Conducted emissions at the AC side of the inverter in the presence and in the absence of the EMI filter.

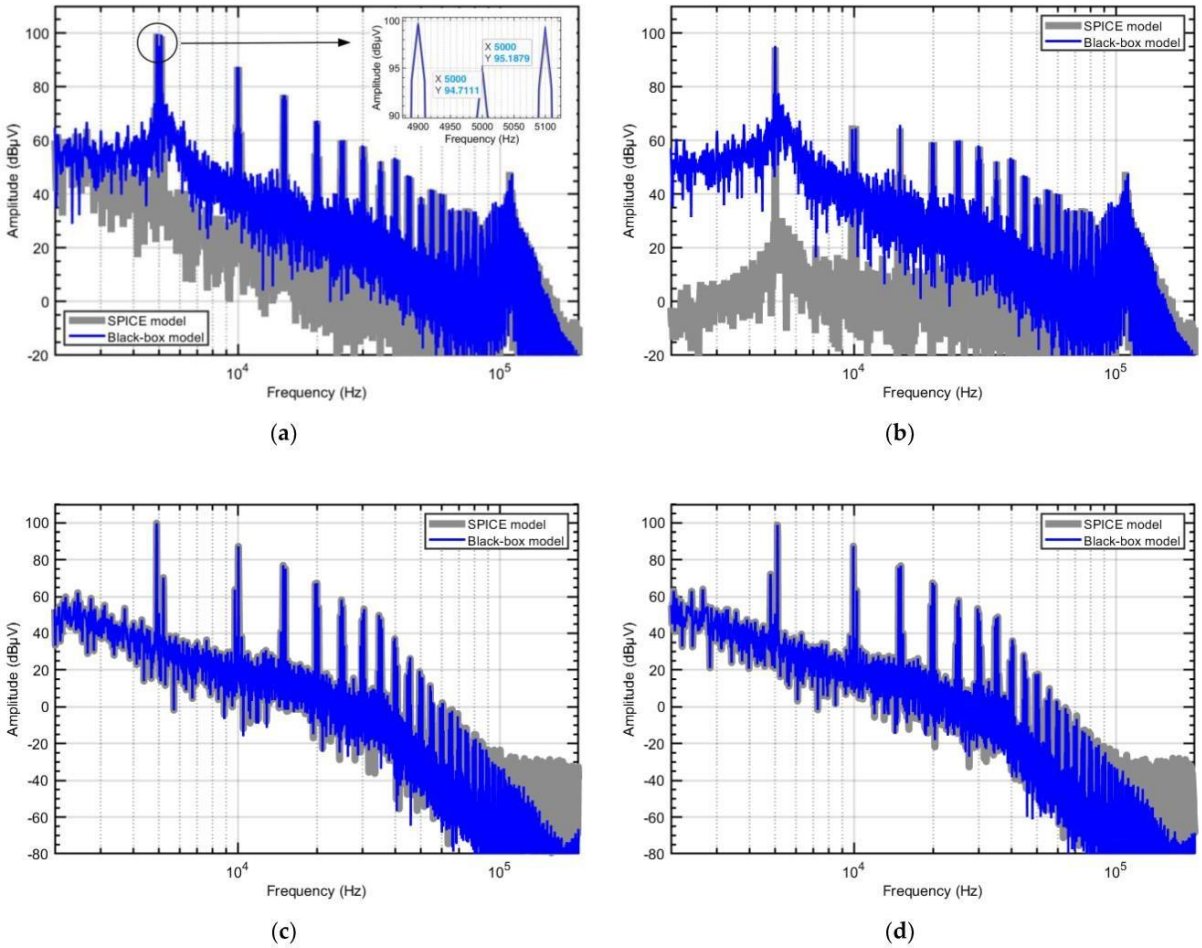

Figure 2.23: Conducted emissions obtained by the SPICE model in Section 3 and predicted by the black-box model (**a**) phase voltage (**b**) zero-sequence voltage (**c**) positive sequence voltage and (**d**) negative sequence voltage.

Figure 2.23 shows the CE with and without EMI filter, where there is a significant difference between the two spectra, and this confirms the effectiveness of introducing the EMI filter to generate a new set of working conditions for validation purposes.

The CEs obtained by the SPICE model of the whole test setup described in Section 2.3.1 and those predicted by the black-box model are compared in Figure 24 (a) in the frequency range from 2 kHz to 200 kHz. The CEs above 200 kHz are not plotted, as they are significantly attenuated (below 10 dBµV). The comparison proves that the black-box model can effectively predict the emissions exiting the converter, with maximum deviations within 3 dB around 110 kHz, where the system exhibits a resonance. The corresponding comparison in terms of zero sequence and positive/negative sequence is shown in Figure 24(b–d), respectively, and confirms the effectiveness of the proposed black-box model also in predicting modal quantities. The zero-sequence and the positive/negative sequences dominate above and below 35 kHz, respectively. The discrepancies observed above 100 kHz are mainly owing to numerical processing of data, due to the extremely low CE levels at high frequency.

2.3.4. Limitations of Black-Box Modelling

2.3.4.1. Influence of the Mask Impedance

To investigate the role of the masking effect due to the LCL filter on model effectiveness, the LCL filter was removed, and the procedure for model parameter extraction was repeated. The obtained predictions are compared versus SPICE simulations in Figure 2.25 (a).

Specifically, for the system without the LCL filter, obvious mismatches are observed in predictions of CEs obtained by the black-box model from 100 to 400 kHz with respect to the accurate circuit simulation. In Figure 2.25(b–d), three sequences of emissions are compared. It is observed that the discrepancies in this frequency interval are mainly from the positive and negative sequences instead of the zero sequence. With respect to Figure 24, the discrepancies observed in Figure 25 are to be ascribed to the inaccuracy of black-box modelling in the absence of the LCL filter, rather than to the noise floor of data-processing. As a matter of fact, in Figure 25 CE levels from 100 kHz to 400 kHz are still significantly larger (above 40 dBµV) than the noise floor. This investigation puts in evidence that in the absence of an LCL filter (and its masking effect), the nonlinear and time-variant characteristics reflect the prediction of positive/negative sequence components. In this case, the black-box modelling approach is less accurate in the prediction of DM emissions, especially in the high frequency range.

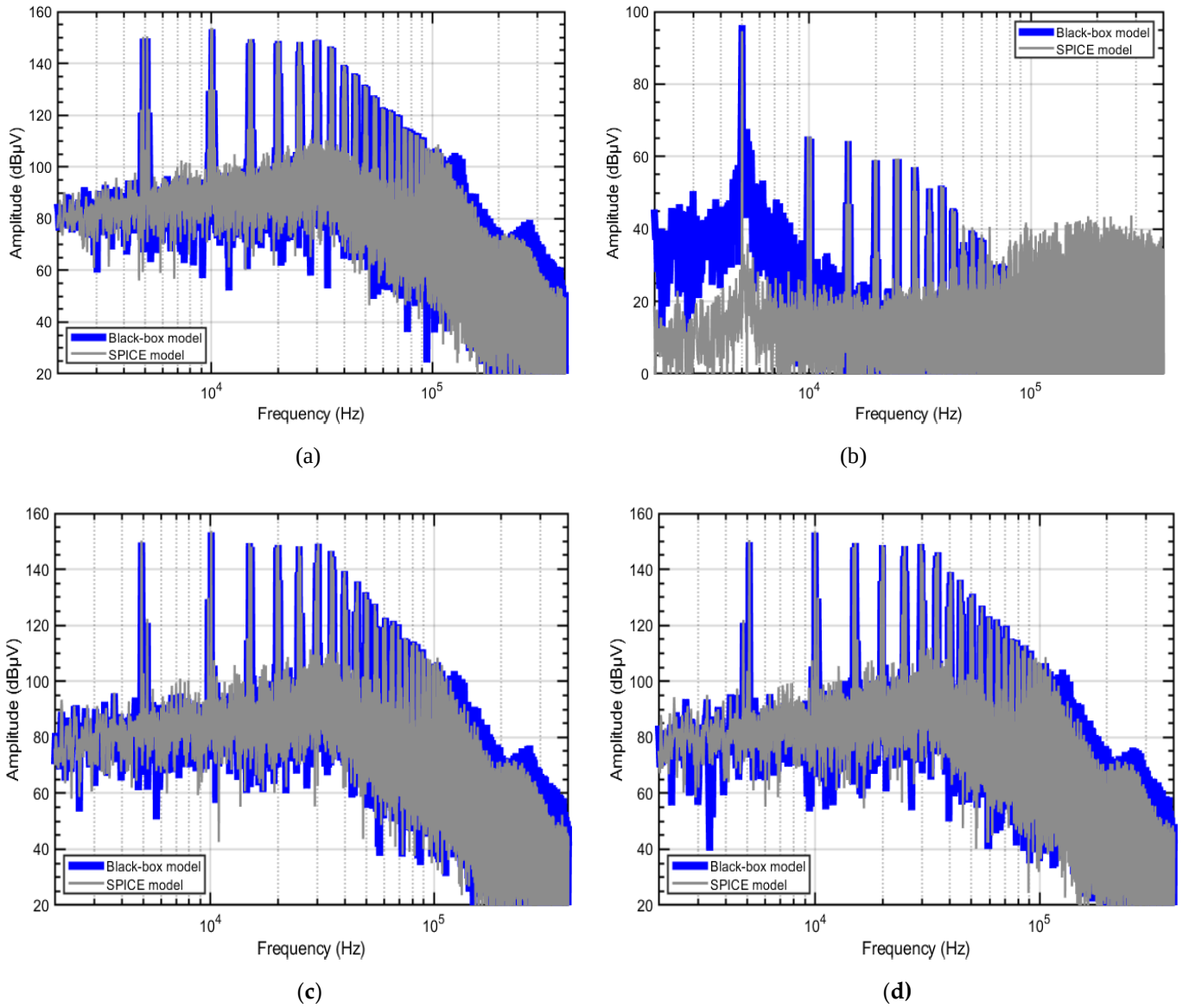

Figure 2.24: Conducted emissions in the absence of LCL filter obtained by SPICE model and predicted by the black-box model (**a**) phase voltage (**b**) zero-sequence voltage (**c**) positive sequence voltage and (**d**) negative sequence voltage.

2.4. Conclusion

This chapter discussed the modelling of noises sources mainly power electronics converters. In this regard, both white-box and black-box modelling techniques were investigated in detail considering their application in predicting EMI emissions in complex networks such as the LV distribution network and their respective application limitations.

The white box modelling approach have been implemented to study the CE propagation from the LV network to the main grid with the help of PSpice MATLAB co-simulation where different noise sources are modelled in PSpice considering parasitic elements and MATLAB SIMULINK was used to implement control schemes for synchronizations. The work started from detail modelling of the LV network components such as transmission lines, inverter, load, transformer, and shunt capacitor. The effects of the PFC capacitors, circuit breakers, transmission lines and power factor of the loads, on the CE propagation of the LV network to the main grid has been investigated thoroughly. Simulation results

showed that the PFC capacitor plays an important role in the CE propagation from the LV network to the main grid. For example, when PFC capacitors are connected in grounded star configuration, the CE propagated to the AC grid showed significant reduction compared to delta and ungrounded star connection, since the grounded star connection provides a path to ground. Therefore, connecting PFC capacitors in grounded star has a great advantage to reduce CE even if the required size of the capacitors are three times larger than delta connection to have the same power factor improvement. Besides, the parasitic elements of the PFC capacitor such as ESL significantly affected the propagation of the noise. Indeed, the shunt capacitor no longer works as a capacitor above its resonant frequency, and it becomes inductive which intern creates large impedance at high frequency. Therefore, most of the noise from the inverter propagates to the LV grid compared to the ideal shunt capacitors. Another important parameter is the load power factor. Results confirmed that poor power factor (pf values below 1) caused significant noise current to propagate to the AC grid compared to the ideal power factor (pf=1) since the impedance of the linear load where power factor is less than one is significantly higher compared to unity load power factor and this forces more noise current to propagates to the main grid than the linear load. Finally, the effects of the parasitics of the circuit breakers on the CE propagation where the breakers are in open status have been investigated and results showed that considerable noise current propagate to the AC grid where the non-ideal circuit breaker is considered even when the breaker is in open status. Therefore, it is necessary to consider the parasitic capacitor of the CBs when performing EMI simulation.

The black-box modelling approach has been applied to a three-phase inverter connected with a PV panel, and the procedures and the possible limitations of this modelling approach have been investigated. The procedure foresees separate characterization of the active and passive part of the model. Specifically, a suitable procedure was proposed to identify the noise sources (active part of the model), which resorts to the time-domain measurement of the voltages at the output of the LISN, instead of the currents exiting the converter, to filter out the 50 Hz fundamental component, whose contribution could impair the identification of higher frequency components. The comparison versus SPICE simulation proved the effectiveness of the proposed black-box modelling approach in predicting the CEs exiting the AC side of the grid-tied three-phase inverter system under analysis in the frequency range starting from 2 kHz. The proposed analysis allowed a systematic investigation of two main limitations, possibly degrading the prediction accuracy of the proposed black-box modelling technique during the measurement. The former limitation is related to the assumption that the system under analysis should be treated, at least approximately, as a linear and time-invariant system. In this regard, the fundamental role played by the LCL filter (installed at the converter output) in masking the inherent non-linear and time-invariant behavior of the inverter switching modules has been proven. In general, this assumption needs to be confirmed prior to the application of the black-box modelling procedures. The latter limitation is related to the bandwidth of the LISN exploited to extract from measurement the frequency response of the noise sources (active part of the model). In this regard, it has been proven that using a LISN foreseen for CE measurement starting from 150 kHz, as foreseen by several EMC standards, may lead to significant degradation of prediction accuracy in the lower part of the spectrum (i.e., below 150 kHz), since the frequency response of the extracted noise sources is strongly influenced by the impedance connected at the output of the LISN. To eliminate the influence of power network impedance, it is necessary to develop a new type of LISN with stable impedance starting from 2 kHz, otherwise, the mains impedance must be measured or estimated to improve the accuracy of the black-box model predictions at low frequency.

CHAPTER 3

Random Pulse Width Modulation

3.1. Random Pulse Width Modulation

In RPWM, one of the switching parameters of the PWM signal, such as switching period, pulse position and pulse width are varied randomly in order to spread the noise exiting power converters. Therefore, RPWM can be classified as Random Frequency Modulation (RFM), Random Pulse Position Modulation (RPPM) and Random Duty-Cycle Modulation (RDM), depending on the parameter which is made random [48]. Figure 3.1 shows the RPWM signal, where 'T' is switching period, 'Δ' is the pulse position and 'd' denotes pulse width. Applying RPWM to reduce the CE's of power converters is not new and has been deployed in many converters to pass the EMC compliance tests. Indeed, plenty of research activities were carried out towards finding specific RPWM techniques suitable to the specific converter topologies [49-51].

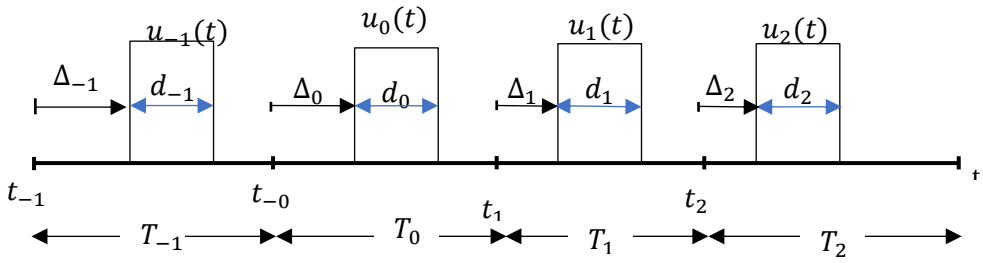

Figure 3.1: Random switching signal.

This chapter is aimed at introducing the most common RPWM techniques which are being deployed in many converter topologies considering their effectiveness at reducing CE and aiming at comparing them with regards to their advantages and possible limitations, with the final goal of using RPWM to the study of coexistence issues with PLC system in the coming chapter (chapter 4). Besides, this chapter is also aimed at introducing the procedures on how those types of RPWM techniques can be implemented using both simulation software like PSpice-Simulink cosimulation and in practical laboratory experiments considering the main challenges of programming the micro-controllers to generate RPWM signals. Moreover, the main parameters which affect the effectiveness of the specific RPWM techniques on the reduction of the CE of power converters as well as the coexistence issue will be discussed in detail. Therefore, an introduction of the RPWM, its implementation in simulation software and its practical implementation in laboratory experiment are summarized in the following sections.

3.1.1. Random Frequency Modulation

Random Frequency Modulation (RFM) or alternatively spread spectrum modulation is the most deployed random modulation technique for EMI reduction. It is also the first random modulation technique introduced. RFM is an extension of a very common modulation technique called Frequency Modulation (FM) [52].

In conventional FM, the frequency of the carrier wave (f_c) is varied according to the message signal ($\xi(t)$) with frequency deviation of Δf as shown in Figure 3.2.

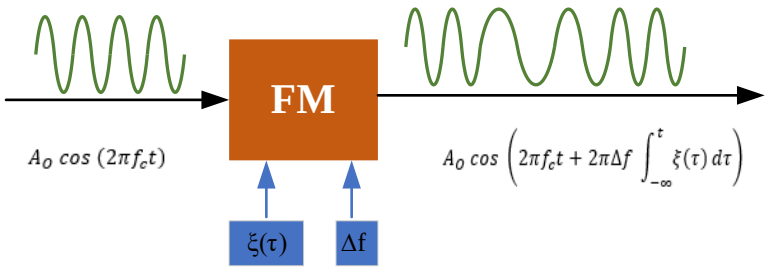

Figure 3.2: Classic approach for spreading a sinusoidal tone based on frequency modulation using a generic driving signal ξ(t).

The resulting signal s(t) from center-spread FM modulation of a simple sinusoidal tone can be defined as:

$$s(t) = A_0 \cos\left(2\pi f_c t + 2\pi\Delta f \int_{-\infty}^{t} \xi(\tau)\, d\tau\right) \qquad (3.1)$$

where, the message signal ξ(t) (in this case modulation profile), varies between -1 and 1 as $-1 \leq \xi(t) \leq 1$.

Therefore, in classical FM, the instantaneous frequency of the signal varies from fc − Δf (when $\xi(t) = -1$) to fc +Δf (when $\xi(t) = 1$) linearly with ξ(t) as (3.2).

$$f(t) = f_0 + \Delta f \times \xi(t) \qquad (3.2)$$

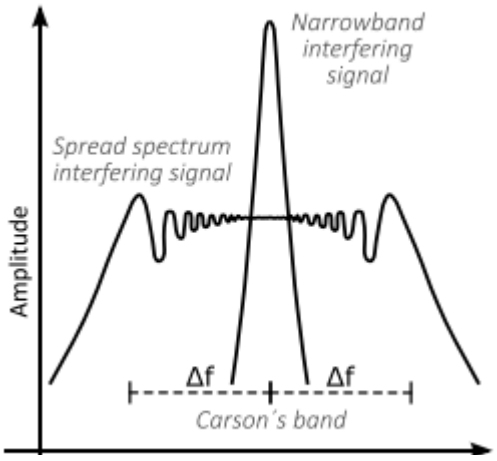

Figure 3.3: Sketch comparison between the power spectra of an unmodulated narrow-band interfering signal and of a spread spectrum one (center-spread).

Hence, the power of s(t) is spread linearly in the Carson's bandwidth [fc − Δf; fc+ Δf] as shown in Figure 3.3. RFM is an extension of the FM where (3.1) applied to each signal harmonic, with the only difference that the n^{th} harmonic is spread within a bandwidth of amplitude 2nΔf. Of course, the actual shape of the spectrum of s(t) depends on the modulation parameters, i.e., Δf and ξ(t). When ξ(t) is a periodic function with period T, the spectrum of s(t) is discrete, with components located at fc ± k/T, k € Z.

There are important parameters which play a significant role in RFM such as spreading factor, modulation index and the type of the modulation profile signal. The spreading factor (α) determines the rate by how much the switching frequency deviates from the reference central switching frequency of the PWM signal, and can be expressed in percentage as:

$$\alpha\ (\%) = \frac{\Delta f}{f} \times 100 \qquad (3.3)$$

and the modulation index defines the rate by how much the switching frequency deviates with respect to the frequency of the modulation profile signal ξ(t) and can be expressed as:

$$m = \frac{\Delta f}{f_m} \qquad (3.4)$$

Where '*f' is* the central switching frequency of the PWM signal and f_m is the frequency of the modulation profile.

The spreading factor and modulation index plays a crucial role in spreading the spectrum of the RFM signal. For example, the larger value of spreading factor, α, results more spread spectrum and more EMI reduction compared to lower values as it will be outlined both in simulation and experimental results in the coming sections. Besides, the modulation index plays a big role in spreading the

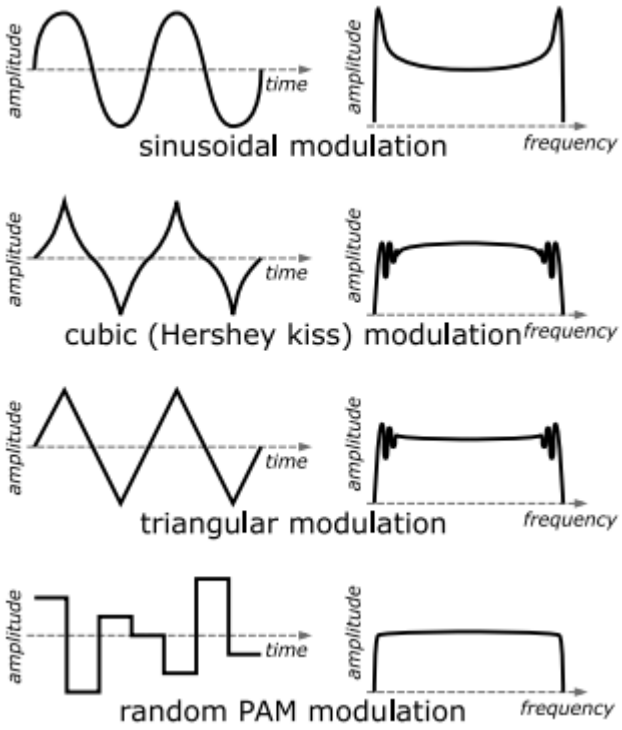

Figure 3.4: Sketch comparison between the output power spectra achieved with different ξ(t) modulating signal. From top to bottom: sinusoidal modulation, cubic (Hershey kiss) modulation, triangular modulation, random PAM modulation.

spectrum where large value results the (discrete) spectrum of s(t) to have many components very close each other that can be assumed to be continuous in the Carson's bandwidth which results better EMI reduction compared to lower values and the result is independent of the resolution of the measurement instrument.

The shape of the spectrum of RPWM with different types of modulation profile is shown in Figure 3.4. As it can be seen, a truly continuous power spectrum is obtained only with a non-periodic ξ(t) such as that obtained using a true random generator. However, it is really difficult to obtain a true random wave generators specially in simulation software since they are periodic at some instant.

3.1.2. Random Pulse Position Modulation

Random Pulse Position Modulation (RPPM) is similar to the classical PWM scheme with constant switching frequency. However, the position of the gate pulse is randomized within each switching period, instead of commencing at the start of each cycle. RPPM offers fixed switching frequency and duty cycle so that the passive parts of power converters function properly.

The instantaneous pulse position can be determined as:

$$\Delta(t)= \Delta ref + \Delta\_\Delta \times \xi(t) \qquad (3.5)$$

In order to investigate the properties of RPPM, it is important to consider the Power Spectral Density (PSD). For conventional PWM, the PSD can be directly determined from the Fourier Series expansion of the PWM signal (1).

$$S(f) = \sum_{n=-\infty}^{\infty} |a_n|^2 \delta(f - nf_1) \qquad (3.6)$$

or indirectly, by using the autocorrelation/PSD relationship [53,54]:

$$S(f) = \int_{-\infty}^{\infty} R(\tau) e^{-i\omega\tau} d\tau \qquad (3.7)$$

where, *S(f)* is the PSD of PWM signal, $|a_n|$ is the magnitude of the Fourier Series coefficients, f_1 is the switching frequency and $R(\tau)$ is the autocorrelation of the switching signal respectively.

However, it is not straightforward to apply the above formulas to find the PSD of RPWM signals, since they are random and can be described only by a probabilistic level using the theory of stochastic processes such as wide-sense stationary (WSS) random processes.

The PSD of a RPPM is derived in [52] by assuming constant switching period and pulse width of the RPWM shown in Figure 3.1.

$$S(f) = \frac{1}{T}|U(f;d)|^2 \left[1 - \left|E\{e^{-i\omega\Delta}\}\right|^2 + \frac{1}{T}\left|E\{e^{-i\omega\Delta}\}\right|^2 \sum_{n=-\infty}^{\infty} \delta\left(f - \frac{n}{T}\right)\right] \qquad (3.8)$$

where, *U* (*f*; *d*) is the Fourier transform of the sampling pulse *u*(*t*):

$$u(t)= \begin{cases} 1, & \text{for } 0 \le t \le d \\ 0, & \text{otherwise} \end{cases} \qquad (3.9)$$

$E\{e^{-j\omega\Delta}\}$ is the expectation of the probability density function of the random pulse position, which depends on the distribution of the random number, and $\omega = 2\pi f$.

As an example, the PSD of RPPM with 5 kHz switching frequency and 0.5 duty ratio is shown in Figure 3.5 (a). In this case, a uniformly distributed random number is used to vary the random pulse position. Of course, the shape of the spectrum may change if the distribution of the random number changes, e.g., if a normal distribution is used. However, the spectrum always exhibits both the density and the harmonic part unlike other modulation schemes. For instance, the RFM spectrum only exhibits the density part as shown in Figure 3.5 (b) [52]. This makes RPPM less effective compared to RFM in minimizing the CE of power converters. Nevertheless, this property will play a significant role in making RPPM more compatible than RFM with communications systems which will be discussed in Chapter 4.

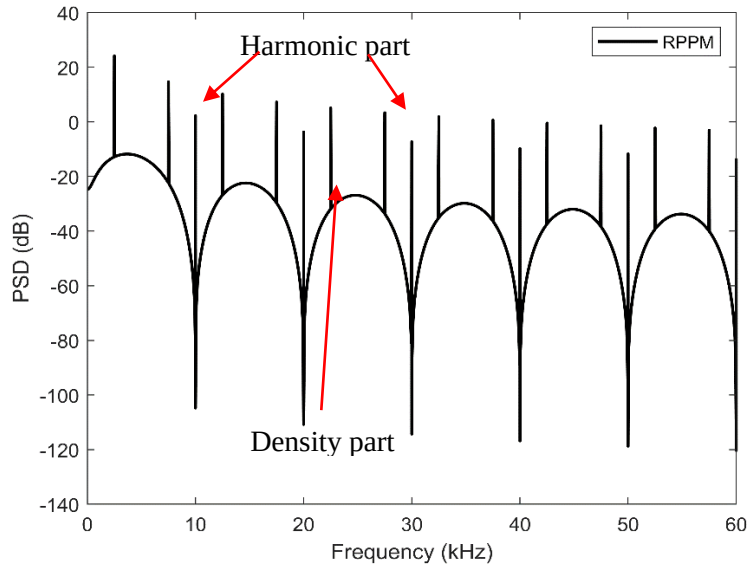

(a)

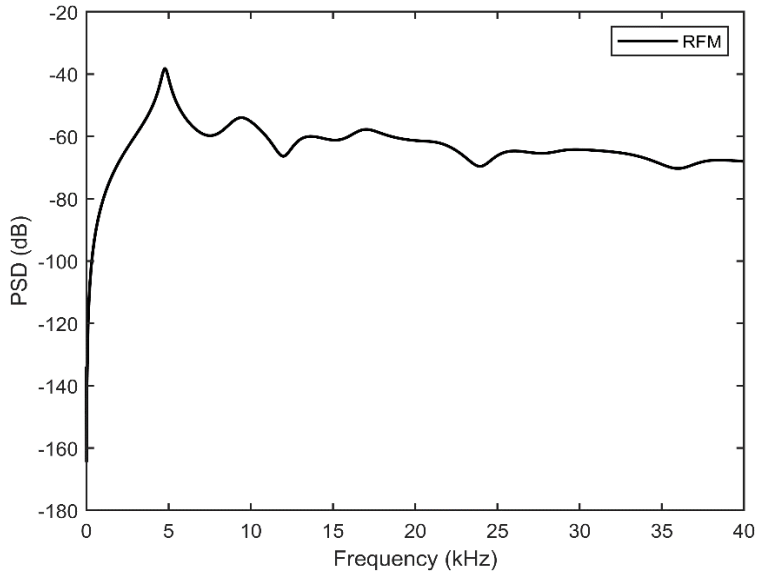

(b)

Figure 3.5: PSD of the switching signal with uniformly distributed random pulse position (a) Random Pulse Position Modulation and, (b) Random Frequency Modulation.

There are parameters which can play a significant role in the effectiveness of RPPM in spreading the noise coming out of power converters such as Random Number Update Rate (RNUR) and spreading factor. The RNUR determines how fast the pulse position of RPPM should change, and it obviously affects the operation of the RPPM. Besides, the spreading factor specifies by how much the pulse position of the RPPM should vary with respect to the switching period. CE reduction is proportional to the spreading factor since higher value results in higher reduction of the CE peak. Indeed, the maximum pulse position variation Δ_max should be:

$$\Delta\_max \leq (T-d) \tag{3.10}$$

3.1.3. Random Duty Cycle Modulation

Unlike RFM and RPPM, in RDM the pulse width is made random**.** RDM is less common compared to RFM and RPPM since duty cycle is being used for many closed loops control of converters. Besides varying the duty cycle will result in output voltage ripples in time domain.

The same as the other two random modulation techniques, the instantaneous duty cycle can be determined as:

$$d(t) = d_{ref} + \Delta d \times \xi(t) \tag{3.11}$$

where d(t) is the instantaneous duty cycle and Δd is the amount of pulse width varied from the reference pulse width, d_{ref}.

The spreading factor α can be defined as

$$\alpha = \frac{\Delta d}{d_{ref}} \tag{3.12}$$

The following sub-sections summarize both the simulation and experimental test campaign to test the effectiveness and possible constraints of the different RPWM schemes.

3.2. PSpice-Simulink Co-Simulation of the CEs of a DC-DC Converter with RPWM

This work investigates the beneficial effects of RPWM strategies in reducing the CE's generated by DC-DC converters. Most of the research related to EMC analysis of switched power supplies are based on converters made up of IGBTS and Si MOSFETs, whereas a little has been done so far to investigate the emissions generated by SiC-technology converters, which are relatively new and still under development. In this part, a simulation tool to investigate spectral characteristics of the CE's of a SiC based DC-DC converter driven by a RPWM Modulation scheme is presented. The comparison versus traditional PWM is carried out by exploiting PSpice-Simulink co-simulation. PSpice is preferable to model a converter, since it allows performing realistic simulations based on actual specification and datasheet of components like SiC MOSFETs, diodes, inductors, and capacitors. However, MATLAB Simulink can be conveniently used to generate RPWM signals and of course for signal visualization.

3.2.1. Circuit implementation in PSpice

The setup modelled and implemented in PSpice is shown in Figure 3.6. It is composed of a battery (leftmost block), a DC-DC converter (rightmost block) and two LISNs. The corresponding circuit models implemented in PSpice are shown in Figure 3.7 and Figure 3.8 and will be presented in the following sub-sections.

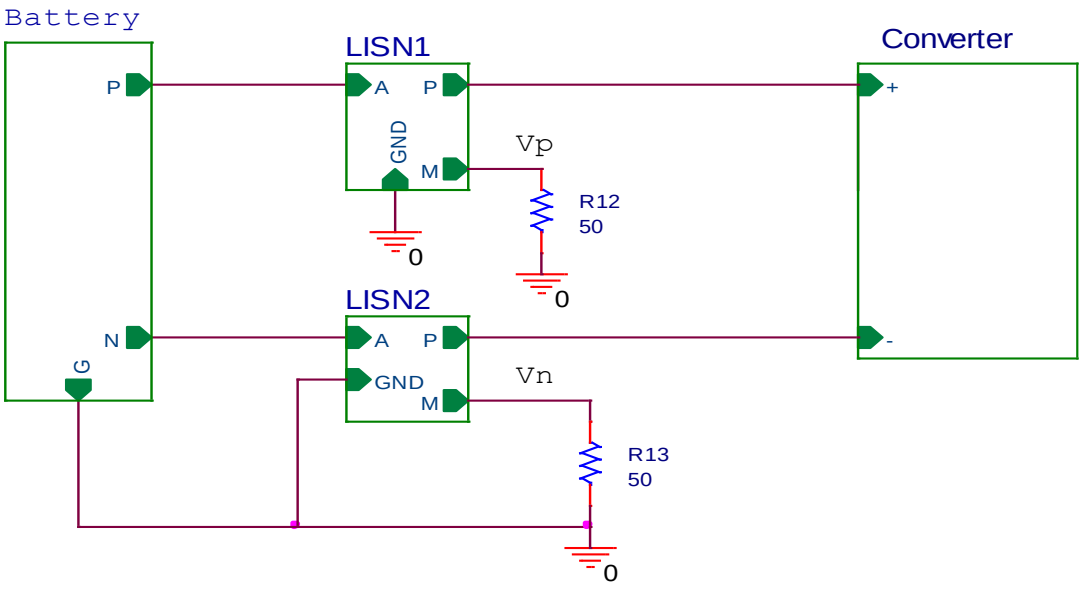

Figure 3.6: Overall schematic of the test setup implemented in PSpice. In this representation, the DC-DC converter, the battery, and the two LISNs are represented by blocks, whose circuit representation is shown in Figure 3.7, Figure 3.8 and Figure. 2.21

3.2.1.1. Converter Model

The circuit model of the 20-kW boost converter considered for simulation is shown in Figure. 3.7. The converter boosts the input voltage from 400 V to 800 V and has a switching frequency of 35 kHz. SiC MOSFETs are used in this converter design. The second-generation CREE SiC MOSFET, C2M0040120D was chosen from the Wolfspeed manufacturer spice library and integrated into the PSpice software library.

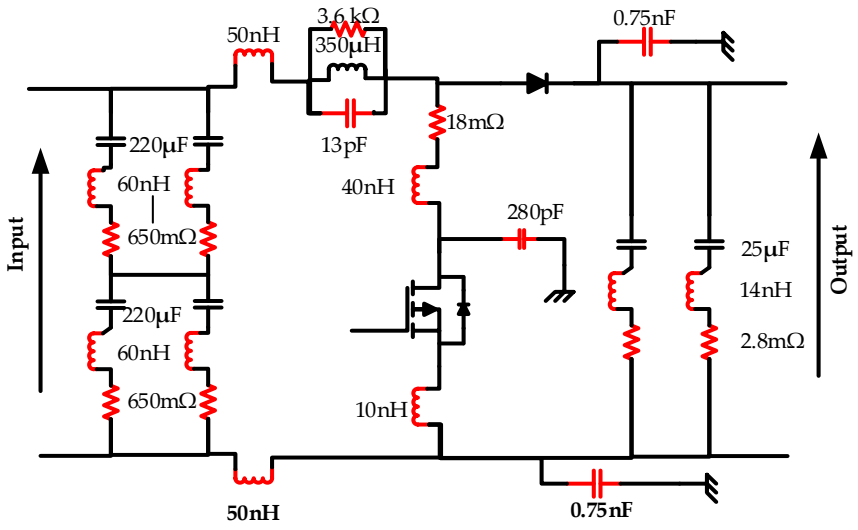

Figure 3.7: PSpice model of the DC-DC converter under analysis: wideband model including parasitic elements.

To make the simulation more realistic, the thermal operation of the SiC MOSFETs are also considered. To this end, the case and junction temperatures are assumed to be equal to 40°C and 150°C, respectively. Besides, parasitic components (e.g., parasitic capacitors and wiring resistance and inductance), whose presence is of key importance in order to perform effective prediction of the converter CEs in the frequency interval of interest for EMC analyses, are included and drawn by the

red color. Values for the equivalent series resistance and inductance of capacitors, the leakage inductance and insulation resistances are taken from the component datasheet. Conversely, for the other parasitic elements, some assumptions are taken, and reasonable values of these components are inferred from [55].

3.2.1.2. Circuit Model of the Battery

Figure 3.8. shows the circuit model of the battery. Likewise in Figure 3.7, parasitic elements are sketched by the red color and are used to represent the high-frequency behavior of the battery. In this model, V_{dc} represented the DC voltage source. The specific topology and numeric values of the red elements are inferred from [49].

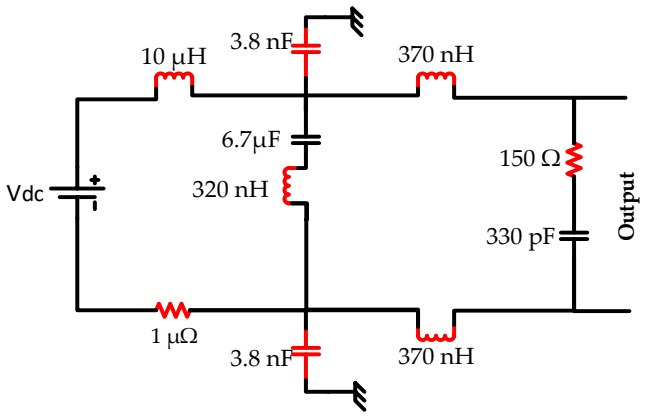

Figure 3.8: PSpice model of the DC battery.

3.2.1.3. Circuit model of the LISN

The LISN topology exploited for simulation is designed based on CISPR16-1-2 standard as shown in Figure 2.21 (see Chapter 2).

3.2.2. PSpice-Simulink Co-Simulation

3.2.2.1. The basic principle of the implemented RPWM scheme

The schematics of the implemented RFM is shown in Figure 3.9. The central switching frequency is multiplied by the spreading factor to get the deviation frequency. The resulting frequency deviation is multiplied by the random number which varies between -1 and 1 and can be different wave form as described in Section 3.1.1 to get the randomized switching frequency. The randomized switching frequency is then converted to PWM signal or RFM by using MATLAB code as specified in **Appendix A2**.

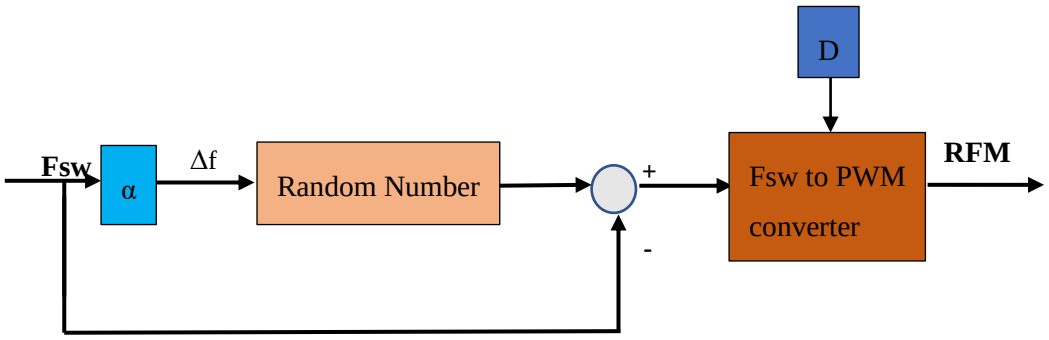

Figure 3.9: Schematics of the implementation of RFM.

Figure 3.10 shows the schematics of the implemented RPPM. The process is the same as RFM except in this case the pulse position is controlled. Hence, the reference pulse position is multiplied by the spreading factor to get the deviation of pulse position. The resulting pulse position deviation is multiplied by the random number which varies between -1 and 1 and can be different wave form as described in Section 3.1.2 to make the pulse position random. Then the randomized pulse position is converted to PWM signal or RPPM using MATLAB code as specified in Appendix A2. As can be seen, both the switching frequency and duty cycle are fixed.

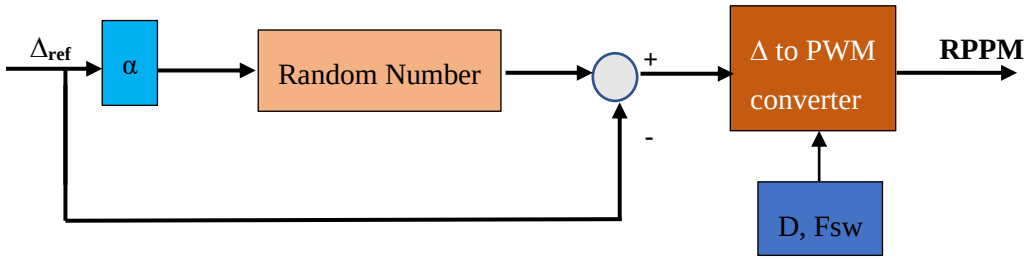

Figure 3.10: Schematics of the implementation of RPM.

The implementation of RDM is the same as RFM and RPPM except the control parameter is here the duty cycle as shown in Figure 3.11.

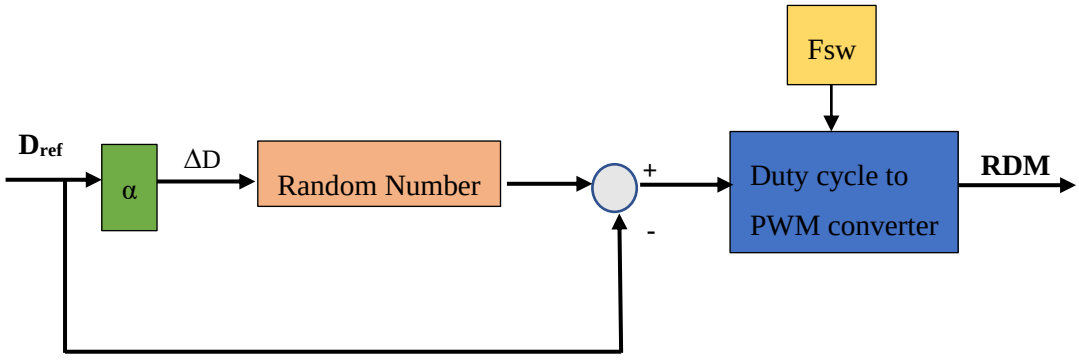

Figure 3.11: Schematics of the implementation of RDM.

3.2.2.2. System Co-simulation

The Simulink schematic implemented to simulate RPWM is shown in Figure 3.12 (the schematic implementing standard PWM is here omitted for brevity). In this configuration, the randomly generated PWM signal is connected to the input of the PSpice system and applied to the DC-DC converter. The top two pins/arrows at the output of the "PSpice system" block (represent all the circuit models deign ed in PSpice such as the DC-DC converter, the battery and the LISN) in Figure 3.12 is used to measure the phase and neutral noise voltages across the 50 Ω LISN resistors. Starting from these quantities, differential mode (DM) and common mode (CM) noise voltages can be directly estimated by exploiting mathematical blocks available in Simulink (see block at the bottom of Figure 3.12).

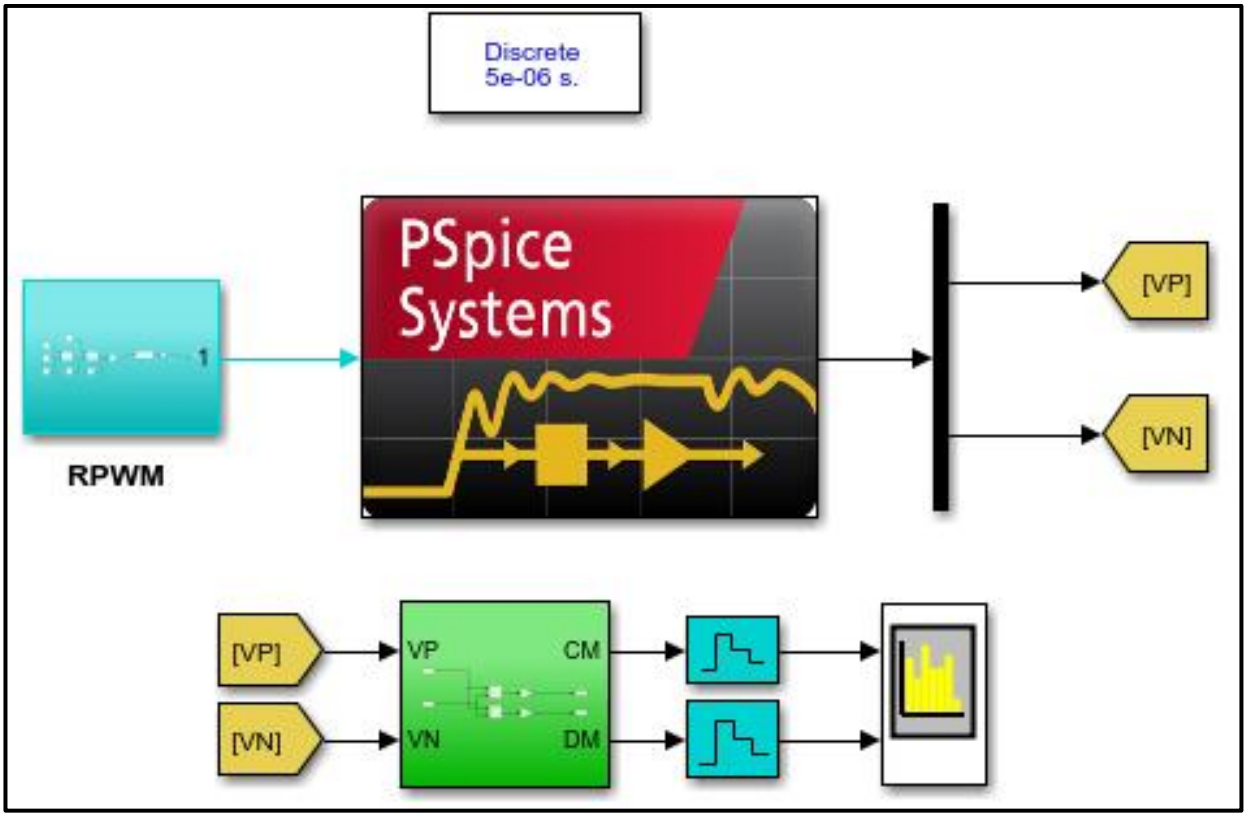

Figure 3.12: Simulink schematic for co-simulation. The "PSpice System" block calls the PSpice circuit model in Figure 3.6.

3.2.3. Simulation Results and Discussions

Examples of the obtained results are discussed in the following sections considering all the three types of RPWM schemes. Besides, the effects of spreading factor and RUNUR is examined. Finally, a comparison among the different RPWM schemes is performed.

3.2.3.1 Simulation of the CEs of the DC-DC converter under RFM

Figure 3.13 (a) presents the comparison of the phase to ground voltage measured at the LISNs 50 Ω terminal when the DC-DC converter is resorted to RFM and conventional PWM. The switching frequency is chosen arbitrary to 20 kHz. The spreading factor ('α') is fixed to 30% so that the switching frequency deviates from 14 kHz to 26 kHz. Moreover, the modulation profile chosen is random PAM modulation. As can be seen clearly, the CE measured with RFM (orange) shows significant reduction compared to the conventional PWM (in black and in this case α= 0%) by more than 15 dB.

To see the effects of the spreading factor of the RFM on the CE of the DC-DC converter, additional simulation was carried out. Therefore, two values of the spreading factor (5% and 30%) are considered, and the CE is investigated again. As depicted in Figure 3.13 (b) the CE coming out of the DC-DC converter did not show significant variation in terms of peak reduction. However, in the case of the 30% spreading factor, the CE was more continuous and spread than the 5% spreading factor. In practice, lower value of spreading factor (below 5 %) is usually preferable in many applications since higher value of α causes ripples in the time domain wave forms.

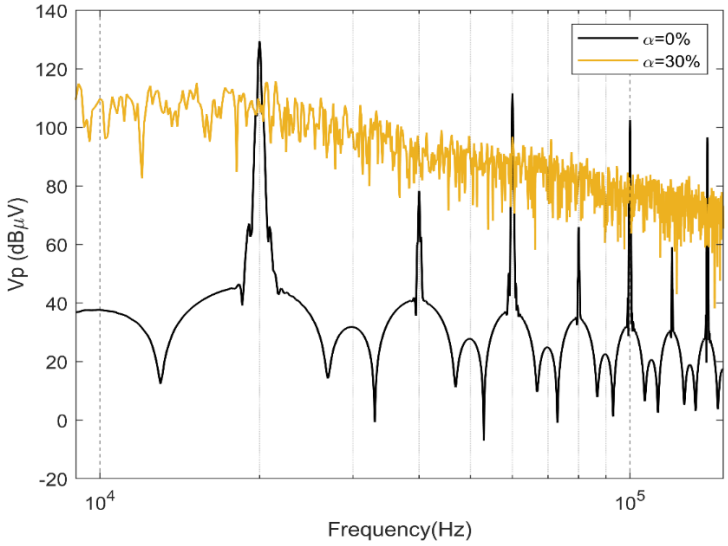

(a)

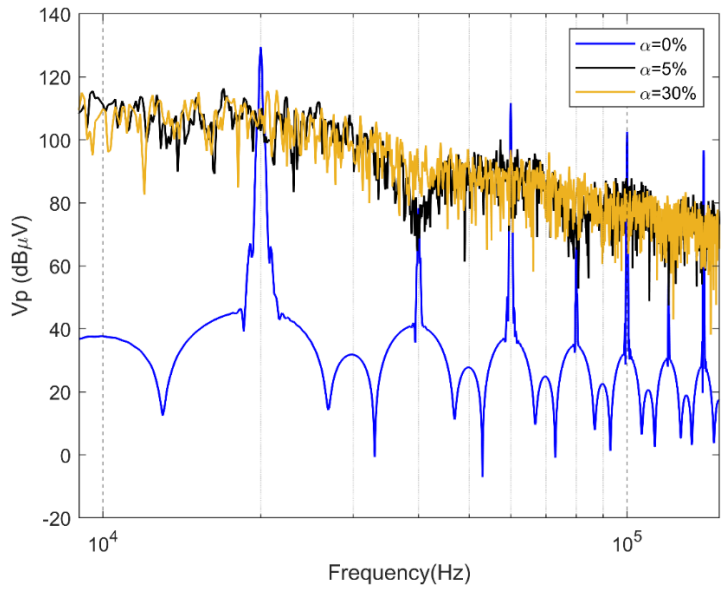

(b)

Figure 3.13: Simulation result of the CEs of the DC-DC converter: (a) PWM Vs RFM, (b) under different values of the spreading factor of the RFM.

3.2.3.2. Simulation of the CEs of the DC-DC converter under RPPM

Another simulation activity carried out was to test the RPPM on the effectiveness of reducing the CE of the DC-DC converter. Figure 3.14 (a) presents the comparison of the phase to ground voltage measured at the 50 Ω LISN terminal of the DC-DC converter under RPPM w.r.t conventional PWM.

The switching frequency and the spreading factor are chosen to 20 kHz and 30% respectively. Again, random PAM modulation profile was chosen.

The CE measured with RPPM (orange) showed remarkable reduction (more than 10 dB attenuation) compared to the conventional PWM (black) starting from the 3rd harmonic frequency (60 kHz). However, the CE attenuation was only 4 dB at the fundamental frequency of 20 kHz. The attenuation at the fundamental frequency was even worse where lower values of spreading factor was chosen. This condition may have an advantage with regards to coexistence issues as it will be discussed in Chapter 3, where RPPM will be preferable to assure coexistence compared to RFM. Apart from the fundamental frequency, the CE showed significant reduction proportional to an increase in the spreading factor in terms of peak reduction as depicted in Figure 3.14 (b).

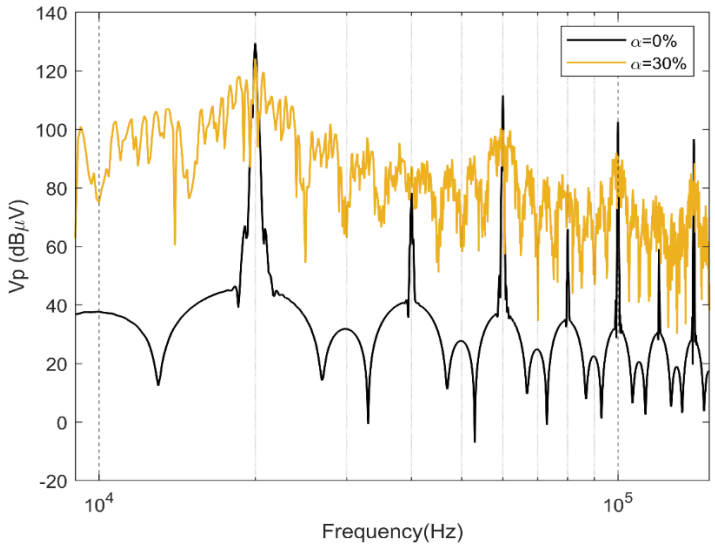

(a)

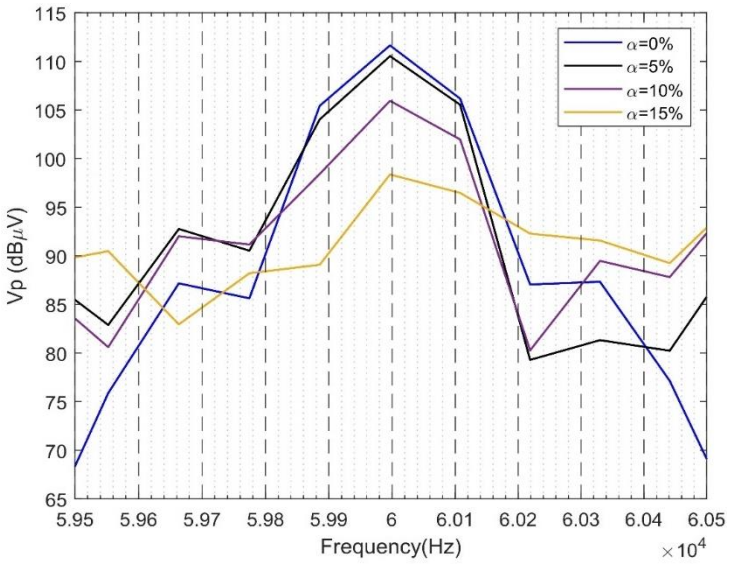

(b)

Figure 3.14: Simulation result of the CEs of the DC-DC converter: (a) PWM Vs RPPM, (b) under different values of the spreading factor of the RPPM.

3.2.3.3. Simulation of the CEs of the DC-DC converter under RDM

Figure 3.15 presents the comparison of the phase to ground voltage measured at the 50 Ω LISN terminal when the DC-DC converter was resorted to RDM/PWM. Again, the switching frequency was chosen to 20 kHz. In this case, the reference duty cycle is 0.5 and the spreading factor was fixed to 80% so that the duty cycle varies between 0.1 and 0.9. As can be seen clearly, the CE measured with RDM shows no significant reduction compared to the conventional PWM. This kind of RPWM is less effective in reducing CE. Besides, varying the duty cycle by this much amount could lead to too much output ripple voltage.

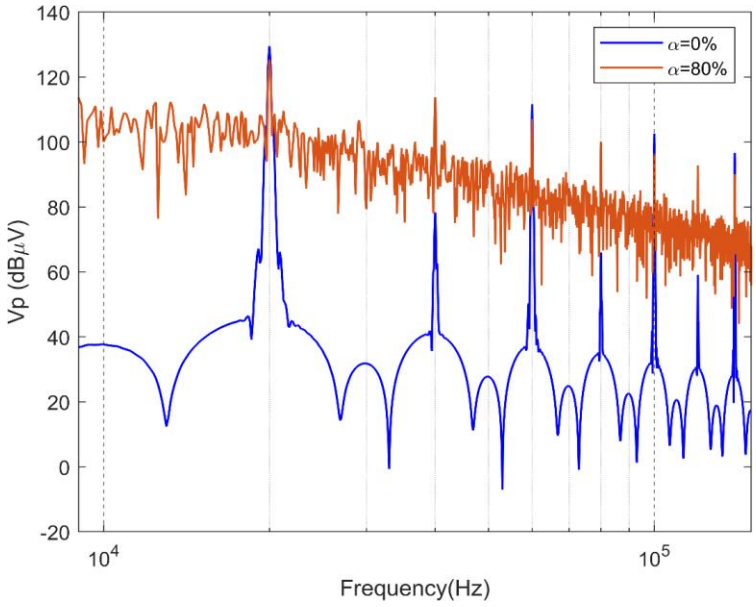

Figure 3.15: Simulation result of the CEs of the DC-DC converter under the RDM.

3.2.3.4. Simulation of the CEs of the three- phase inverter under RPWM

In order to examine the effectiveness of RPWM techniques on the CE reduction of the three-phase inverter, further simulations were carried out. In this case only the two types of RPWM techniques

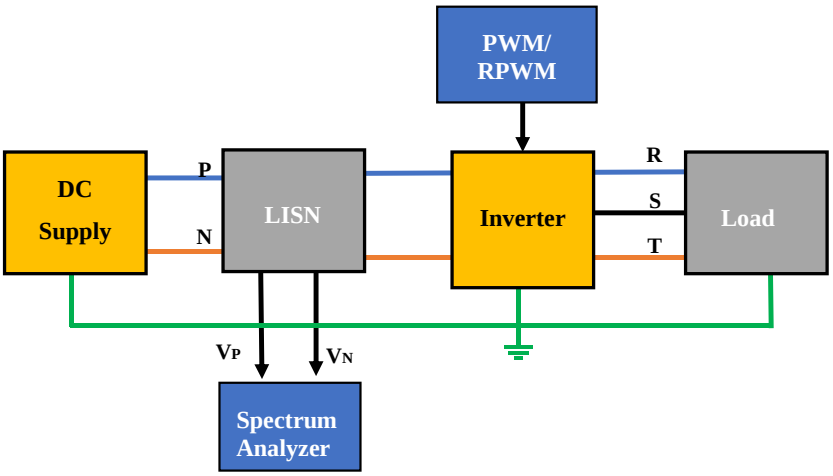

Figure 3.16: Schematics of the simulation setup for the CE measurement of the three-phase inverter at the DC side.

(RFM and RPPM) were considered. Details of the RPWM signal generation for three-phase inverter is available in the **Appendix A2**. The inverter is fed from 600 V dc source to get the required 400 V three-phase ac voltage. The CE is measured from DC side of the inverter as shown in Figure 3.16.

Figure 3.17 presents the CE's of the inverter measured at the DC side where different modulation were applied. Particularly, PWM, RFM and RPPM were considered. The switching frequency was chosen to 20 kHz. The spreading factor was fixed to 30% to the RPWM.

As for the DC-DC converter, the CE measured with RFM and RPPM showed significant reduction compared to the conventional PWM (Figure 3.18 (a) and Figure 3.18 (b)). Moreover, RFM outperforms RPPM in terms of the CE reduction. Further analyses were carried out to see the effects of spreading factor (the plot is not included here for brevity), and the same conclusion as of DC-DC converter can be reached where there was a significant influence of the spreading factor on the CE of the Inverter. Results also showed that, in case of RFM increasing spreading factor above a certain value (in this case above 15%) does not show appreciable difference on the CE peaks (the spreading of the

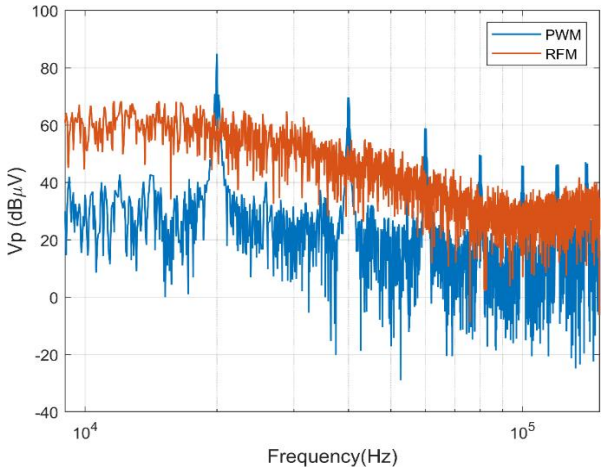

(a)

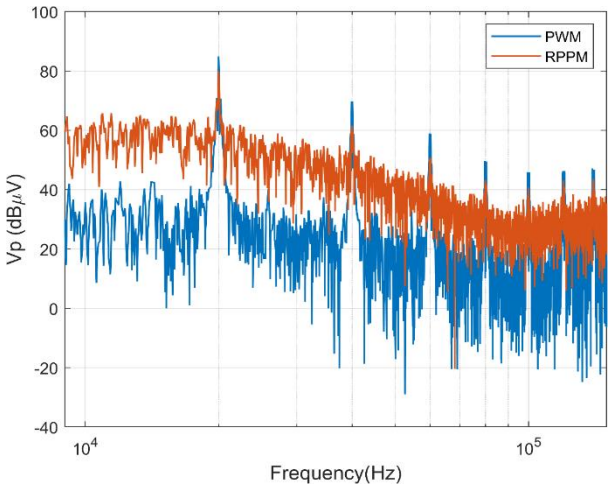

(b)

Figure 3.17: Simulation result of the CEs of the three-phase inverter at the DC side: (a) PWM Vs RFM, and (b) PWM Vs RPPM.

noise saturates at a certain level). Therefore, even a small variation of the switching frequency could give satisfying reduction of CE peaks.

3.3. Experimental Evaluation of the CE's of Randomly Modulated SiC based DC-DC Converter

The software simulation results needed to be verified using experimental analysis. To this end, an experimental test campaign was held to test the effectiveness of RPWM techniques in reducing the CE of the SiC based bi-directional DC-DC converter. Besides, the effects of different parameters of RPWM needs to be examined. With the final objectives of providing an overview of the implementation of different RPWM schemes using microcontrollers and the evaluation of the CE as well as studying the interaction of randomly modulated converters to the coexisting communications systems, a preliminary test was performed and presented as follows.

3.3.1. Experimental Test Setup

The schematic of the experimental test setup is shown in Figure 3.18 where the randomly modulated DC-DC converter is connected to the DC source through the LISN. The CEs of the DC-DC converter can be measured using the EMI receiver.

The implemented experimental test bench is presented in Figure 3.19. The specific converter chosen for this work was Cree's KIT-CRD-3DD065P/ CRD-3DD12P evaluation board from Wolfspeed (see Table 3.1). Different RPWM signals were generated using F28379D Launch Pad from Texas Instruments (TI). The RPWM signals can be coded using SIMULINK and can be loaded to the TI microcontroller (see Appendix A5). The CE's of the DC-DC converter were measured using CISPR 16 LISN (HV-AN 150 LISN) and DSOX1204G oscilloscope (KEYSIGHT). The DC-DC converter was configured as a boost converter where low input voltage (25 V) was considered for safety reasons and connected to 66 Ω resistive load.

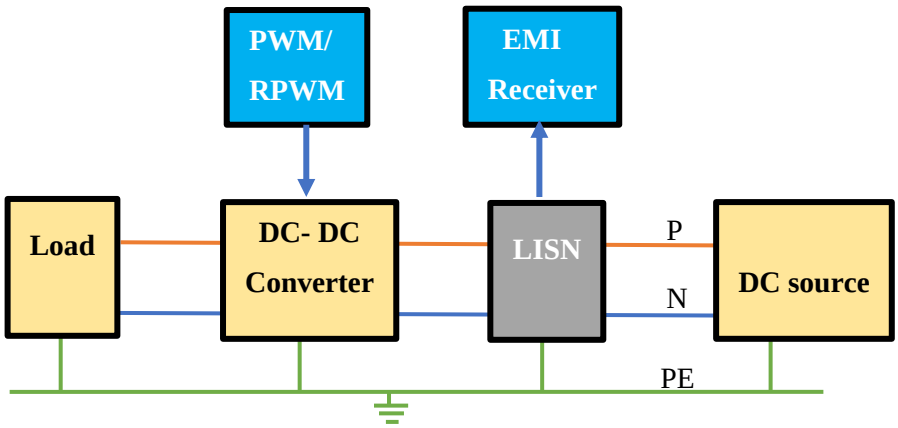

Figure 3.18: Schematics of the experimental test bench to assess the effects of RPWM on the CE's of the DC-DC converter.

Table 3.1: Summary of the specification of KIT-CRD-3DD065P/ CRD-3DD12P evaluation board.

Item	**Values**	
KIT VERSION	CRD-3DD065P (650V)	CRD-3DD12P (1200V)
Max Input Voltage	450	800V
Max Output Voltage	450	800V
Max Output Power	2500W	
VCC (Logic Power)	15VDC	
VCC Input Current (standby)	40mA	
Switching Frequency	100 kHz	

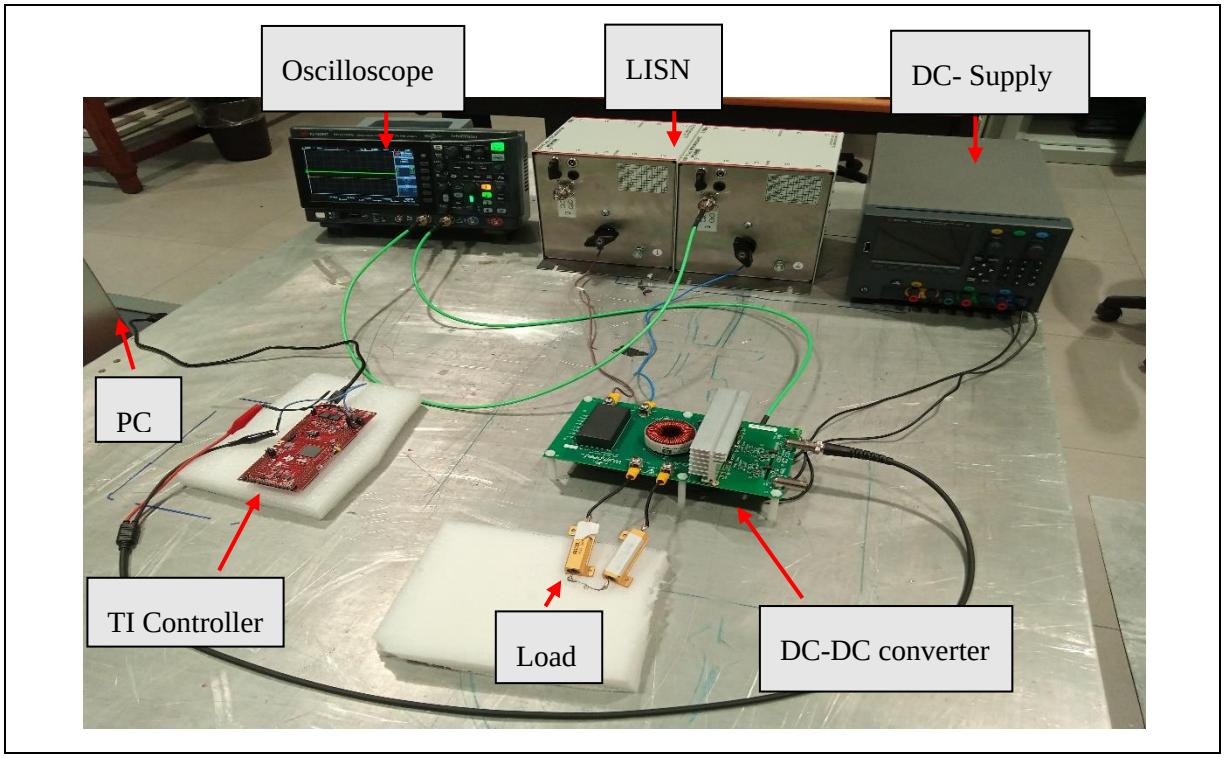

Figure 3.19: Experimental test setup to assess the effects of RPWM on the CEs of a SiC based bi-directional DC-DC converter.

3.3.2. Discussion of Experimental Findings

The first experimental activity in this test setup was to assess the effectiveness of the RFM in spreading the noise coming out of the DC-DC converter. Therefore, Figure 3.20 (a) presents the comparison of the phase to ground voltage measured at the HV-AN 150 LISNs 50 Ω terminal when the DC-DC converter is resorted to RFM and conventional PWM. The same switching frequency and spreading factor (20 kHz and 30% respectively) were considered as that of the simulation activities presented in Section 3.2.3. Experimental results confirmed that the CE measured with RFM shows significant reduction compared to the conventional PWM by more than 15 dB. Besides, the CE is more spread as the spreading factor was increased from 5 to 30 % which is in line with the conclusion reached during simulation (see Figure 3.20 (b)).

Another experimental activity was to examine RPPM. As depicted in Figure 3.21 (a), RPPM offers better attenuation of the CE peaks of the DC-DC converter compared to conventional PWM. Besides, Figure 3.21 (b) shows the dependance the CE's of the RPPM based DC-DC converter on the spreading factor where the same conclusion was reached during simulation activities.

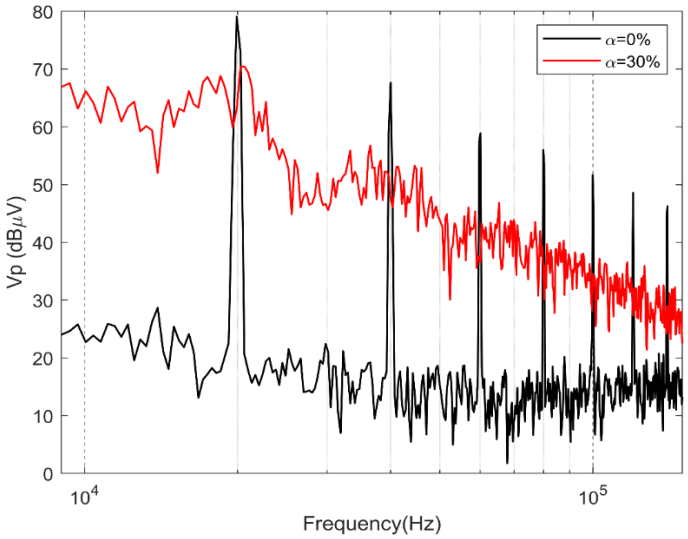

(a)

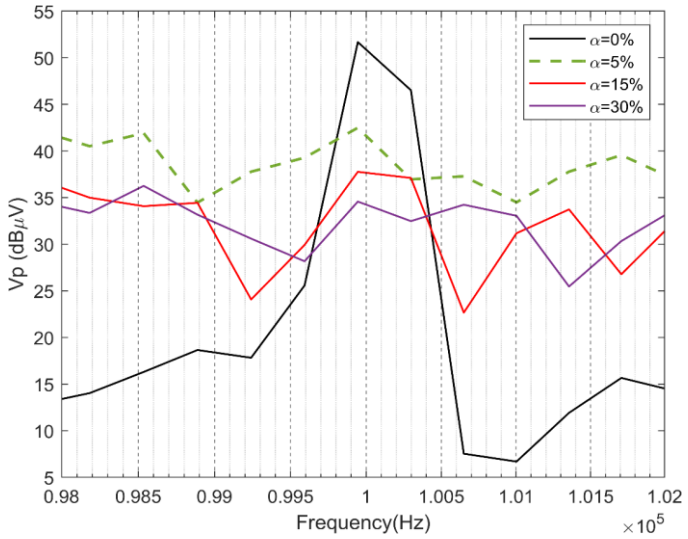

(b)

Figure 3.20: Experimental result of the CE's of the DC-DC converter: (a) PWM Vs RFM, and (b) under different values of the spreading factor of the RFM.

It is also very important to compare RFM and RPPM in terms of CE reduction. Figure 3.22 (a, b, c) shows the comparison of RFM and RPPM at the 5%,15% and 30% spreading factor. In all cases, RFM outperforms RPPM considering CE reduction. Of course, this comparison may not seem vital since the parameters which are controlled in both RWM techniques are different. However, it is possible to compare them considering maximum possible CE reduction of each RPWM techniques since RFM doesn't show variation in CE above 30% spreading factor and RPPM has a limitation of the maximum pulse position which is possible to vary as defined in (3.10). Therefore, it is possible to conclude that the noise coming out of the DC-DC converter in case of RFM was more spread than RPPM. This may have a negative impact on the coexistence issues which will be outlined in the next chapter of this thesis.

Apart from the CE reduction, RFM is easier to implement than RPPM. This is true in both software simulation and experimental test setups. However, the latter provides fixed switching frequency and

can be used in applications where switching frequency is a priority. Besides, the additional consideration in choosing the right modulation scheme is coexistence issue.

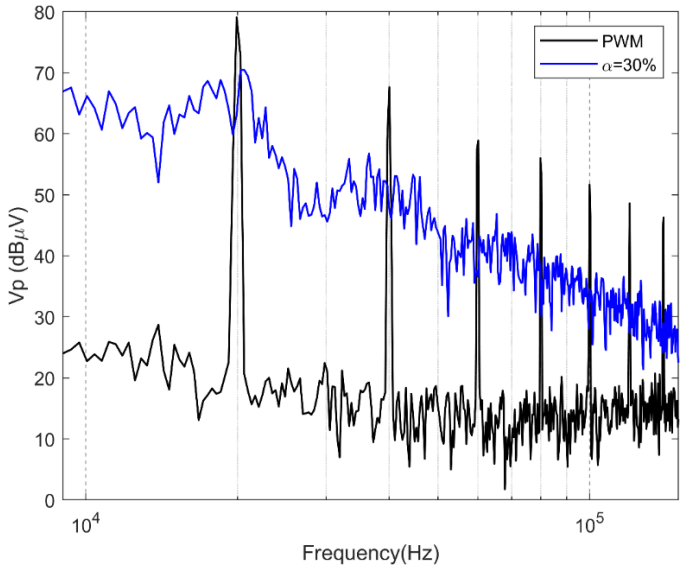

(a)

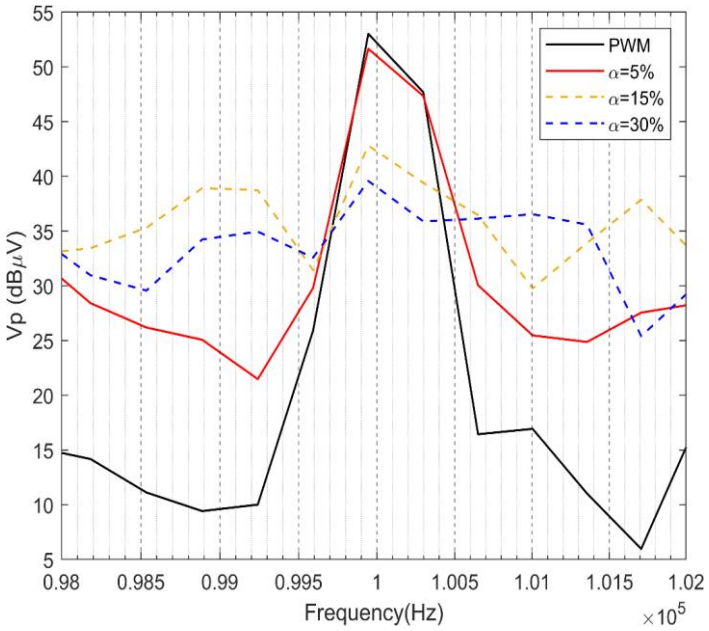

(b)

Figure 3.21: Experimental result of the CE's of the DC-DC converter: (a) PWM Vs RPM, and (b) under different values of the spreading factor of the RPPM.

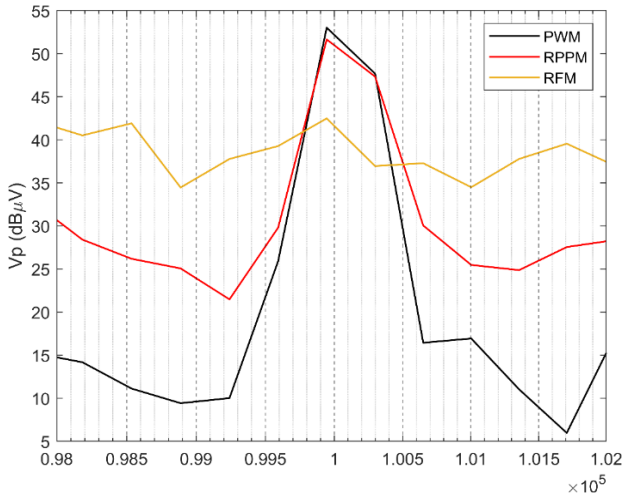

(a)

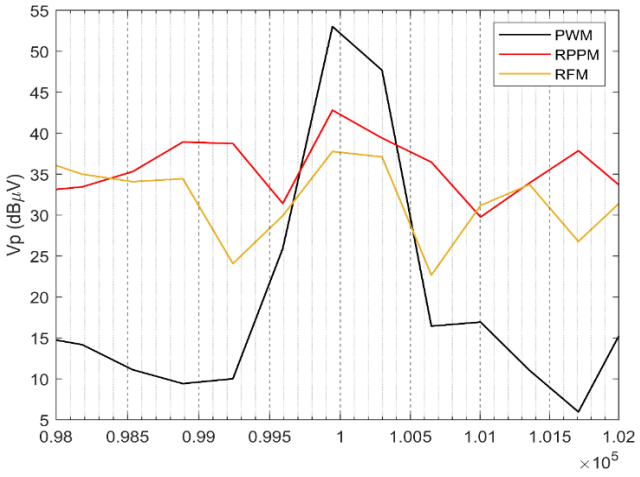

(b)

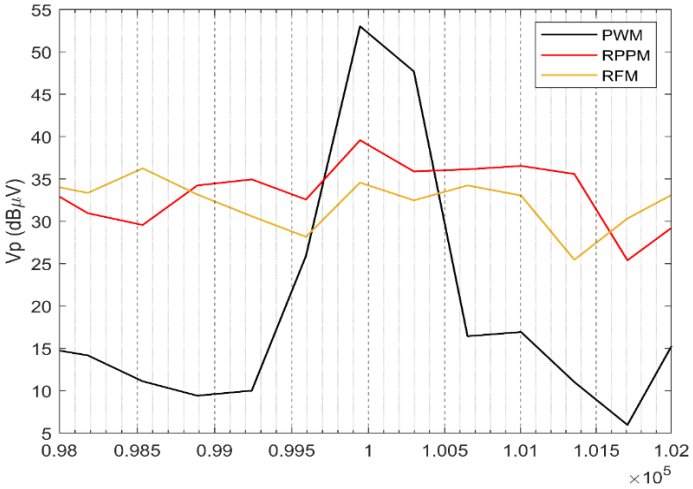

(c)

Figure 3.22: Experimental result of the CE's of the DC-DC converter where RFM and RPPM are compared with PWM at the spreading factor of : (a) 5%, (b) 15% and (c) 30%.

3.4. Conclusion

In this chapter, the most common RPWM techniques which are being deployed to reduce the CE's of many converter topologies are discussed. The chapter summarized the details of the implementation of different RPWM techniques both in simulation software and practical experiments as well as the comparison of those RPWM techniques in terms of CE reduction. Besides, the main parameter which affects the effectiveness of the specific RPWM techniques mainly the effects of the spreading factor on the reduction of the CE of power converters is discussed. Firstly, a simulation activity using PSpice-Simulink co-simulation was carried out aiming at comparing the CE's of SiC based DC-DC converter and Inverter under different modulation schemes. The obtained results proved the effectiveness of RPWM techniques in spreading conducted noise spectra, thus leading to an overall reduction of the CE peaks obtained by standard PWM schemes. Indeed, more than 15 dB CE reduction was obtained by resorting to RPWM. Results also showed that RFM outperforms RPPM and RDM in terms of CE reduction. In fact, RFM is the most common and the easiest one compared to the other RPWM techniques. Besides, the simulation result confirmed that the spreading factor in all RPWM techniques plays a significant role in their effectiveness of CE reduction, i.e., higher value of spreading factor results more spread noise and better CE attenuation. Also, this chapter has presented the advantages of PSpice-Simulink co-simulation, which despite not be a multiphysical simulation, it means that the reliability of results is not enough to consider all the possible circuit's parasitics couplings, is proven to be a suitable tool. Indeed, the features available in Simulink allow us to easily implement a whatever control scheme, and the PSpice allows accurate modelling of the converter as well as the inclusion of realistic models of the involved circuit component. In this regard, it is worth mentioning here that the same simulations carried out by neglecting parasitics in the converter, would have led to inconsistent results, since the non-ideal behavior of components significantly determines the generated noise in the CE frequency range.

The simulation results were confirmed by laboratory experiments where different RPWM signals were generated by using F28379D microcontroller and applied to KIT-CRD-3DD065P SiC based bidirectional DC-DC converter. Indeed, the experimental results were in line with the simulation results in such a way that the advantages of using RPWM on reducing the CEs of the DC-DC converter were clearly outlined. Besides, experimental results also showed the positive effect of the spreading factor in spreading the CE of the DC-DC converter, which is indeed a nightmare to the coexistence issues associated with coexisting communication systems as it will be discussed in the coming chapter.

CHAPTER 4

Electromagnetic Coexistence Issues in PLC Systems

4.1. EM coexistence issues in PLC systems

PLC technology requires further investigation to solve possible coexistence issues. The presence of power electronics converters in the AC mains represents a source of high frequency conducted noise, which may cause coexistence issues with the PLC signal. Besides, there is urgent need to study the interference between randomly modulated converters and PLC systems since the spreading of the noise spectrum resulting from random modulation may cause problems with the communication system. In fact, enough research has not been conducted in this area. Undoubtedly, random modulation offers the benefit of reducing the CEs by spreading the noise spectrum in the frequency range of interest. However, this may cause an increase in transmission errors and the random modulated EMI can have detrimental effects over a wider bandwidth.

The following section covers the research activity towards studying the effects of randomly modulated power converter on the coexisting communication system mainly PLC systems. The research work aimed to provide both simulation and laboratory activities towards this goal. Therefore, Section 4.2 discusses the simulation campaign to model and study the interference between randomly modulated power converter and PLC systems in SG applications. Section 4.3 summarizes the laboratory test result of the cross interference between randomly modulated DC-DC converter and G3-PLC system.

4.2. Simulation of the EMI of Power Converter with Random Modulation on the PLC System

It was discussed in Chapter 3 that RPWM allows controlling the switching signal of power converters to reduce the harmonic peaks by spreading the noise spectrum. However, when the converters coexist with PLC systems, such as in Smart Grid (SG) applications, resorting to RPWM needs further investigations since it potentially affects the communication channel by increasing the bit error rate. In contrast, enough research has not been conducted on the effects of power converter modulation schemes on PLC systems. Undoubtedly, random modulation offers the benefit of reducing the CEs by spreading the noise spectrum in the frequency range of interest. However, this may cause an increase in transmission errors and the random modulated EMI can have detrimental effects over a wider bandwidth.

In [57], the model of PLC system for SG application is presented. The main objective in [57] is to model a PLC system for smart metering application using SIMULINK. However, a systematic analysis of the interference between the communication system and the noise exiting the power converters with different modulation schemes is not addressed. In fact, in that paper, only PWM modulation is considered for power converters. In [58], it is proven that applying RPWM on an AC/DC converter causes more signal errors or delays in the PLC system compared to conventional PWM. Contrary to this, in [59], it is presented that resorting to RPWM modulation allows improving transmission performance.

In [60], the effects of power converter modulation scheme on low frequency digital communication systems were studied, and it was proven that RPWM does not have significant effect on digital communication systems. Recently, in [61], the influence of a random modulated SiC-based buck converter on the G3-PLC channel performance is presented, where it was shown that the use of RPWM reduces the channel capacity compared to conventional PWM. However, in that work, only a specific random modulation technique was implemented (i.e., random frequency modulation), and other strategies (such as the random pulse position modulation considered in this work) were not considered. Therefore, further investigations are still needed to investigate the advantages/disadvantages of different RPWM in power grids involving PLC systems. Besides, simulation models combining accurate modeling of both the power and communication parts of the systems still need to be developed. Indeed, although several models of each separate part of the system are already available, there is a lack of simulation models in which both the power system and the communication system are modeled as a whole.

Therefore, this work is intended to investigate the effects of power converter modulation schemes on PLC system, to understand the conditions under which RPWM can be considered as an effective alternative to conventional modulation schemes using software tools. To this end, the PLC system is implemented for AMR application in SG, that is to measure the load voltage remotely. The proposed model combines accurate models of both the power part and communication part of the PLC system using simulation tools. Particularly, SIMULINK is used to implement the PLC modem and the power circuit, including the RPWM scheme. Furthermore, this work also investigates the detrimental effects that unsymmetrical AC wires play on the PLC system.

4.2.1. Description of the System under Analysis

Figure 4.1 shows the principal diagram of the system under analysis, which is divided into two parts: the power part, i.e., the AC system which is used to deliver power, and communication part, i.e., the system which enables data communication through the power line. The power part of the system represents a grid connected PV based renewable energy system and composed of Photovoltaics (PV)/battery, boost converter, an inverter, three phase transmission line, and AC grid. The boost converter boosts the battery/PV voltage to the desired DC link voltage of the inverter. The output of the inverter is connected to the AC grid through a three-phase transmission line. The three-phase load is fed from the PV and the grid simultaneously [57].

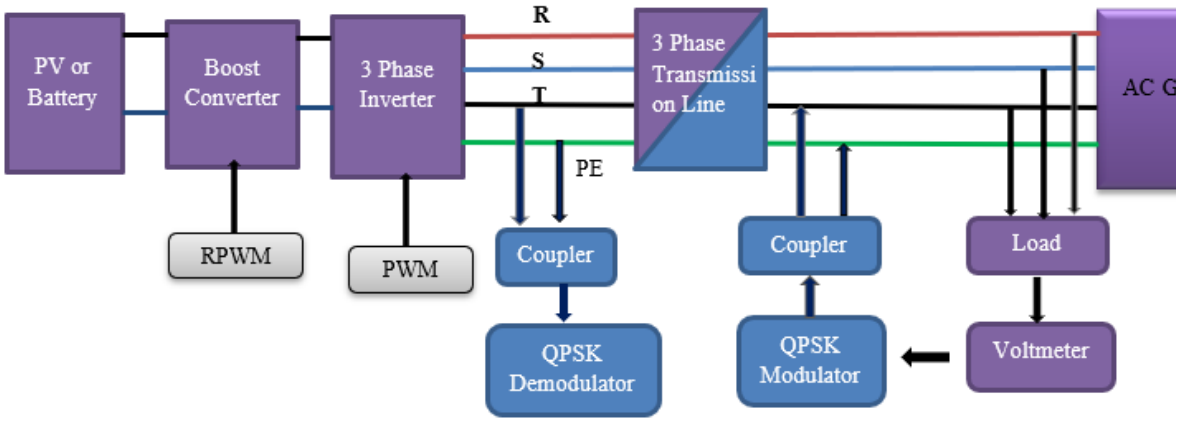

Figure 4.1: Block diagram of the PLC system under analysis.

The measured load voltage (in this case, the communication signal) is transmitted to the inverter side by using PLC. To this end, the communication signal is modulated by QPSK modulation and coupled to the AC system using RC couplers and demodulated by the QPSK demodulator connected at the inverter output. In addition to this, RPWM is implemented and applied to the DC-DC converter, whereas conventional PWM is applied to the inverter in order to analyze only the effects of Random Modulated DC-DC converter on the PLC system.

4.2.2. Simulation Implementation

MATLAB SIMULINK is used to implement the overall system, as shown in Figure 4.2. The top box represents the power part (Section 4.2.2.1), the bottom represents the communication system (central box), and the control part, i.e., RPWM generator for the DC-DC converter (bottom-left box) and PWM generators for the inverter (bottom-right box). A detailed description of these models will be provided in the following sections.

4.2.2.1. Circuit Model of the AC system

This subsection provides a detailed description of the circuit models adopted to implement the power part of the system under analysis. The PV panel is represented by an equivalent battery source. Besides, the same circuit discussed in Chapter 3 was used in this part to represent the battery, DC-DC converter, and the inverter while considering parasitic elements. The inverter output is synchronized with the AC grid by using a Phase-locked loop (PLL) circuit. The PLL determines the frequency of the AC grid, and this frequency is used to generate the sinusoidal PWM signals for the inverter so that both the inverter and the grid are kept synchronized.

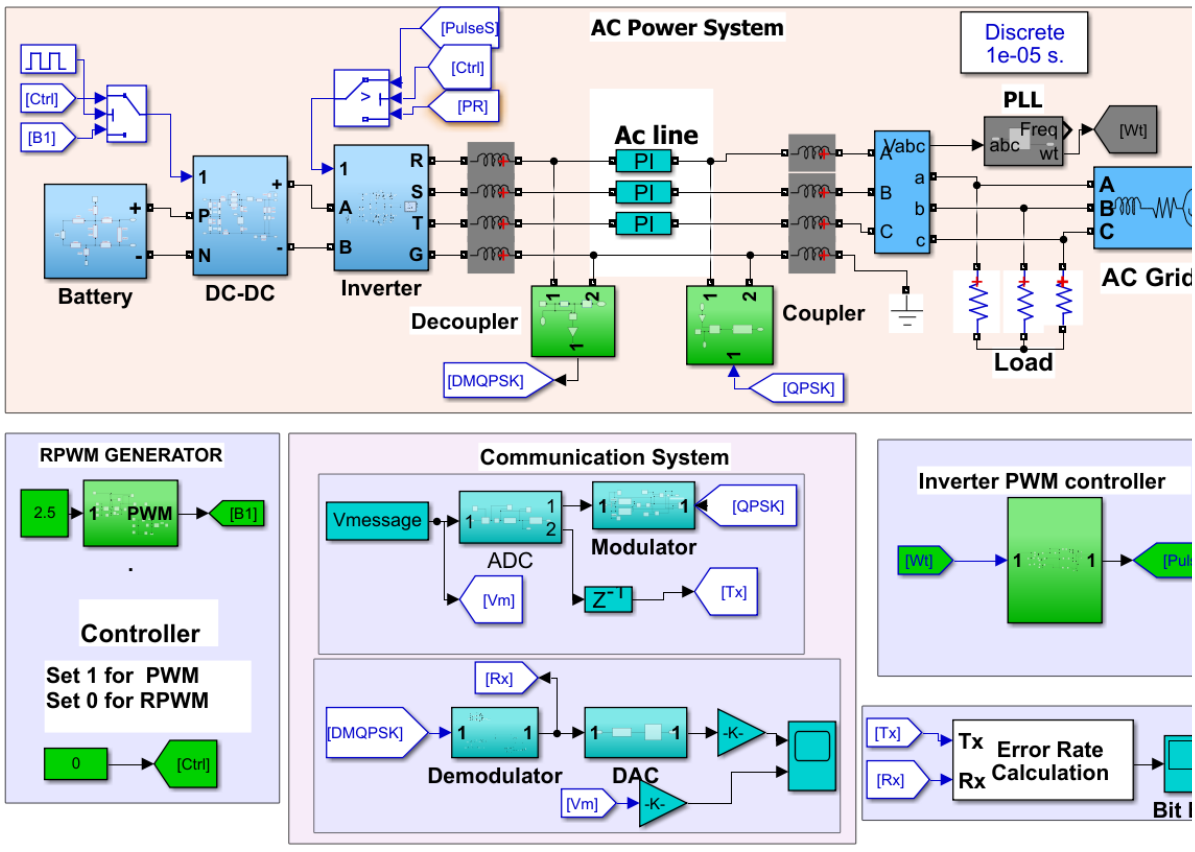

Figure 4.2: SIMULINK schematics of the PLC system under analysis.

A short transmission line model is adopted to represent the AC line. The length of this line is assumed as 100 m, and the frequency of interest is 250 kHz (up to 10th order harmonics of the DC-DC converter). Therefore, the three-phase transmission line is approximated by lumped element model considering only the per-unit resistance, inductance, and capacitance of a four-conductor copper wire, each with size of 4 mm2 [62]. The specific RPWM scheme considered in this work is RPPM.

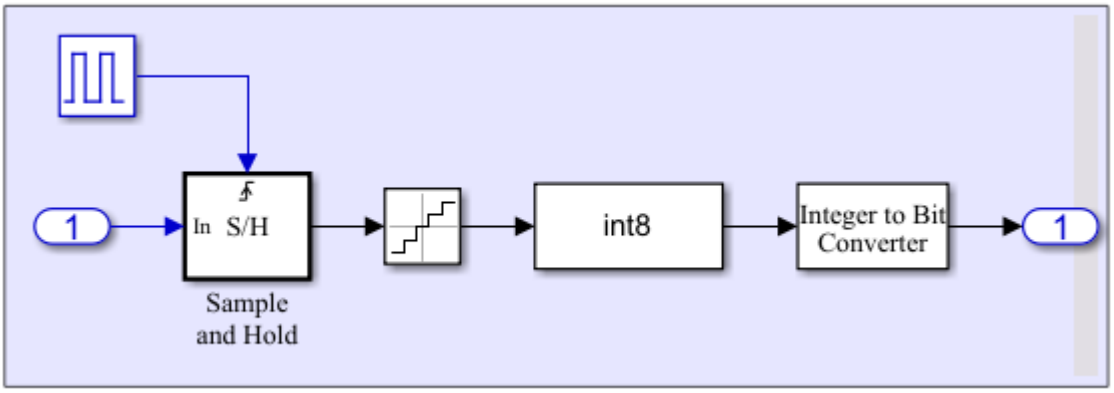

Figure 4.3: SIMULINK implementation of the analog to digital converter.

4.2.2.2. Implementation of the Communication System

Key ingredients of the communication systems are:

1. analog-to-digital conversion (ADC) of the load voltage,
2. modulation of the digital signal,
3. coupling/decoupling, and
4. demodulation

A detailed description of the implementation of the above features is provided in the next paragraphs.

4.2.2.2.1. Analog-to-Digital Conversion

The first step is to measure the load voltage (rms), scale it down to a suitable value and convert the resulting analog signal into an equivalent digital signal. The ADC is implemented first by sampling the analog signal with sampling frequency of 50 kHz. After that, the sampled signal is quantized with the quantization level of 0.4 V. The quantized signal is converted or approximated to the nearest integer value and converted to bits by using the integer to bit converter block available in SIMULINK, as shown in Figure 4.3.

4.2.2.2.2. Signal Modulation

The digital signal is then modulated by using QPSK modulator. Two sinusoidal carrier waves in quadrature to each other are used for implementing QPSK. The carriers have a frequency of 5 kHz and have phase difference of 90 degrees. The bits from the ADC are split into odd and even bits and converted from unipolar to bipolar. Then, even bits are multiplied with the in-phase carrier (cosine), and odd bits are multiplied with the quadrature carrier (sine), thus leading to two independent Phase Shift Key (PSK) modulated signals. The two PSK signals are added to obtain the QPSK modulated signal. The overall process of QPSK modulation is implemented in SIMULINK by the schematics shown in Figure 4.4.

4.4.2.2.3. Coupling/Decoupling with the AC Mains

In order to couple the modulated signals through the AC mains, the capacitive coupling/decoupling circuit topology shown in Figure 4.5 are used.

4.4.2.2.4. Signal Demodulation

To recover the modulated signal, the signal received from the decoupling circuit, which inherently includes also high frequency noise exiting the converters, is multiplied by the in-phase and in-quadrature carrier waves. This results in the separation of the PSK waves. Each wave passes through an integrator and low pass filter in order to avoid the high frequency components and then compared in the comparator to retrieve the odd and even bits. The obtained bits are then converted into integer numbers. Figure 4.6 shows the demodulation circuit implemented in SIMULINK.

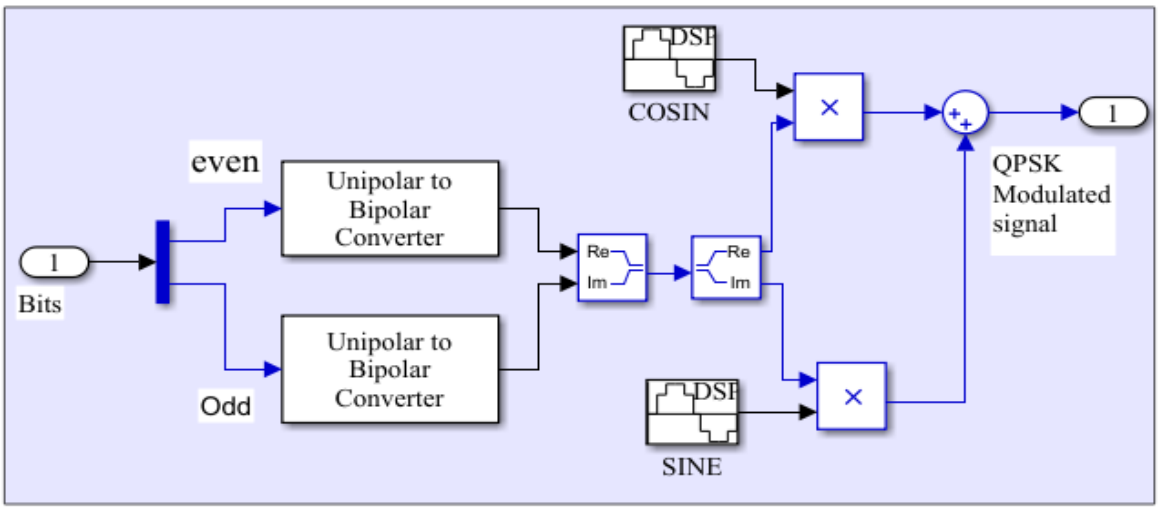

Figure 4.4: QPSK modulator circuit implemented in SIMULINK.

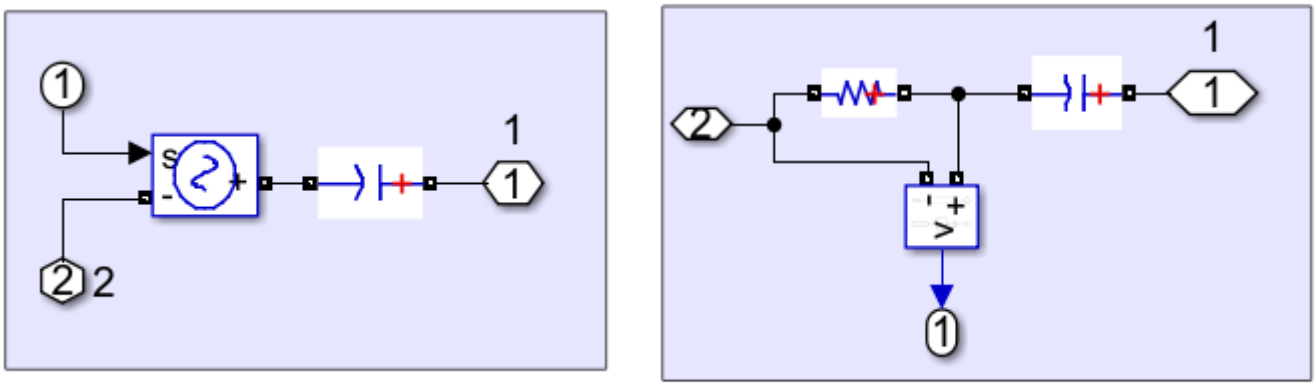

(a) (b)

Figure 4.5: Capacitive (a) coupling and (b) decoupling networks implemented in SIMULINK.

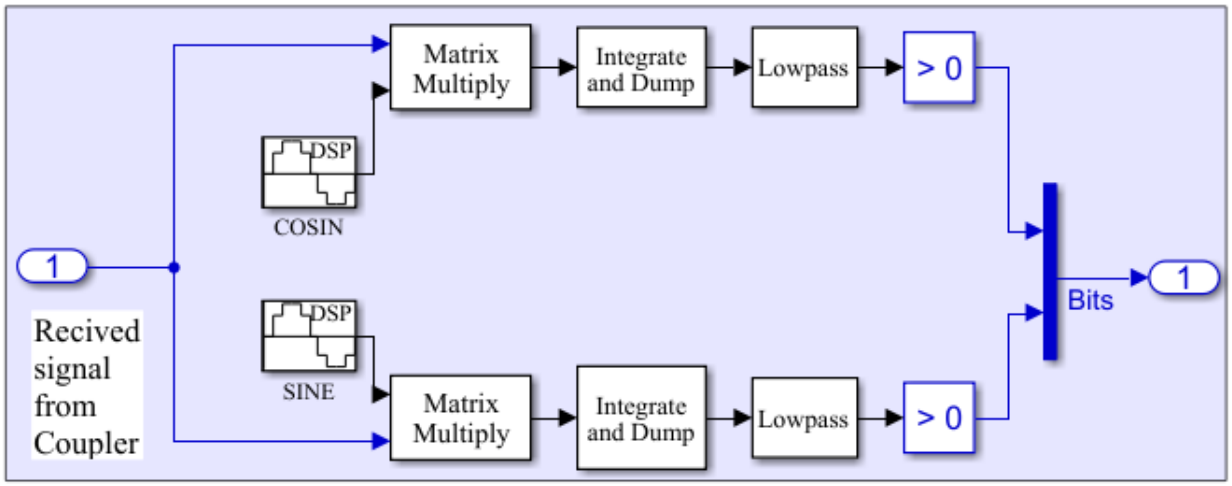

Figure 4.6: SIMULINK implementation of the QPSK demodulator.

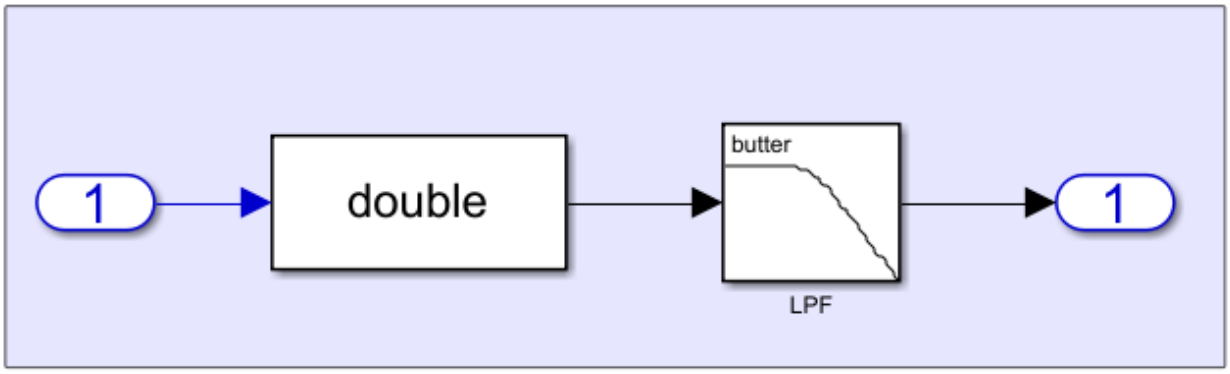

Figure 4.7: SIMULINK implementation of the digital-to-analog converter.

4.2.2.2.5. Digital-to-Analog Conversion

Eventually, the demodulated signal is converted into the corresponding analog signal, to allow the comparison with the original one. To this end, an analog filter with cutoff frequency 100 Hz is used for digital-to-analog conversion, as shown in Figure 4.7. Figure 4.8 shows the even (brown) and odd (black) bits obtained from the message signal and the resulting QPSK modulated signal (blue). As can clearly be seen, the QPSK modulated signal has four phase shifts according to the input bit combinations, as expected from QPSK modulator.

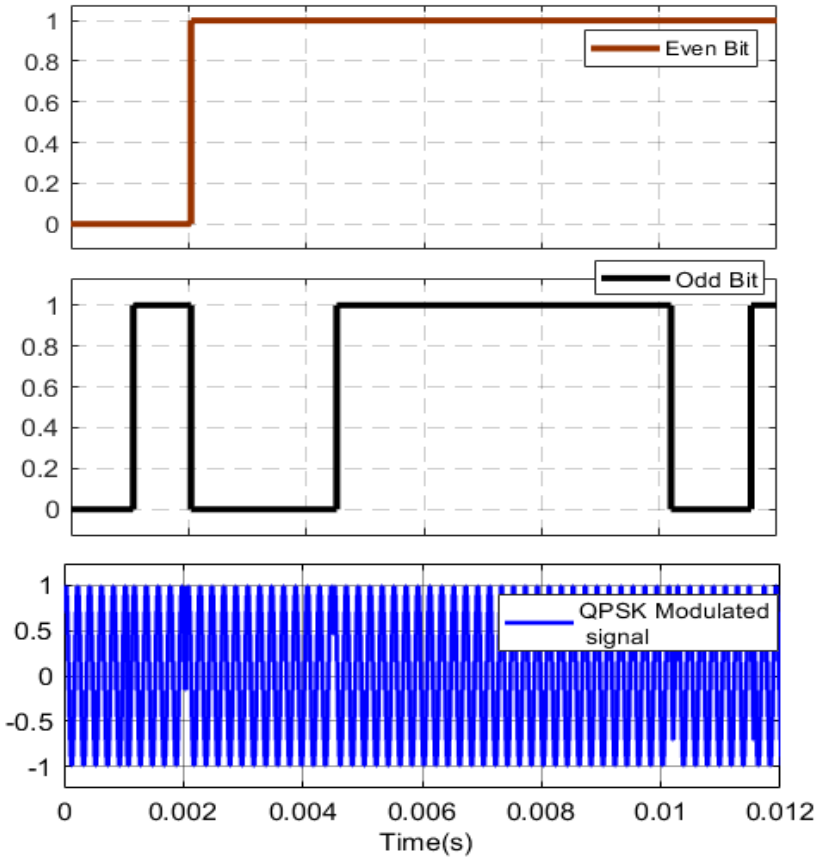

Figure 4.8: Binary bits and QPSK modulated signal waveforms.

Figure 4.9 illustrates the original message signal (red) and its scaled down version (black) to 3 V. The scaled down signal is transmitted to the PLC system and recovered using the QPSK demodulator.

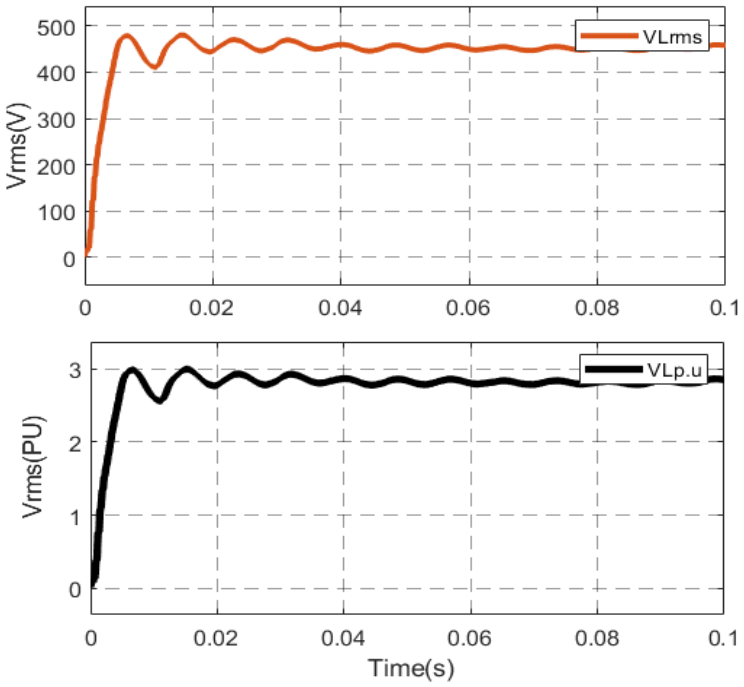

Figure 4.9: Message signal: (top) original signal, (bottom) scaled down signal.

4.2.3. Results and Discussion

Toward the objective of assessing the influence of RPWM in power grids involving PLC systems using simulation tools, two test cases will be considered as follows.

In the first test case, the switching frequency of the DC-DC converter is set to 25 kHz, and the modulation frequency of the QPSK modulator to 5 kHz. In this case, RPWM led to an increased bit error rate (1016 errors out of 10,000 samples) with respect to PWM (572 errors), as shown in Figure 4.10. This is because the peaks of the noise exiting the DC-DC converter do not affect the communication signal, i.e., the frequency of the communication signal does not overlap with the significant noise peaks from the DC-DC converter. This is shown in Figure 4.11, where the CEs of the DC-DC converter with conventional PWM (blue) and RPWM (red) are shown and compared with the QPSK modulated message signal (black). It is shown that resorting to RPWM modulation reduces the noise peaks by more than 10 dB compared to the conventional PWM. However, RPWM spreads the noise spectrum, which exhibits higher amplitude than the conventional PWM in the frequency range around 5 kHz (see the black box in Figure 4.11), with a consequent increase of the interference with the communication signal. This conclusion is in line with the one drawn in [61], where it was proven that RPWM causes more frame error rate than the conventional PWM. However, the RPWM scheme considered in [61] is based on varying the switching frequency of the pulse signal, i.e., the RPWM strategy adopted in that work is different from the one exploited here.

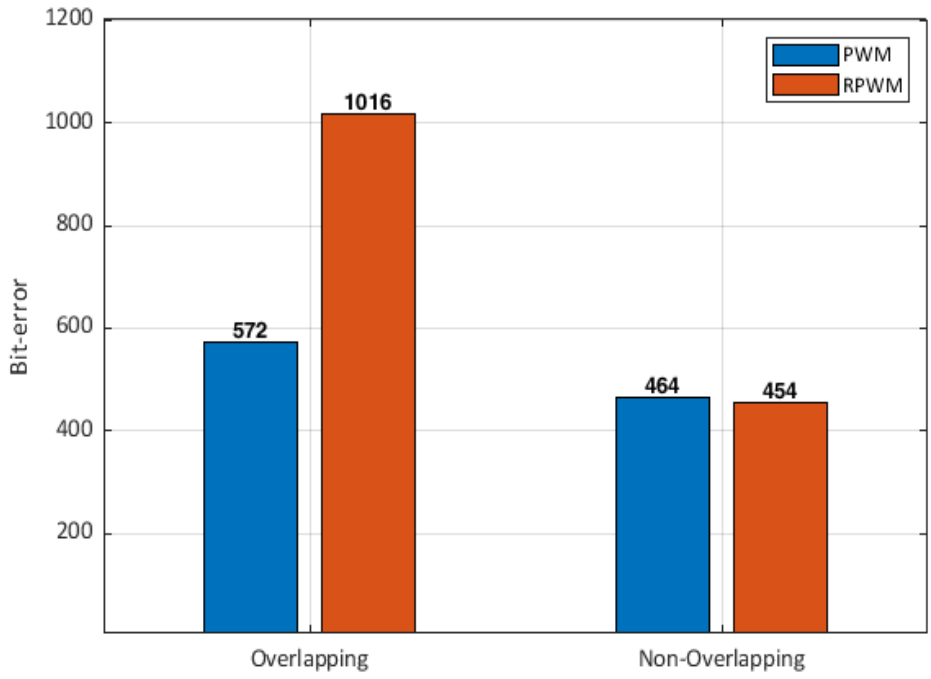

Figure 4.10: Bit error rate: PWM (blue) versus RPWM (orange).

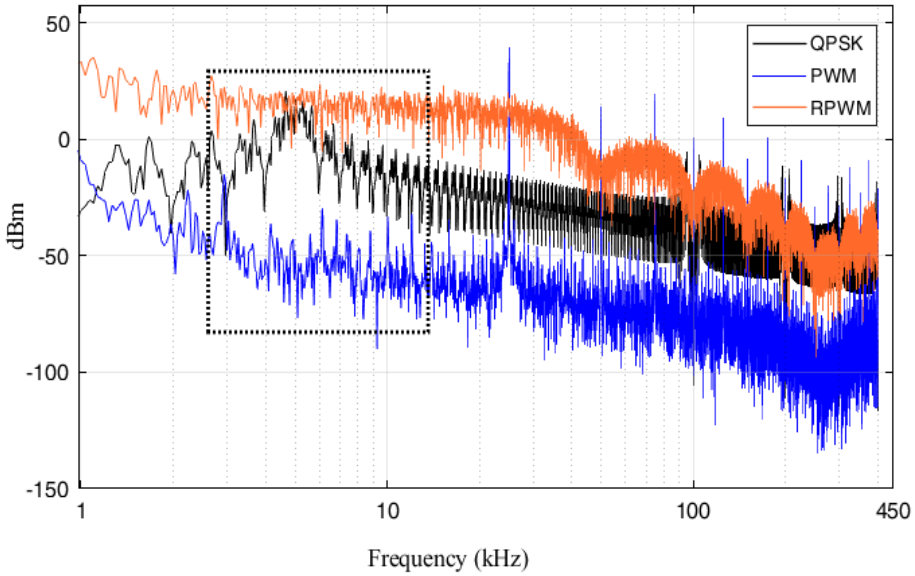

Figure 4.11: Voltage harmonics at the DC-DC converter output: PWM versus RPWM (25 kHz switching frequency) and frequency spectrum of QPSK modulated signal. The x-axis is in logarithmic scale.

Conversely, the advantages of RPWM modulation can be seen if the switching frequency of the DC-DC converter is reduced to 10 kHz, and the modulation frequency of the QPSK modulator is increased to 15 kHz. Figure 4.12 shows the frequency spectrum of the noise exiting the DC-DC converter with PWM (blue) and RPWM (red), along with the spectrum of the QPSK modulated signal (black). In this case, the peaks of the noise spectra of the DC-DC converter overlap with the spectral components of the modulated signal. Since the amplitude of the noise peaks is reduced, thanks to RPWM, the bit error rate with RPWM reduces from 1016 to 454, while the bit error rate with PWM reduces from 572 to 464, as shown in Figure 4.10. It is worth noticing that lower switching frequency, even for PWM, also results in less interference to the communication signal.

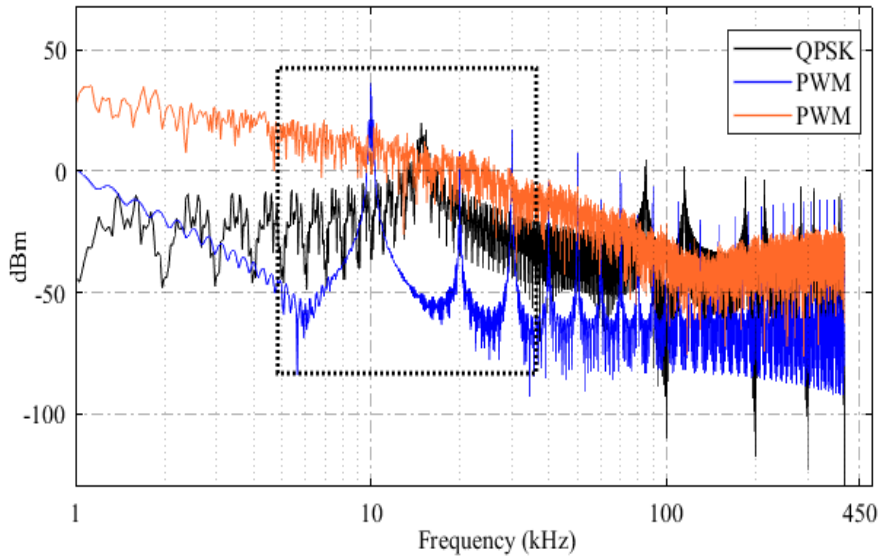

Figure 4.12: Voltage harmonics at the output of the DC-DC converter: PWM versus RPWM (10 kHz switching frequency) and frequency spectrum of QPSK modulated signal. The x-axis is in logarithmic scale.

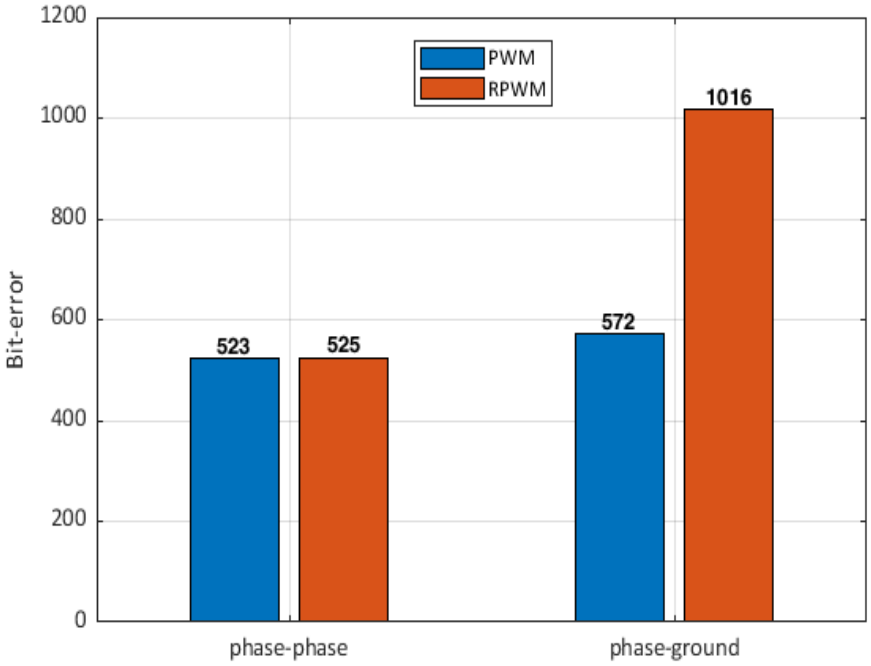

Figure 4.13: Bit error rate with coupling/decoupling networks connected between two phases or between one phase and ground (25 kHz switching frequency).

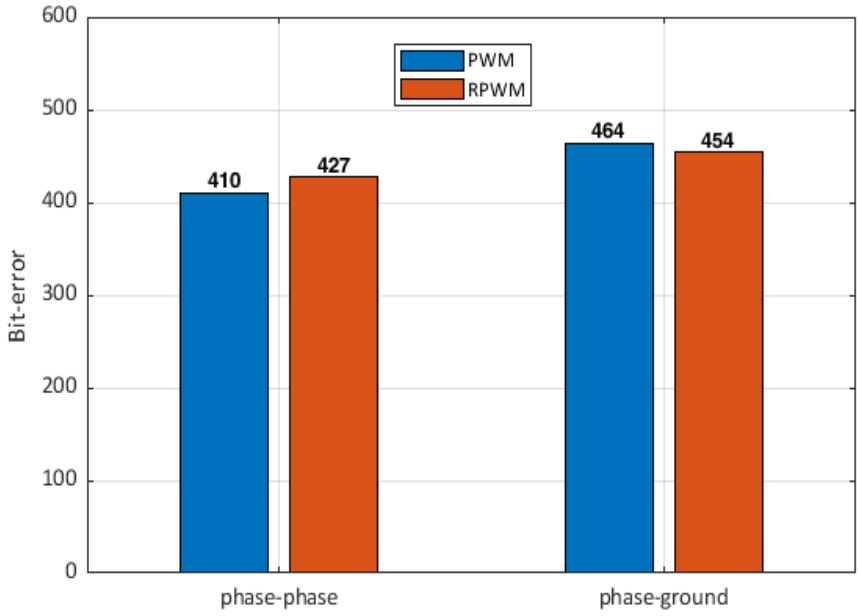

Figure 4.14: Bit error rate with coupling/decoupling networks connected between two phases or between one phase and ground (10 kHz switching frequency)

To assess the effects that symmetry/asymmetry of the power cables plays on the PLC system, an additional example is simulated. To this end, the communication signal was connected between two phases rather than one phase and ground as in the previous examples. Figure 4.13 shows the bit error rate obtained when the communication signal is transmitted between the two phases (the switching frequency of DC-DC converter, in this case, is 25 kHz). The bit error rate drops from 572 to 523 for

conventional PWM and from 1016 to 525 for RPWM when the communication signal is connected between the two phases of the AC system. Likewise, Figure 4.14 shows the bit error rate obtained when the communication signal is transmitted between the two phases (in this case, the switching frequency of the DC-DC converter is 10 kHz). The bit error rate drops from 464 to 410 for conventional PWM and from 454 to 427 for RPWM. This is because connecting the modems between two phases assures better balancing with respect to phase-to-ground connection; hence, signal transmission is affected by less interference.

4.3. Influence of Random Modulated Power Converter on G3-PLC

This section presents an experimental test campaign to study the interference between the power converters and G3-PLC system. G3-PLC is a widespread communication protocol in many PLC applications such as in the SG framework. However, recent research results put in evidence that it may suffer from potential coexistence issues associated with the power converter modulation scheme being used. In particular, RPWM modulated converters have been found to interfere with the PLC.

As summarized in section 4.2.1 there are contributions discussing the comparison between conventional PWM and RPWM effects on the PLC system [33-35]. In general, only specific random modulation schemes (mainly RFM) were investigated in the literature and further investigations on other random modulation strategies are required. Moreover, additional investigations are required to determine which random modulation scheme is most suitable for power converters in applications involving PLC. Besides, there are also many parameters which influence the random modulation schemes such as the switching frequency of the RPWM, the spreading factor and the RNUR. Hence, more analysis is required to identify constraints on these parameters, assuring coexistence with PLC. For instance, the switching frequency of the randomly modulated power converter is not constant, i.e., it depends on the specific application, and it is very difficult to draw general conclusions about coexistence issues, by considering specific switching frequencies only. Besides, the spreading factor specifies by how much the pulse position of the RPPM should vary and it surely plays a significant role on the coexistence issues. The RNUR determines how fast the pulse position of RPPM should change, and it obviously affects the operation of the RPPM as well.

In line with these objectives, this part is aimed at investigating the effects of the RPPM on G3-PLC system and at comparing the results with previous experimental findings obtained with other modulation strategies (such as the RFM) to understand which modulation scheme could better to assure coexistence. To this end, an experimental test campaign aimed at examining the effects of the main parameters which affect the RPPM such as the switching frequency, spreading factor and the RNUR on the performance of G3-PLC is carried out. The performance of the G3-PLC is assessed by considering the FER, the Channel Capacity and the Channel Capacity Loss.

4.3.1. Overview of G3-PLC

The G3-PLC selected for this activity works in the low frequency CENELEC A band with specific frequency between 35 kHz and 91 kHz (see Table 4.1 for details).

Table 4.1: Specifications of the G3-PLC considered in this work.

Layer	*Feature*	
PHY	Modulation	OFDM
	No. of sub carriers	36
	Frequency Band	CENELEC A (35 kHz-91 kHz)
	Sub carrier modulation	DBPSK
	Max data rate	up to 34 kbps
	Sent frames	3000
	Time between frames	100 ms

4.3.2. Experimental test setup considering DC-DC converter as a noise source.

A principle drawing of the test bench is shown in Figure 4.15. Two G3-PLC modems are used as transmitter and receiver, in the frequency band 35 kHz - 91 kHz (see spectra in Figure 4.16) and, are connected by a 42-meter-long 230 V AC cable to transmit the communication signal between the two AC line terminals. An isolation transformer is used to separate the AC line from the grid. The AC line is coupled with the random modulated DC-DC converter through a coupling capacitor of 10 nF. Indeed, in this work a three-phase inverter (one of its legs) is used as a buck DC-DC converter (step-down 50 V DC source to 25 V with a duty cycle of 0.5). The converter has a maximum DC link voltage capacity of 450 V with a 2200 µF DC link capacitor. Six IXGH40N60C2D1 IGBTs are deployed in this specific converter circuit. The output of the DC-DC converter is connected to a variable resistor load fixed at 8 Ω.

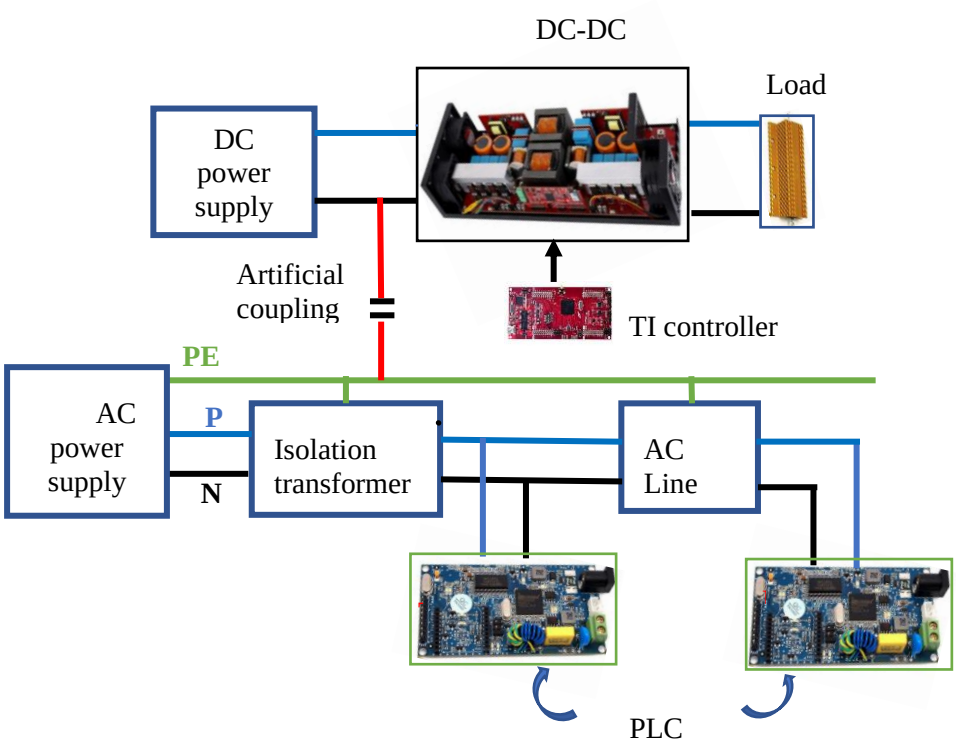

Figure 4.15: Schematics of the experimental test bench with the G3-PLC system coupled with the DC-DC converter through a coupling capacitor.

PWM/RPPM can be easily implemented using microcontroller and SIMULINK. Hence, the code for a specific modulation technique is generated using SIMULINK and deployed to F28379D launchpad for

real time operation (see **Appendix A2**). A picture of the experimental test setup is shown in Figure 4.17.

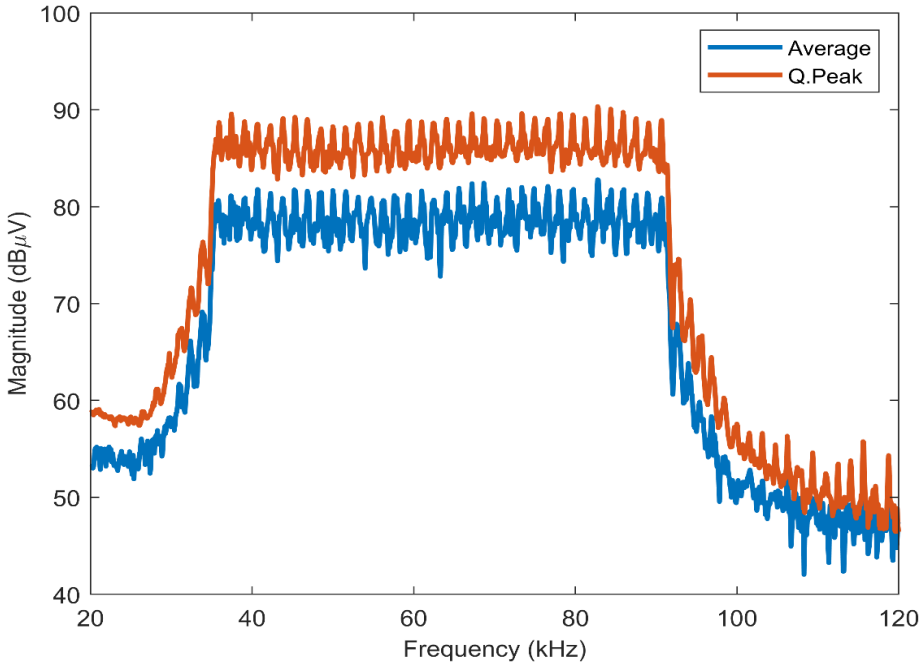

Figure 4.16: Frequency spectrum of the exploited G3-PLC signal.

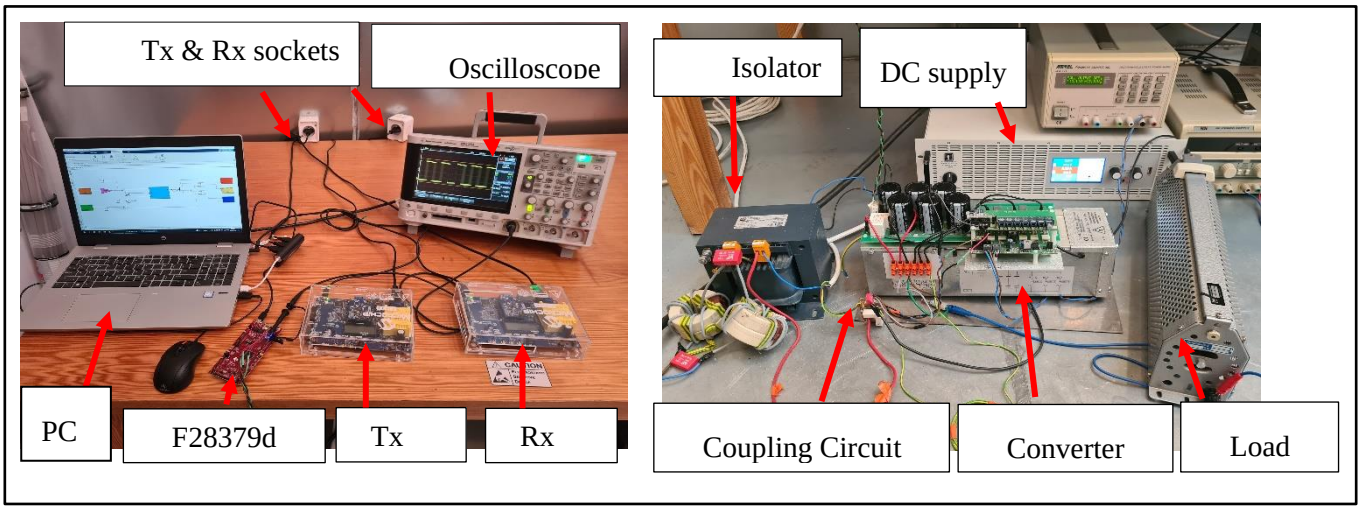

Figure 4.17: Experimental test bench.

4.3.3. Results and Discussion

The performance of the G3-PLC is assessed by considering the FER, the Channel Capacity and the Channel Capacity Loss metrics. The FER indicates the percentage of data frames correctly received over the total data frame sent through the communication system, and can be determined as:

$$FER(\%) = \frac{(Sent\ frames - Received\ frames)}{(Sent\ frames)} x100 \qquad (4.1)$$

The Channel Capacity, *C*, indicates the maximum bits of data that the communication system can in the unit time [59], and is defined as:

$$C = \int_{f_1}^{f_2} \log_2\left(1 + {S(f)}/{N(f)}\right) df \qquad (4.2)$$

where, f_1 and f_2 are the lower and upper frequency bands of the G3-PLC, *S*(*f*) is the PSD of the G3-PLC and N(f) is the PSD of the noise which encompasses two contributions:

$$N(f) = N\_0\ (f) + N\_\text{EMI}\ (f) \qquad (4.3)$$

where, N_0 (*f*) denotes the PSD of the background noise and *N*_EMI (*f*) denotes the PSD of the noise from DC - DC converter. Eventually, the Channel Capacity Loss is defined as:

$$\mathrm{C_{Loss}}(\%) = \frac{(\mathrm{C_0} - \mathrm{C_{G3}})}{\mathrm{C_0}} x100 \qquad (4.4)$$

where, C_{G3} and C_0 denote the Channel Capacity of the G3-PLC with and without the noise from the DC-DC converter (*N*_EMI).

4.3.3.1. Effects of the Converter Switching Frequency

This section presents experimental results showing the effects of the switching frequency of a randomly modulated power converter on the G3-PLC system. Hence, different switching frequencies from 10 kHz to 100 kHz are considered for this analysis.

Figure 4.18 shows the FER calculated from 3000 frames of data transmitted through the G3-PLC when different switching frequencies are applied to the DC-DC converter resorting to RPPM. The input

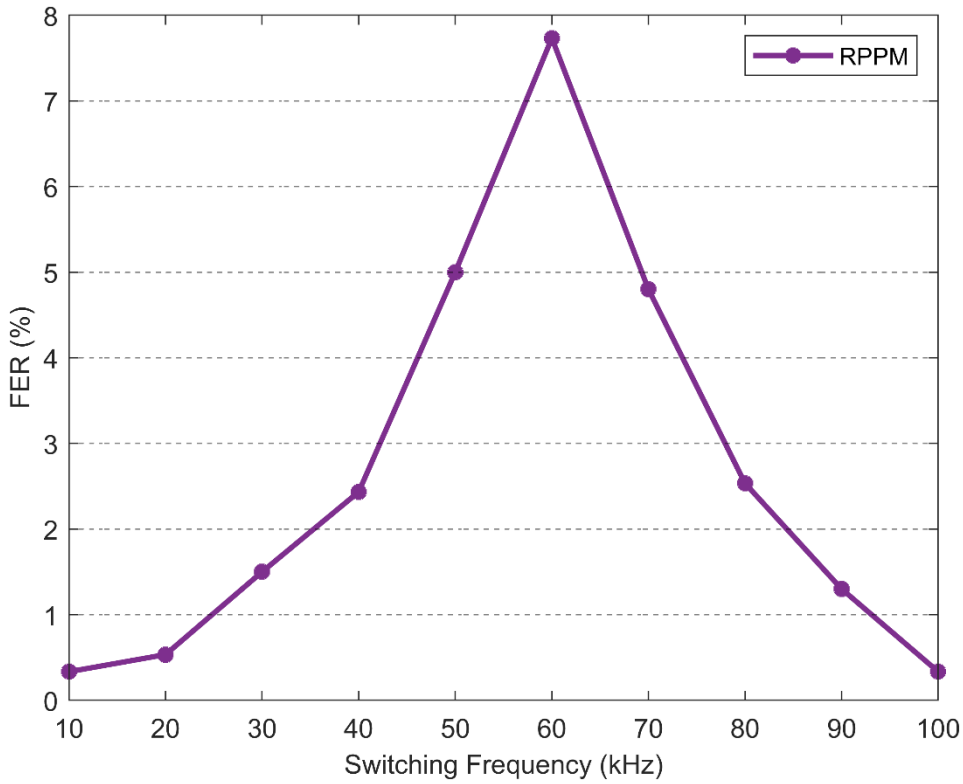

Figure 4.18: FER of the G3 PLC vs. switching frequency of the DC-DC converter modulated with RPPM.

of the DC-DC converter is fixed to 50 V. The FER is significantly higher in the G3-PLC bandwidth (when the switching frequency of the DC-DC converter is in the range 35 kHz - 91 kHz) with maximum

value of around 60 kHz (i.e., the center frequency of the PLC bandwidth). However, the FER is not significant where the switching frequency of the DC-DC converter is out of the bandwidth of the G3-PLC. This result allows drawing the conclusion that RPPM could influence the G3-PLC only when the switching frequency of the power converter is in the bandwidth of the G3-PLC system.

A similar analysis involving RFM was carried out in [35], with the same input voltage of the DC-DC converter (50 V) and switching frequency varied from 50 to 75 kHz. Some of the results obtained in [35] are summarized in Table 4.2. The comparison allows appreciating that RFM (with 15-30% spreading factor) causes significantly larger FER (more than 40%) compared to RPPM with maximum FER of 8% obtained at 20 % spreading factor (which is the maximum possible pulse position variation as defined in (4.5)) around the intermediate switching frequency (60 kHz). Even with lower spreading factor, RFM causes higher FER than RPPM. This is because the bandwidth of the noise generated by a DC-DC converter with RFM is wider (i.e., the noise is more spread) than with RPPM. This can be easily appreciated in Figure 4.19, where the CE exiting the same DC-DC converter driven by different modulation schemes (PWM, RFM and RPPM at the 20 kHz switching frequency) are compared. The comparison unveils that even if RFM is more effective than RPPM for EMI reduction, RPPM offers significant advantages in terms of assuring coexistence with communications systems. Of course, better performance of RFM can be obtained by adjusting the working parameters, i.e., by reducing the spreading factor of RFM it is possible to have lower interference to the G3-PLC but with lower CE reduction. This corroborates the conclusion that choosing the right modulation scheme is to be intended as a trade-off between EMI reduction and the coexistence issues.

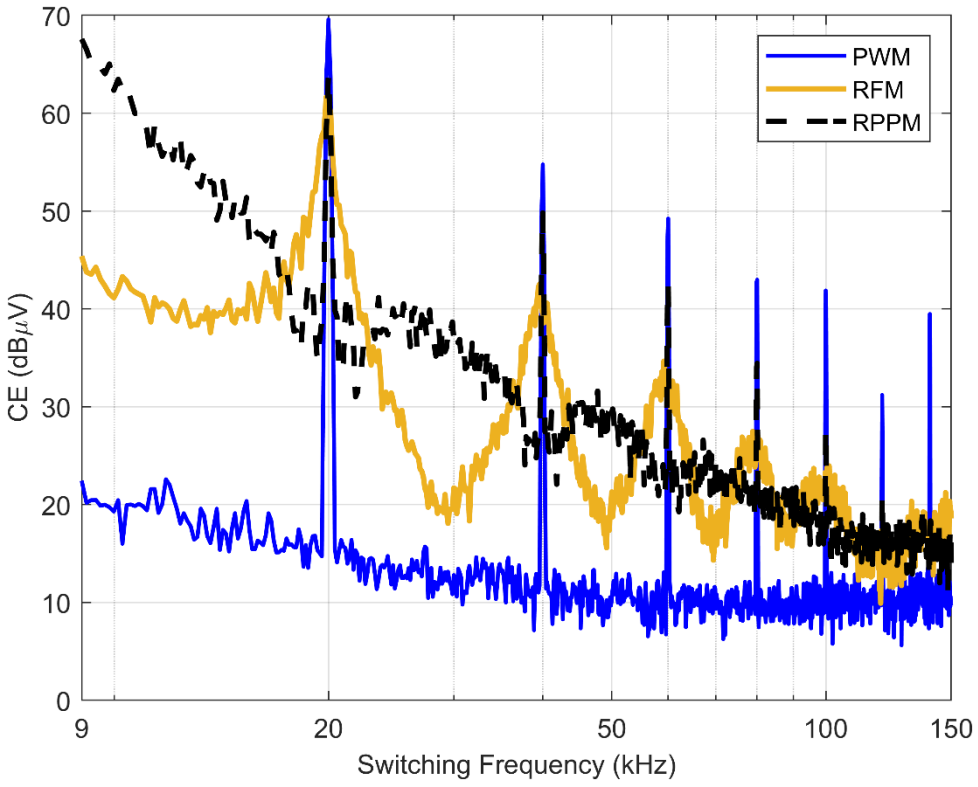

Figure 4.19: Comparison of the CE exiting the same DC-DC converter driven by different modulation schemes.

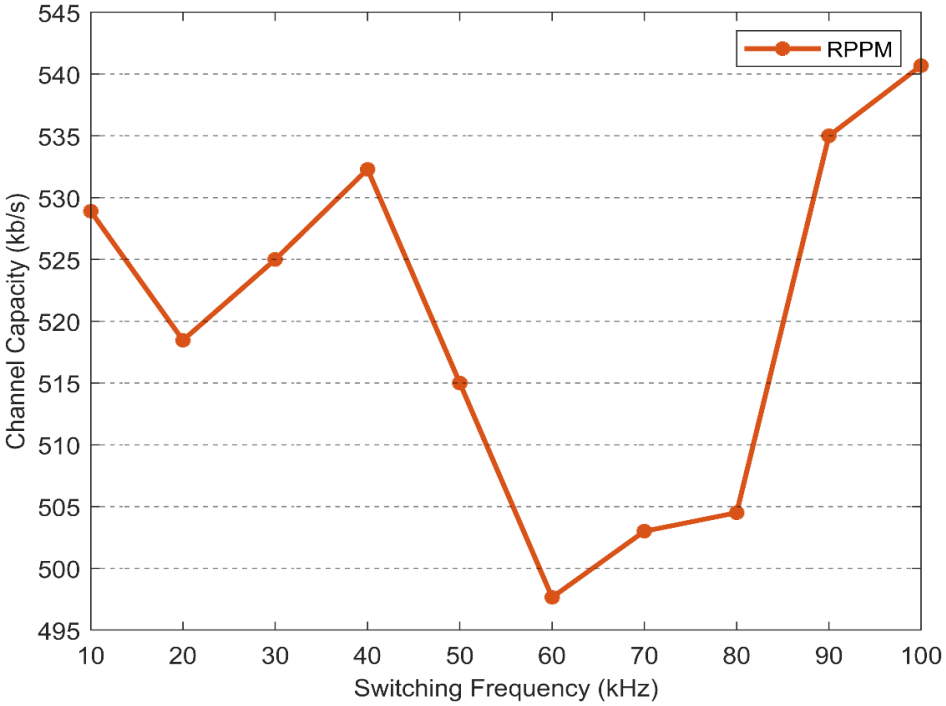

Figure 4.20: Channel Capacity of the G3-PLC with different switching frequencies applied to the RPPM modulated DC-DC converter.

This conclusion is also confirmed when the Channel Capacity is considered. As depicted in Figure 4.20. The Channel Capacity of the G3-PLC reduces when the switching frequency of the converter is near the intermediate frequency of the G3-PLC system. However, for switching frequencies out of the bandwidth of the G3-PLC, the Channel Capacity is not significantly affected. The worst Channel Capacity in case of RPPM obtained is at switching frequencies around 60-63 kHz (498 kb/s) and results to be significantly higher than the minimum Channel Capacity obtained in [35] with the DC-DC converter driven by the RFM (390 kb/s at the spreading factor 'α=30%' and 63 kHz switching frequency).

These observations are confirmed also in terms of Channel Capacity Loss. Indeed, Figure 4.21 shows that the G3-PLC Channel Capacity Loss takes maximum value (18%) at 60 kHz, which results in being significantly lower than the maximum Channel Capacity Loss (48%) observed in [35] for RFM (with spreading factor 'α=30%').

Table 4.2: Comparison of the performance of G3-PLC assessed with RFM and RPPM applied to the DC-DC converter [35]

Frequency (kHz)	**G3-PLC performance**					
	FER (%)		**Channel Capacity (kb/s)**		**Channel Capacity Loss (%)**	
	RFM	**RPPM**	**RFM**	**RPPM**	**RFM**	**RPPM**
60-63	50	8	390	498	48	18
50	8	5	460	515	40	16
75	4	3.5	370	503	50	17

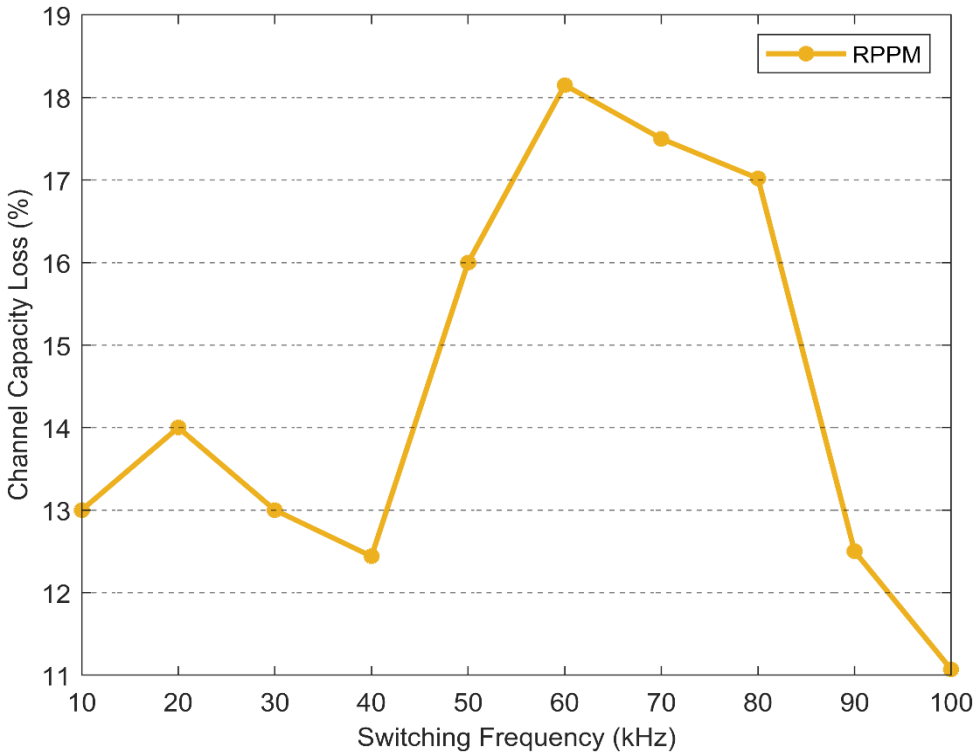

Figure 4.21: Channel Capacity Loss of the G3-PLC with different switching frequencies applied to the RPPM modulated DC-DC converter.

4.3.3.2. Effects of Random Number Update Rate and Spreading Factor

In this section, the effects of the RNUR and the spreading factor of randomly modulated power converter on the G3-PLC system are investigated.

The RNUR of the random number (see **Appendix A2**) plays a significant role on signal transmission since, with higher RNUR of the random number the pulse position of the RPWM changes rapidly.

The spreading factor determines how much the pulse position could be varied with respect to the switching period. CE reduction is proportional to the spreading factor since higher value results in higher reduction of the CE peak. Indeed, the maximum pulse position variation Δ_{max} should be:

$$\Delta_{max} \leq (T - d) \qquad (4.5)$$

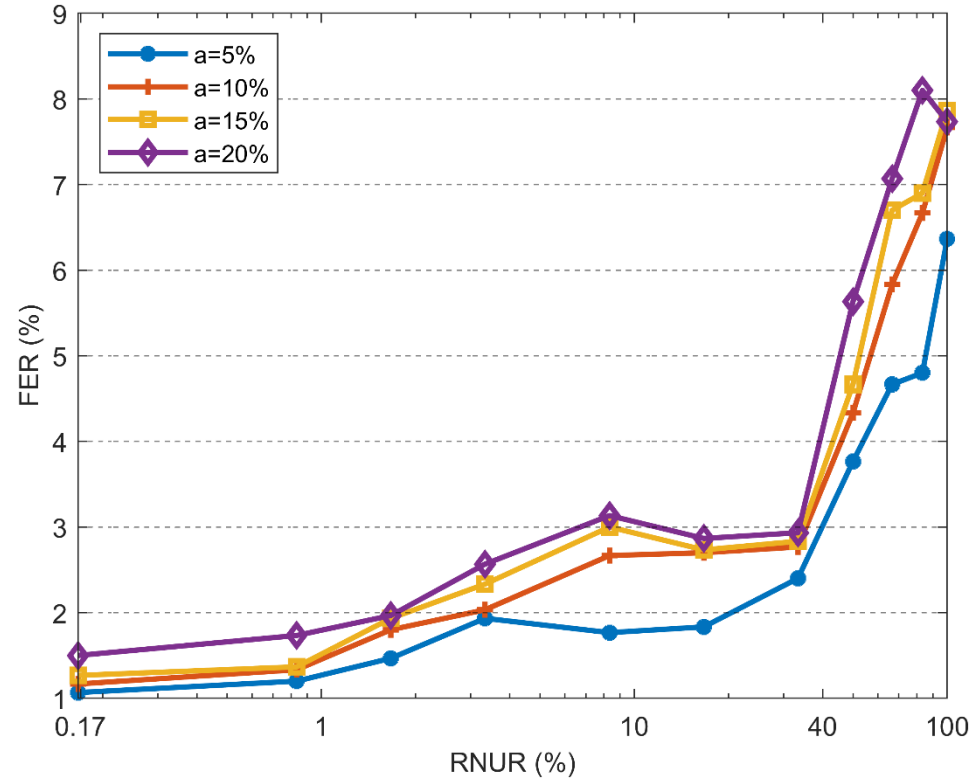

Figure 4.22: FER of the G3 PLC measured with different values of RNUR and spreading factor of the RPPM modulated DC-DC converter @ 60 kHz switching frequency.

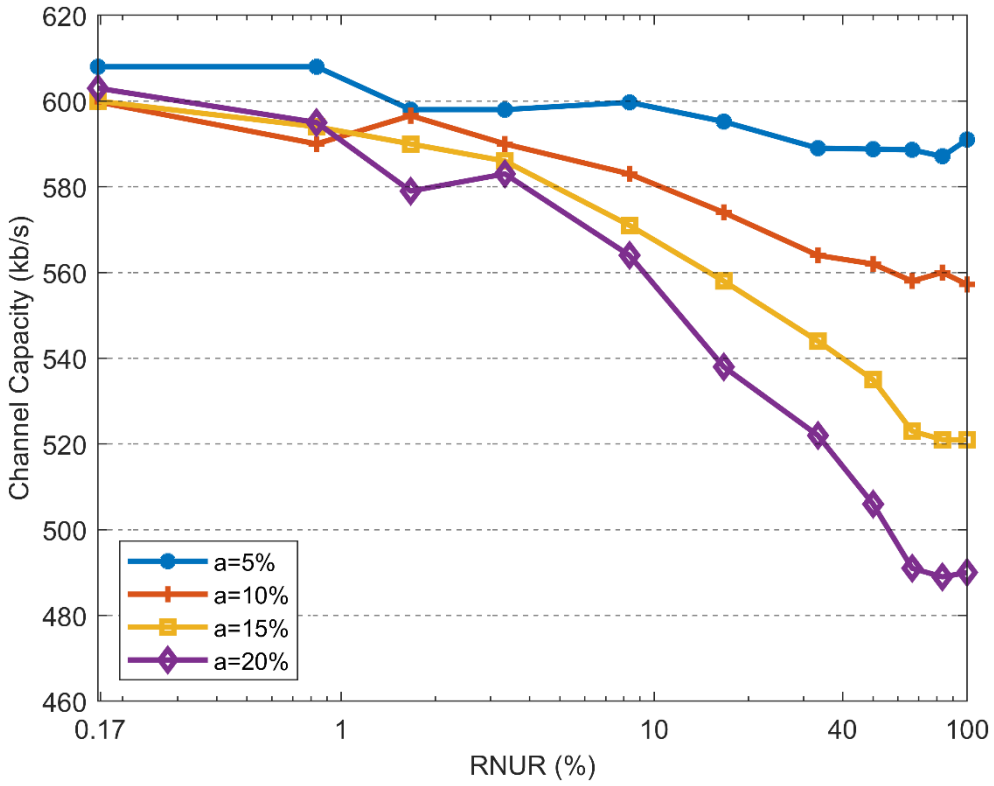

Figure 4.23: Channel Capacity of the G3 PLC measured with different values of the RNUR and the spreading factor of the RPPM modulated DC-DC converter @ 60 kHz switching frequency.

Based on the results obtained in Section 4.3.3.1, to analyze the effects of the RNUR of the random number and the spreading factor, three switching frequencies are chosen in which one is around the intermediate frequency of the G3-PLC (60 kHz) where maximum disturbance due to random modulation is registered (see Section 4.3.3.1) and the other two are out of the frequency band of the G3-PLC (10 kHz and 100 kHz). A range of RNUR and spreading factor values are considered to assess the performance of the G3-PLC.

Figure 4.22 shows the FER obtained when the switching frequency of randomly modulated converter is 60 kHz, and the RNUR and the spreading factor take values in the intervals (0.16 % - 100 %) and (5% - 20%) respectively. The obtained result shows that the FER is directly proportional to both the RNUR and the spreading factor. The FER increases when the RNUR and the spreading factor increase. This result further confirms that there is a trade-off between EMI reduction and coexistence issues, i.e., increasing the spreading factor helps reduce the peaks of the converter CE (see Figure 4.25). However, it causes more disturbance to the G3-PLC.

The Channel Capacity of the G3-PLC with respect to the RNUR and the spreading factor is depicted in Figure 4.23. The Channel Capacity exhibits significant reduction when both the RNUR and the spreading factor are increased. The reduction with the RNUR is significant for large values of the spreading factor. Conversely, for small spreading factors, limited variations are observed. These results are also confirmed in terms of Channel Capacity Loss as shown in Figure 4.24. Normally, also the Channel Capacity Loss increases with an increase in both the RNUR and the spreading factor.

The performance of the G3-PLC for switching frequencies outside the PLC bandwidth are shown in Figure 4.26 and Figure 4.27 respectively, confirming an increase of the FER when both the RNUR and the spreading factor increase. However, the amount of variation in Figure 4.26 and Figure 4.27 is insignificant compared to the results in Figure 4.22.

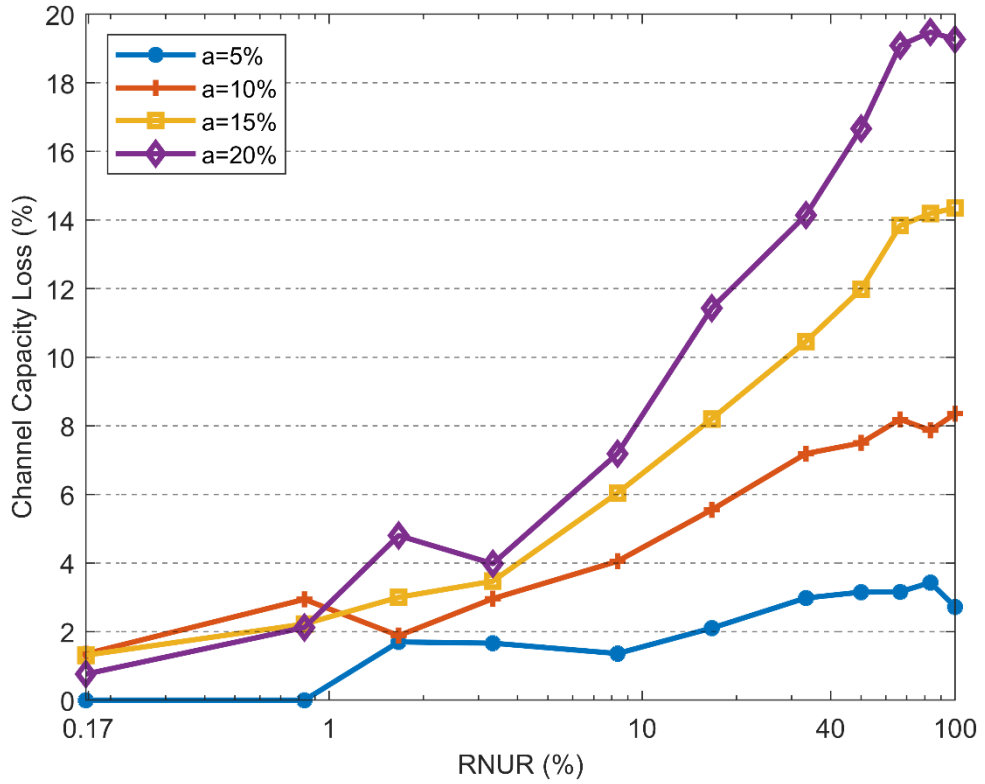

Figure 4.24: Channel Capacity Loss of the G3 PLC calculated with different values of the RNUR and the spreading factor of the RPPM modulated DC-DC converter @ 60 kHz switching frequency.

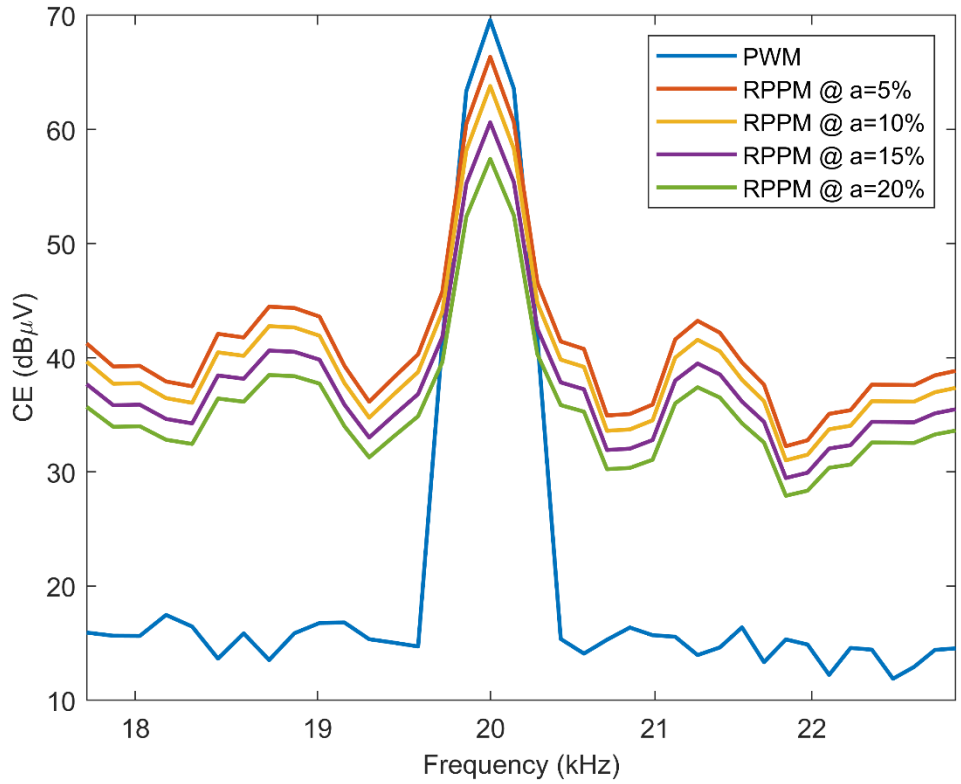

Figure 4.25: CE of the DC-DC converter measured with different values of the spreading factor @ 20 kHz switching frequency and @ 33% RNUR.

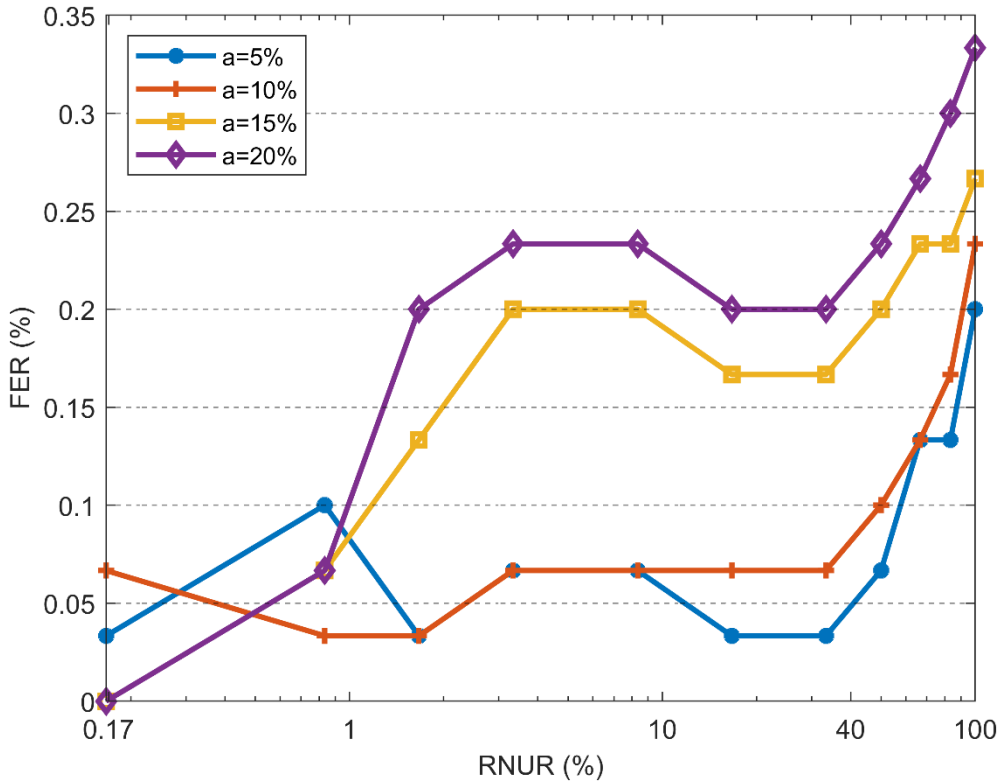

Figure 4.26: FER of the G3 PLC measured with different values of the RNUR and the spreading factor of the RPPM modulated DC-DC converter @ 10 kHz switching frequency.

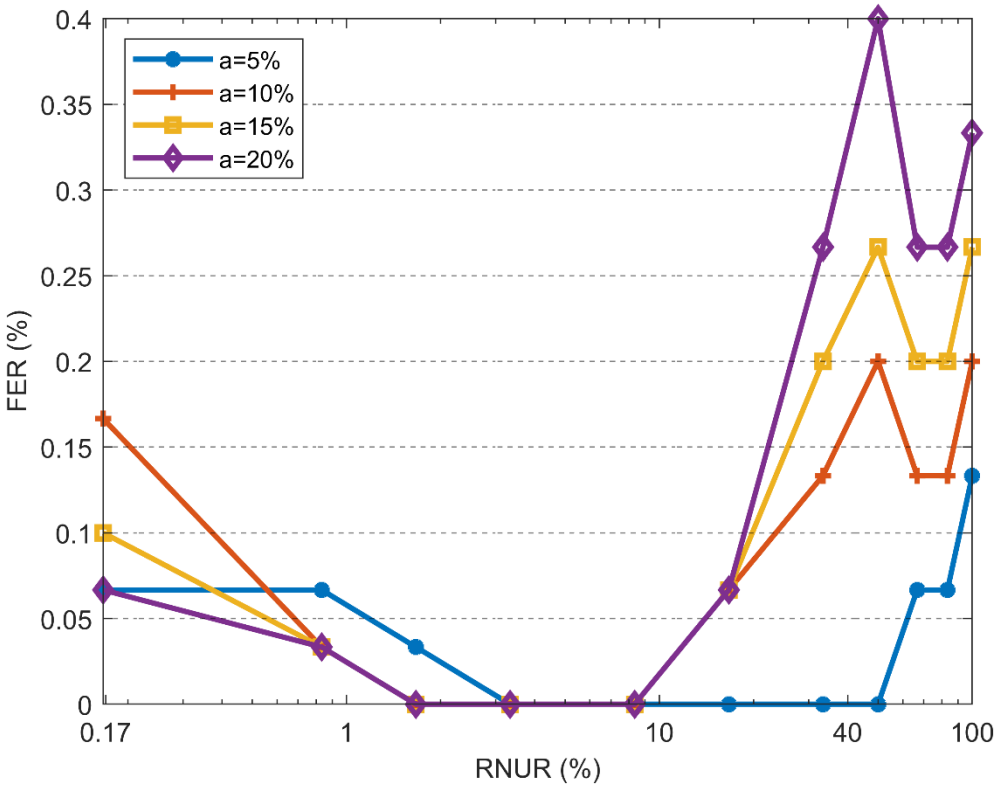

Figure 4.27: FER of the G3 PLC measured with different values of the RNUR and the spreading factor of the RPPM modulated DC-DC converter @ 100 kHz switching frequency.

Therefore, it is possible to conclude that the RNUR and the spreading factor of randomly modulated power converter plays a significant role in affecting the G3-PLC only when the switching frequency of the power converter overlaps with the bandwidth of the G3-PLC, and negligible for switching frequencies out of the bandwidth of the G3-PLC. This conclusion is confirmed also in terms of Channel Capacity and Channel Capacity Loss, whose plots are omitted for sake of brevity.

4.4. Conclusion

This chapter presented the research carried out to study the coexistence issues between randomly modulated power converters and coexisting PLC systems using both simulation tools and laboratory experiments.

Firstly, the effects of using RPWM to control the switching activity of power electronics converters in power systems involving PLC for advanced meter reading are investigated using software tool. To this end, both the power and the communication part of the system were modeled in SIMULINK. The comparison versus traditional PWM is carried out in terms of bit error rate achievable by application of the two modulation schemes. Additionally, the effects of connecting the PLC modems to the power line in different configurations are presented. Based on the obtained results, it is possible to conclude that applying RPWM on the power converter in the PLC system, besides having a significant effect on reducing the CEs, results in less bit error rate compared to the conventional PWM when the modulation frequency of the communication signal and the frequency of the significant peaks of the noise exiting the DC-DC converter are overlapping. Conversely, higher bit error rate will be obtained if the two frequency spectra do not overlap. Of course, the PLC considered in this part is a low data rate PLC with a capacity of 5kb/s data transmission and with QPSK modulation. The results might change with high data rate PLC and with other communication modulation schemes such as OFDM modulation being deployed. But the obtained results give a general conclusion that, whichever modulation scheme

applied, i.e., PWM or RPWM, who has higher noise spectrum in the frequency band of the communication system, causes more communication problem. Results also showed that, to improve the bit error rate, it is preferable to connect the PLC coupling/decoupling networks between two phases of the power line, rather than between a phase and ground, since this assures higher symmetry of the PLC channel.

Next, the coexistence issue between power and data lines in G3-PLC systems in the presence of randomly modulated power converters has been investigated using laboratory experiments. The effects of different parameters of RPWM scheme driving power converter (switching frequency, spreading factor and RNUR) on the G3-PLC are assessed in detail. Communication performance is evaluated in terms of FER, Channel Capacity and Channel Capacity Loss. The obtained results have confirmed that switching frequencies close to the bandwidth of the G3-PLC cause interference in the PLC system more than those out of the frequency bandwidth. Besides, the comparison between different RPWM schemes such as RPPM and RFM applied to power converter on their performance in assuring coexistence is investigated, where experimental results have showed that there is a trade-off between CE reduction and coexistence issue with communication systems. Namely, even if RPPM is not as effective as other schemes (as for instance RFM) in reducing the CE exiting the converter, however this modulation scheme outperforms RFM in terms of assuring coexistence with communication systems. Moreover, the effects of other RPWM parameters, such as the RNUR and the spreading factor, on the PLC system have been experimentally examined to draw general conclusions on the effectiveness of RPWM in assuring coexistence. Results showed that the RNUR and the spreading factor of RPWM have a direct effect on the communication channel performance. Indeed, the performance of the G3-PLC degrades with the increase in the RNUR and the spreading factor. However, this is true only when the switching frequency of the randomly modulated converter overlaps with the bandwidth of the G3-PLC. Otherwise the effect is almost negligible. In general, it is possible to draw two main conclusions based on the experimental analysis. First, randomly modulated power converter may deteriorate G3-PLC performance when the converter switching frequency is near the bandwidth of the communication channel. The interference can be avoided or reduced to the minimum by choosing different/non-overlapping frequency bands for the converters and or the PLC systems. Another conclusion is that among the available RPWM schemes, RPPM is less detrimental than RFM. Obviously, RFM may also result less interference to the G3-PLC if lower spreading factor is chosen but with compromising CE reduction.

CHAPTER 5

Behavioral Modelling of G3-PLC Modems

5.1. Modelling of G3-PLC Modems for Low-Frequency EMI analysis

G3-PLC is among the communication protocols which is mostly deployed in power system networks such as SG application. Modeling the G3-PLC modem for EMI analysis using detail network diagram (white-box modelling) is very challenging since the modem is very complex, and due to the limitation of the detail information of the components being used in. Therefore, this section presents an experimental test campaign to find an alternative modelling approach to represent the G3-PLC modems in their desired frequency band using black-box modelling technique.

Black-box modelling of noise sources, mainly power converter, is a very common subject where many modelling techniques have been studied so far including the Norton Thevenin equivalent model as discussed in Chapter 2 [42,60]. Although such a black-box modelling approach does offers very promising EMI models, there is a limitation which is that the device under analysis should be linear and time-invariant (LTI) system. This limitation is not necessarily affecting the modeling of power converters since they are usually equipped with large input capacitors and inductors, which can mask the nonlinear behavior of the converter semiconductor devices [61-63]. Additionally, power converter control algorithms are designed to track low frequency signals (DC or AC 50/60 Hz), so that they are typically effective up to a few kHz at most. The noise generated by power converters is then marginally affected by control algorithms and can hence be represented by means of a Norton Thevenin model. On the contrary, the linearity assumption may put a constraint on the use of this approach in the modeling of PLC systems, which are designed to inject controlled signals into the grid with a frequency up to some hundreds of kHz. The required control loops affect the validity of the aforementioned linearity assumption, so that the suitability of Norton Thevenin representation for PLC modems is to be verified.

Nevertheless, there is a research gap in finding exact EMI models of PLC systems. There are many research activities to study the modulation being used in PLC systems using white-box modelling approaches [56]. But those models are only approximate models without considering detailed circuit components and cannot be used for EMI analysis in complex systems like SG. There are also very interesting research works about the channel characterization of PLC systems for different applications [64,65]. Some mode-based modeling and analysis methods have also been proposed [66, 67]. However, the coexistence issue between power converters and PLC systems is a relatively new concept despite the latest research developments come to existence these days [33, 35]. Most importantly, the concept of modelling the PLC modem as a black-box is completely new. Accurate modelling of PLC modems is vital since they have many electronics components including some power conversion stages and rigorous closed-loop control systems which will play a significant role in EMI analysis of complex systems.

Therefore, this part aims to provide a behavioral model of the G3-PLC system starting from an experimental test campaign, so that it can be easily integrated into complex networks and could help to

predict EMI. Firstly, to investigate whether G3-PLC modems can be modelled as linear sources, Norton Thevenin equivalent circuit representations are employed. In this case, the transmitting G3-PLC modem (PLC Tx) is considered as an intentional noise source and represented by a Thevenin equivalent circuit, while the receiving PLC modem (PLC Rx) is represented by an impedance matrix. A set of experiments, however, will reveal that when the modem is in transmitting mode, the linearity assumption is no longer satisfied, due to the effect of closed-loop control algorithms. Hence, by the substitution theorem, it is proposed to model the transmitting modem by a pair of ideal voltage sources, while still using an impedance matrix to model the receiver.

5.2. System under analysis

Figure 5.1 shows the most common representation of SG where PLC systems integrated with distributed generations (DG) such as PV and wind, together with different loads such as smart homes and electric vehicles. The PLC systems play significant role by providing real time data exchange between the sources and loads as well as the user. In general, to predict the EMI in such kind of complex networks, we should get first the model of each device. Indeed, the noise sources associated with DG like DC-DC converters and inverters can be modelled using Norton Thevenin equivalent assuming that.

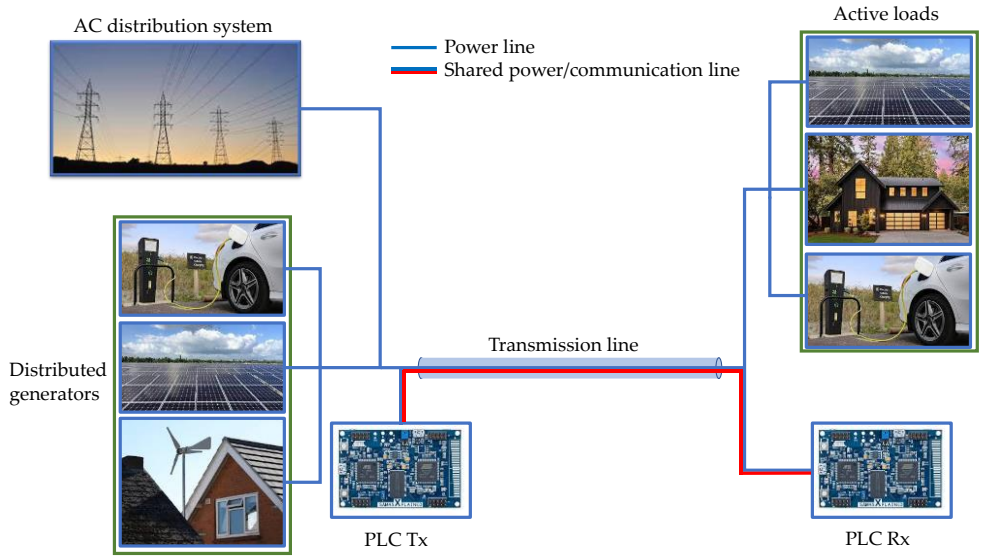

Figure 5.1: Schematics representation of a typical PLC application in modern distribution systems.

they satisfy LTI assumption. The main challenge is modelling the communication protocols inside SG, such as G3-PLC system. Those devices have strong control systems and plenty of electronics components which make them difficult to assume as an LTI system. However, once their model is adopted, it can be used in complex SG networks to study the electromagnetic coexistence between power and communication systems. Besides, it will allow also to predict the electromagnetic emissions in the whole SG network.

The schematics of the system considered in this work is shown in Figure 5.2. The simplified setup is aimed at representing a basic radial distribution network, where the system under analysis is supplied by the AC mains (230 V, single phase) through a short cable, and two PLC modems are connected to the power line. Additionally, two Line Impedance Stabilization Networks (LISNs) are included in the setup with the following three purposes. Firstly, LISNs reject high frequency noise possibly coming from the AC mains and provide a stable impedance in the frequency range of interest. This allows removing possible sources of uncertainty, which is beneficial for the PLC model accuracy. Secondly, they

provide additional measurement ports for measuring EMI. Finally, different LISNs can be used to offer a different set of impedances in the frequency range of interest for PLC modelling, without affecting the low frequency system behavior, allowing to perform multiple tests in well-defined conditions, which provides the data needed to verify the proposed behavioral model. The oscilloscope is connected to the measurement ports of the two LISNs in order to simultaneously measure the EMI coming from the system under analysis. It is worth noting that the schematic shown in Figure 5.2 is used not only for behavioral modeling but also for validation measurement. Specifically, in the validation stage, the circuit layouts of the LISNs are different from the one used for model extraction, providing data from different system working conditions.

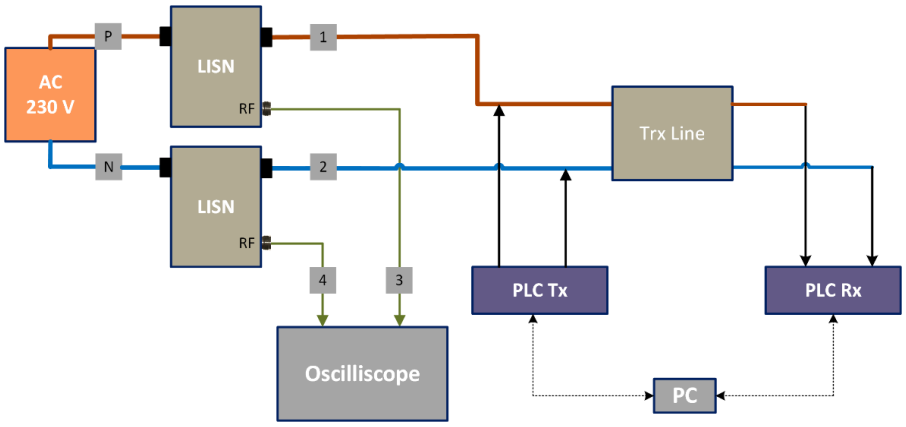

Figure 5.2: Principal diagram of the setup for PLC modelling.

5.3. Behavioral Modelling Procedure

In this section, the procedure used to derive a Thevenin equivalent model representing the considered PLC system is presented. Norton equivalent circuits are not discussed for brevity, as they are a dual (equivalent) representation of the Thevenin model discussed in the following. The procedure to extract the passive part of the Thevenin model and to characterize the other passive elements of the system depicted in Figure 5.2 is described in Section 5.3.1. The procedure to extract the active part of the PLC Thevenin model is presented in Section 5.3.2.

5.3.1. Procedures to Characterize the Passive Elements

The circuit reported in Figure 5.2 can be subdivided into three main blocks: 1) PLC Tx, 2) transmission line and PLC Rx, and 3) AC mains and LISNs. Each of these elements is characterized by VNA measurement in terms of S-parameters. The following subsections present the procedure to determine the equivalent circuit representation of the passive part of those elements.

5.3.1.1. Characterization of the PLC Tx and Rx Modems

Since one of the PLC modems is operated as transmitter (PLC Tx) while the other one is operated as receiver (PLC Rx), it is reasonable to use an extracted Thevenin equivalent circuit for the PLC Tx unit, while the PLC Rx unit is modelled simply by an impedance matrix, *i.e.*, the passive part of the Thevenin model. The Thevenin equivalent circuit for a two-port circuit element, used in the following for the PLC Tx, is shown in Figure 5.3(a), while the equivalent passive model, used in the following for the PLC Rx, is depicted in Figure 5.3(b).

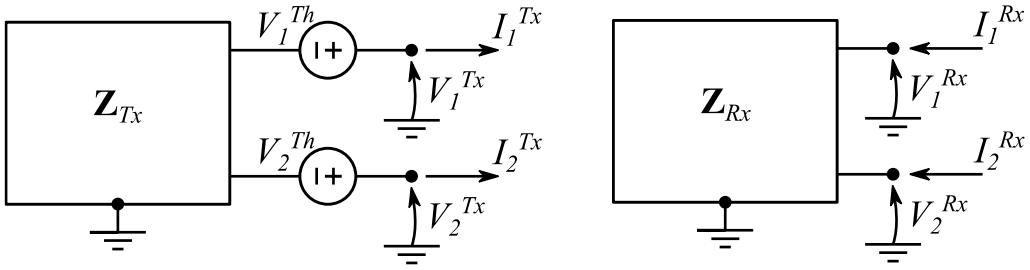

(a) (b)

Figure 5.3: Proposed behavioral model representation: (a) Complete Thevenin equivalent circuit, used to represent the PLC Tx, and (b) impedance representation used to represent the PLC Rx.

The PLC Tx and Rx modems are characterized independently by means of a VNA measurement. The PLC Tx is characterized as a two-port network, as shown in Figure 5.4(a), while it is switched off. The measurement results in a 2×2 *S*-parameters matrix, denoted hereon as $\mathbf{S}_{Tx}$, from which the passive part of the Thevenin model is extracted. To simplify the model verification procedure, the PLC Rx is directly characterized together with the transmission line, as shown in Figure 5.4(b). The measurement results in a 2×2 *S*-parameter matrix, denoted hereon as $\mathbf{S}_{Rx}$.

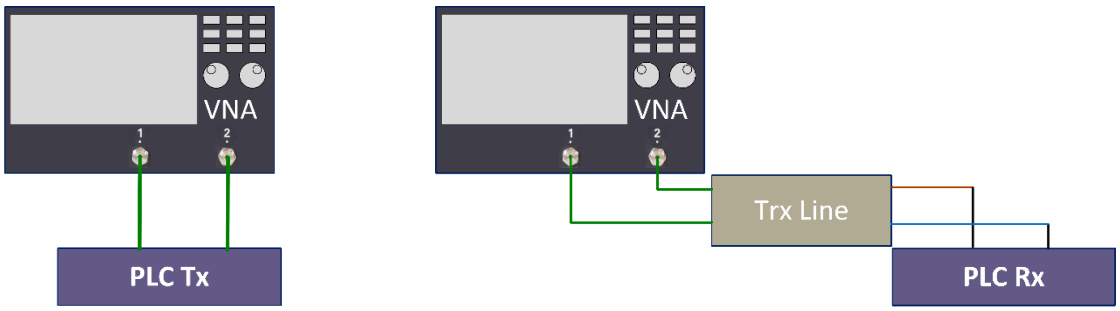

(a) (b)

Figure 5.4: Characterization of: (a) PLC Tx, and (b) PLC Rx and transmission line.

The corresponding impedance matrices $\mathbf{Z}_{Rx}$, $\mathbf{Z}_{Tx}$ are obtained as:

$$\mathbf{Z}_{Rx,Tx} = Z_0 \left(\mathbf{I}_2 + \mathbf{S}_{Rx,Tx}\right)\left(\mathbf{I}_2 - \mathbf{S}_{Rx,Tx}\right)^{-1} \qquad (5.1)$$

where Z_0 is the reference impedance, in this case equal to 50 Ω, and $\mathbf{I}_2$ is the 2×2 identity matrix.

5.3.1.2. Characterization of the LISNs

The considered setup includes two identical LISNs (HV-AN 150, [68]) connected to the phase and neutral wires of the AC mains. In addition to the two ports connected to the AC mains (P and N in Figure 5.2), each LISN has two ports: one for power connection (1 and 2 in Figure 5.2) and one for EMI measurements (3 and 4 in Figure 5.2). In order to accurately determine the relations between quantities at ports 1, 2 and measurements performed at ports 3, 4, it is possible to characterize the two LISNs as a four-port network, as depicted in Figure 5.5, yielding a 4×4 S-parameter matrix, denoted hereon as $\mathbf{S}_{LISN}$. The corresponding impedance matrix $\mathbf{Z}_{LISN}$ is obtained as:

$$\mathbf{Z}_{LISN} = Z_0 \left(\mathbf{I}_4 + \mathbf{S}_{LISN}\right)\left(\mathbf{I}_4 - \mathbf{S}_{LISN}\right)^{-1} \qquad (5.2)$$

where $\mathbf{I}_4$ is the 4×4 identity matrix.

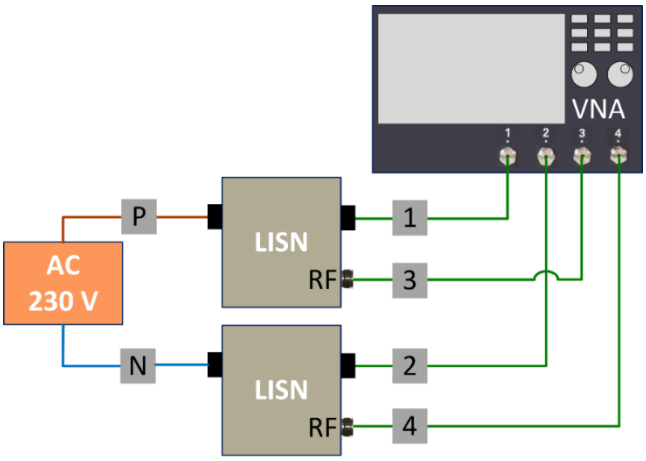

Figure 5.5: Characterization of the two LISNs as a four-port network.

5.3.2. Procedures to Characterize the Active Elements

The setup depicted in Figure 5.2 has been selected with the twofold purpose of determining a Thevenin model for the considered PLC systems and allowing the variation of LISNs impedances in order to verify the obtained model. In these regards, the corresponding circuit representation is depicted in Figure 5.6, where the PLC Tx is represented by its Thevenin equivalent circuit, while PLC Rx and LISNs are represented by impedance matrices.

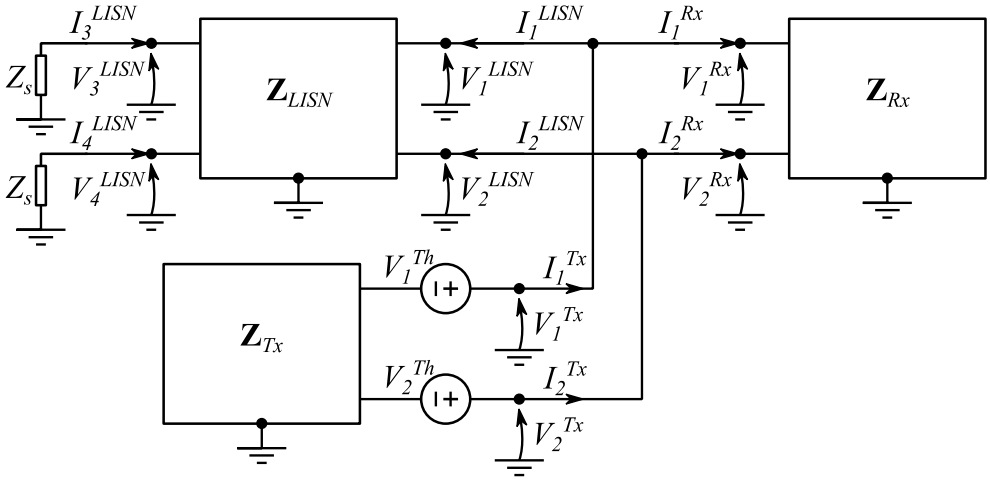

Figure 5.6: Reference circuit for the calculation of PLC Tx Thevenin equivalent circuit voltages.

To evaluate open voltage sources, V_1^{LISN}, V_2^{LISN}, the measurement of the voltages at the LISNs signal ports by means of an oscilloscope is the first step. The spectrum of the time-domain measured voltages is hence evaluated by FFT. The obtained frequency-domain voltages are hereinafter labelled as V_3^{LISN}, V_4^{LISN}. Therefore, neglecting the coaxial cables contributions, the currents drawn from the LISNs signal ports I_3^{LISN}, I_4^{LISN} can be determined as:

$$I_3^{LISN} = -\frac{V_3^{LISN}}{Z_S} \qquad (5.3)$$

$$I_4^{LISN} = -\frac{V_4^{LISN}}{Z_S} \tag{5.4}$$

where Z_S is the oscilloscope input impedance.

Then, the voltages V_1^{LISN}, V_2^{LISN} and the currents I_1^{LISN}, I_2^{LISN} at the LISNs power ports can be determined by means of the ABCD representation of the LISN block, which is directly obtained from the measured S-parameters as:

$$\begin{bmatrix} V_1^{LISN} \\ V_2^{LISN} \\ I_1^{LISN} \\ I_2^{LISN} \end{bmatrix} = \begin{bmatrix} \mathbf{A}_{LISN} & \mathbf{B}_{LISN} \\ \mathbf{C}_{LISN} & \mathbf{D}_{LISN} \end{bmatrix} \begin{bmatrix} V_3^{LISN} \\ V_4^{LISN} \\ -I_3^{LISN} \\ -I_4^{LISN} \end{bmatrix} \tag{5.5}$$

Once voltages and currents at the LISN power ports are obtained from (5.5), the circuit reported in Figure 6 can be solved to determine the voltage sources of the PLC Tx Thevenin equivalent circuit. To this end, a two-port representation of all elements is required. Hence, the port constraints at the PLC Tx and PLC Rx and related transmission line ports are hence represented by the following constitutive relations:

$$\underbrace{\begin{bmatrix} V_1^{Rx} \\ V_2^{Rx} \end{bmatrix}}_{\mathbf{V}_{Rx}} = \mathbf{Z}_{Rx} \underbrace{\begin{bmatrix} I_1^{Rx} \\ I_2^{Rx} \end{bmatrix}}_{\mathbf{I}_{Rx}} \tag{5.6}$$

$$\underbrace{\begin{bmatrix} V_1^{Tx} \\ V_2^{Tx} \end{bmatrix}}_{\mathbf{V}_{Tx}} = \underbrace{\begin{bmatrix} V_1^{Th} \\ V_2^{Th} \end{bmatrix}}_{\mathbf{V}_{Th}} - \mathbf{Z}_{Tx} \underbrace{\begin{bmatrix} I_1^{Tx} \\ I_2^{Tx} \end{bmatrix}}_{\mathbf{I}_{Tx}} \tag{5.7}$$

where voltages and currents are defined as in Figure 5.6.

It is similarly needed to determine a 2×2 impedance representation of the LISNs. This requires converting the full 4×4 S matrix $\mathbf{S}_{LISN}$ in the corresponding 4×4 impedance matrix $\mathbf{Z}_{LISN}$, according to (5.2). Successively, the desired 2×2 impedance matrix is obtained considering that the LISNs signal ports are terminated on the oscilloscope ports impedances Z_s (which is not necessarily equal to 50 Ω), as depicted in Figure 5.6. The port constraints at the LISN ports read:

$$\underbrace{\begin{bmatrix} V_1^{LISN} \\ V_2^{LISN} \\ V_3^{LISN} \\ V_4^{LISN} \end{bmatrix}}_{\mathbf{V}_{LISN}} = \mathbf{Z}_{LISN} \underbrace{\begin{bmatrix} I_1^{LISN} \\ I_2^{LISN} \\ I_3^{LISN} \\ I_4^{LISN} \end{bmatrix}}_{\mathbf{I}_{LISN}} \tag{5.8}$$

Substituting port constraints in (5.3), (5.4) into (5.8), the equivalent 2×2 impedance matrix $\mathbf{Z}_{LISN}^{2\times2}$ seen from port 1 and 2 of the LISNs is obtained as:

$$\underbrace{\begin{bmatrix} V_1^{LISN} \\ V_2^{LISN} \end{bmatrix}}_{\mathbf{V}_{LISN}^{2\times2}} = \underbrace{\begin{bmatrix} Z_{11}^{LISN} + k_{31}Z_{13}^{LISN} + k_{41}Z_{14}^{LISN} & Z_{12}^{LISN} + k_{32}Z_{13}^{LISN} + k_{42}Z_{14}^{LISN} \\ Z_{21}^{LISN} + k_{31}Z_{23}^{LISN} + k_{41}Z_{24}^{LISN} & Z_{22}^{LISN} + k_{32}Z_{23}^{LISN} + k_{42}Z_{24}^{LISN} \end{bmatrix}}_{\mathbf{Z}_{LISN}^{2\times2}} \underbrace{\begin{bmatrix} I_1^{LISN} \\ I_2^{LISN} \end{bmatrix}}_{\mathbf{I}_{LISN}^{2\times2}} \tag{5.9}$$

Where:

$$k_{31}=\frac{Z_{34}^{LISN}Z_{41}^{LISN}-Z_{31}^{LISN}\left(Z_{44}^{LISN}+Z_S\right)}{\left(Z_{33}^{LISN}+Z_S\right)\left(Z_{44}^{LISN}+Z_S\right)-Z_{34}^{LISN}Z_{43}^{LISN}},\ k_{32}=\frac{Z_{34}^{LISN}Z_{42}^{LISN}-Z_{32}^{LISN}\left(Z_{44}^{LISN}+Z_S\right)}{\left(Z_{33}^{LISN}+Z_S\right)\left(Z_{44}^{LISN}+Z_S\right)-Z_{34}^{LISN}Z_{43}^{LISN}}$$
$$k_{41}=\frac{Z_{43}^{LISN}Z_{31}^{LISN}-Z_{41}^{LISN}\left(Z_{33}^{LISN}+Z_S\right)}{\left(Z_{33}^{LISN}+Z_S\right)\left(Z_{44}^{LISN}+Z_S\right)-Z_{34}^{LISN}Z_{43}^{LISN}},\ k_{41}=\frac{Z_{43}^{LISN}Z_{32}^{LISN}-Z_{42}^{LISN}\left(Z_{33}^{LISN}+Z_S\right)}{\left(Z_{33}^{LISN}+Z_S\right)\left(Z_{44}^{LISN}+Z_S\right)-Z_{34}^{LISN}Z_{43}^{LISN}} \quad (5.10)$$

and Z_{xy}^{LISN} indicates (x,y) entry of matrix $\mathbf{Z}_{LISN}$.

Since the three two-port circuit elements are connected in parallel, i.e.:

$$\mathbf{V}_{LISN}=\mathbf{V}_{Rx}=\mathbf{V}_{Tx} \quad (5.11)$$

Combining (5.6), (5.7), (5.9), and (5.11), the equivalent voltage sources of the Thevenin equivalent circuit V_1^{Th}, V_2^{Th} are hence obtained as:

$$\mathbf{V}_{Th}=\left(\mathbf{Z}_{LISN}^{2\times2}+\mathbf{Z}_{Tx}+\mathbf{Z}_{Tx}\mathbf{Z}_{Rx}{}^{-1}\mathbf{Z}_{LISN}^{2\times2}\right)\mathbf{I}_{LISN} \quad (5.12)$$

5.4. Experimental Investigation the Proposed Behavioral Model

5.4.1. Test Setup

The experimental test setup is shown in Figure 5.7. The PLC Tx and Rx modems communicate through a short AC transmission line, which is connected to the 230 V AC mains through two HV-AN 150 LISNs, whose measurement ports are connect to the oscilloscope Keysight DSOX1204G with the objective of measuring the noise from the system under test. The oscilloscope input impedance Z_S is set equal to 1 MΩ in parallel with a 16-pF capacitor [69]. This measurement will be used for both the extraction of the active part of the model and model validation, as LISNs offer proper ports for EMI measurement. The specific G3-PLC modems are Microchip ATMEL P360 with a maximum bandwidth of 500 kHz [70]. In this specific task, the two PLC modems communicate in the CENELEC A band between 35 and 91 kHz; in this frequency range, the PLC modem (transmitter) can be regarded as an intentional noise source. 5000 frames of data are sent from the transmitter modem to the receiver modem with a 100 ms lag between consecutive frames. The PHY layer specifications of the G3-PLC modem summarized in Table 4.1 are used again in this part.

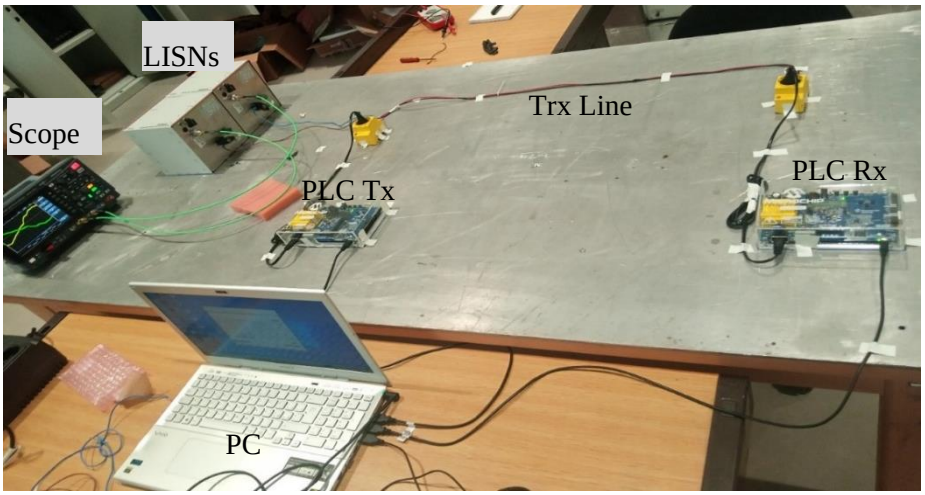

Figure 5.8: Experimental test bench to measure active parts of the proposed behavioral model.

The operating mode of the HV-AN 150 LISN can be switched to comply with several EMC standards, including the most common CISPR 16-1-2, CISPR 25, MIL-STD 461F, and DOG-160G standards [68]. Therefore, they can be easily exploited to realize different working conditions. To extract the active parts of the behavioral model, the LISNs are configured to work for DOG-160G (LISN A); this will be referred to as the "reference case" hereafter. Then, the following two cases are considered for model validation. In the former test case (case #1), the DOG-160G standard LISNs are modified by adding 0.047 uF capacitors at the EUT sides (LISN B1). The second test case (case #2) is obtained by adding the same 0.047 uF capacitors at the EUT sides of the CISPR 25 LISNs (LISN B2). The reference and test cases are shown in Table 5.1 and Figure 5.8.

Table 5.1: LISN setups used to realize different working conditions.

Case	Implementation
Reference (LISN A)	DOG-160G
#1 (LISN B1)	DOG-160G + 0.047uF capacitors at the EUT sides
#2 (LISN B2)	CISPR 25 + 0.047uF capacitors at the EUT sides

Figure 5.9 shows the test setup to characterize the LISN. The LISN is characterized by the four-port VNA Keysight E5080B ENA. The measured input impedance of the LISNs looking from port 1 and port 2 is shown in Figure 5.10. As seen clearly, all the three LISNs show different impedance and it is possible to use LISN B1 and LISN B2, to verify our results both above and below 100 kHz.

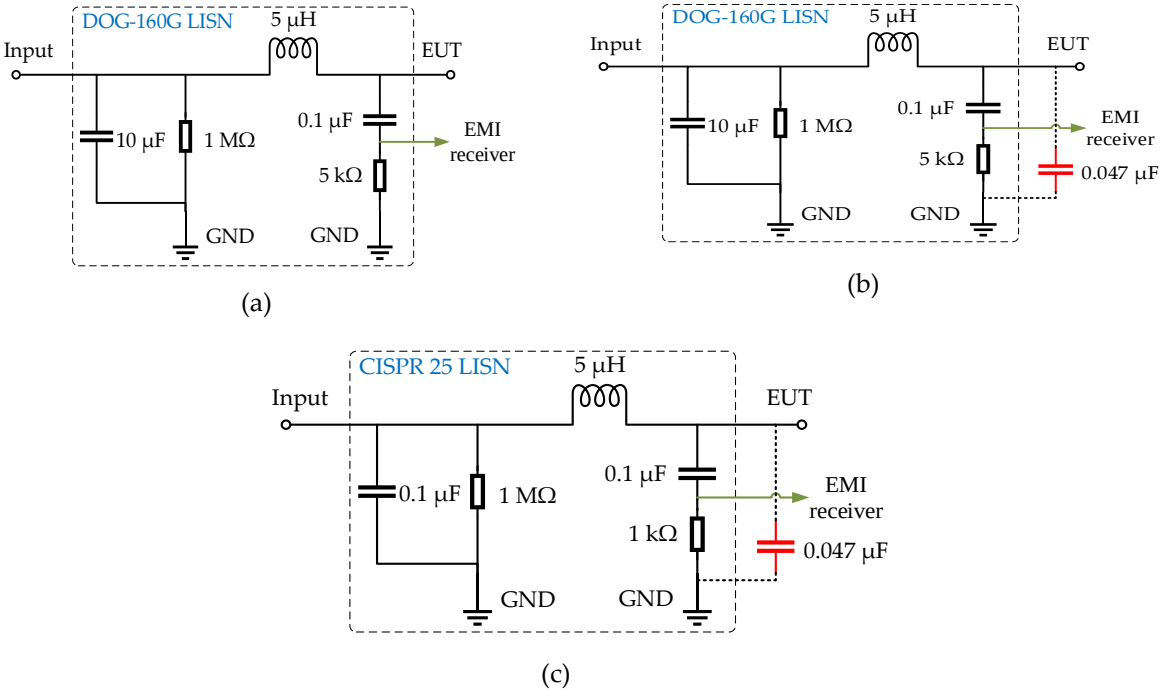

Figure 5.9: Circuit representation of: (a) DOG-160G LISN (LISN A), (b) LISN B1, and (c) LISN B2 exploited in this work for model extraction (a), and verification (b), (c). Only one polarity (either P or N with reference to ground) is shown as an example.

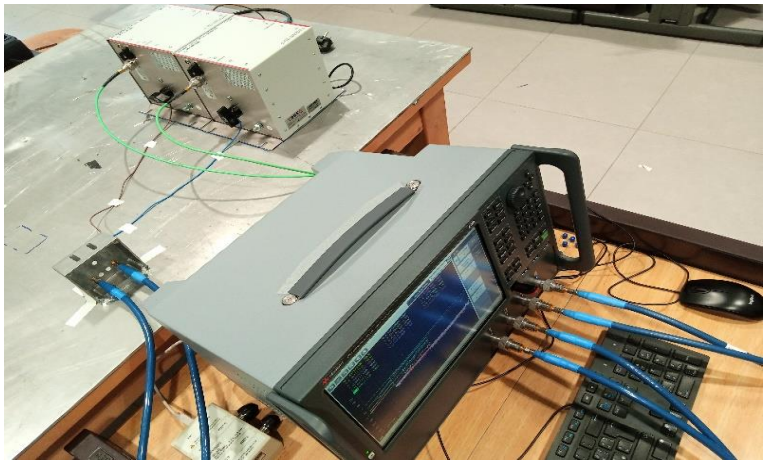

Figure 5.10: Experimental test bench to characterize the LISN.

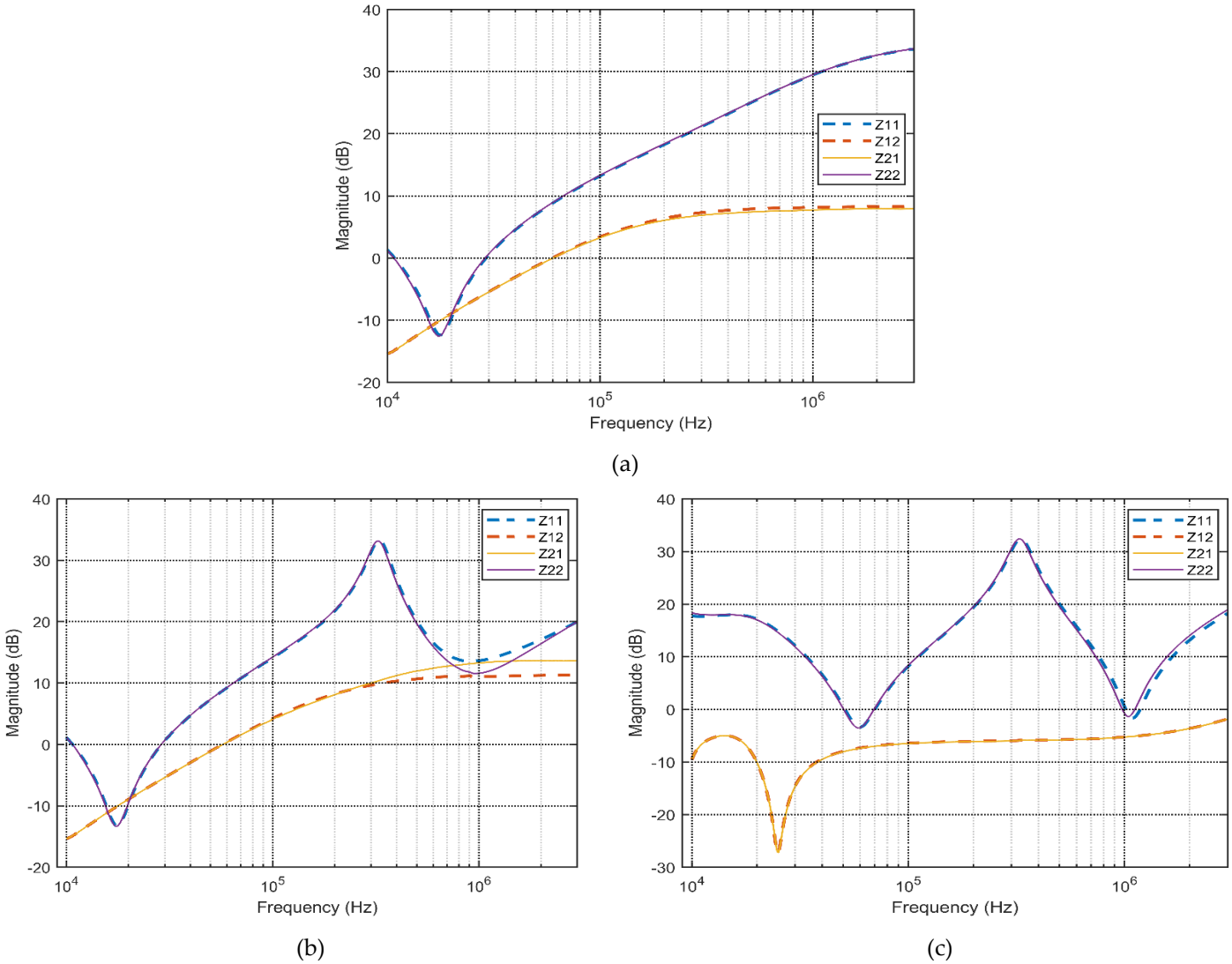

Figure 5.11: Impedance plot of: (a) DOG-160G LISN (LISN A); (b) LISN B1; and (c) LISN B2.

5.4.2. Extraction of the Behavioral Model

Figure 5.11 shows the experimental test setup to characterize the PLC modems, where the PLC Tx modem is characterized independently, whereas the PLC Rx modem is characterized together with the transmission line and the load. The impedance plots of the G3-PLC modems are summarized in Figure 12(a) and (b).

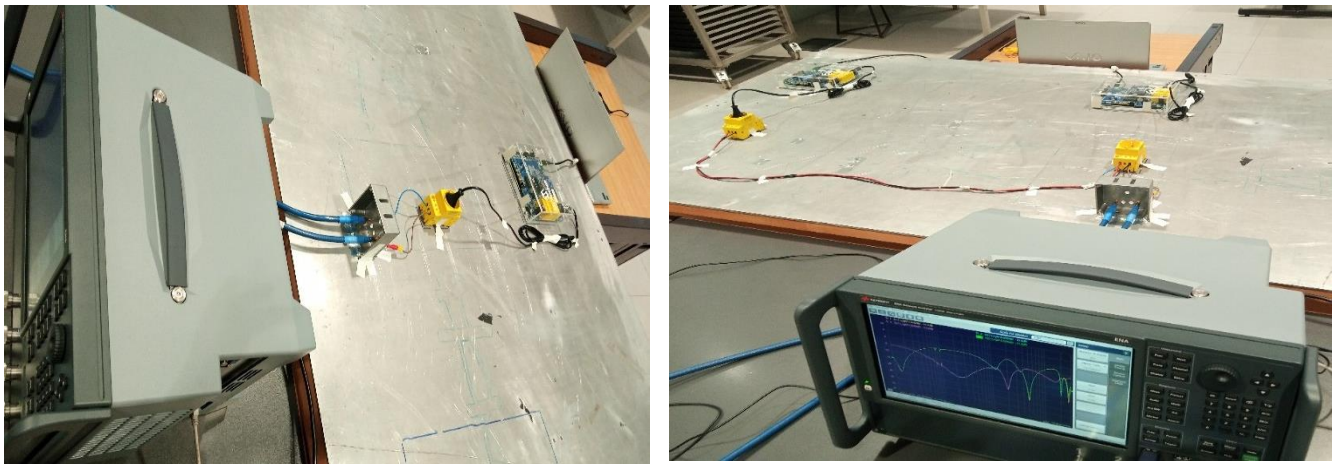

(a) (b)

Figure 5. 12: Experimental test bench to characterize: (a) the transmitting PLC modem, (b) the receiving PLC modem together with transmission line.

To extract the active part of the behavioral model, the noise measurement is carried out with the setup shown in Figure 5.7, in conjunction with the employment of the reference LISN (LISN A). Then, based on (5.12), the equivalent voltage sources $\mathbf{V}_{Th-A}=[V_1^{Th};V_2^{Th}]$ can be obtained, as shown in Figure 12(c).

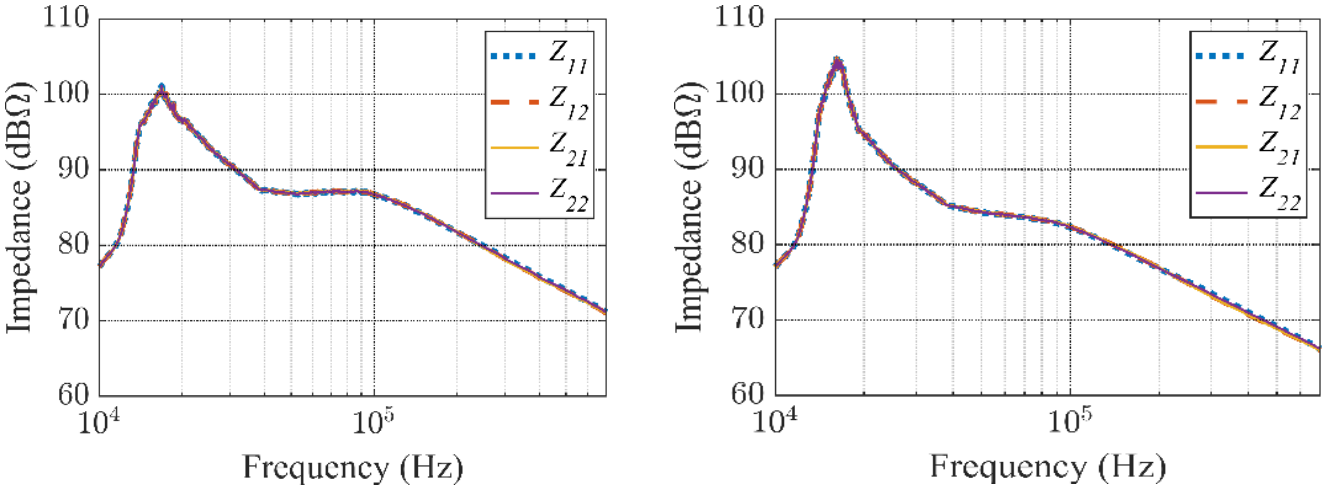

(a) (b)

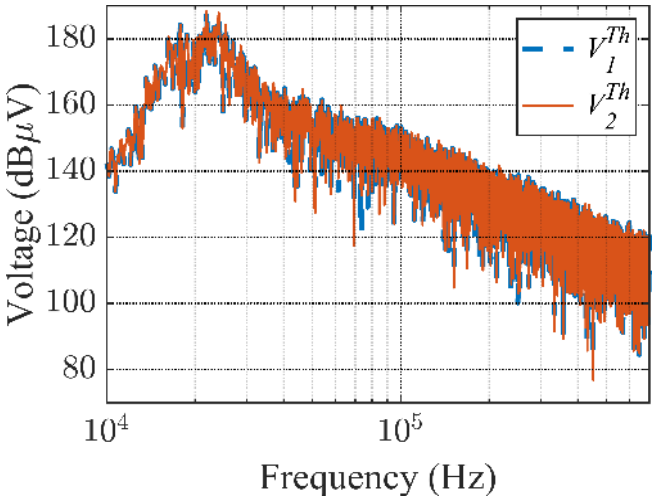

(c)

Figure 5.13: Behavioral model parameters: Impedances of (a) the PLC Tx modem and (b) the PLC Rx modem together with the transmission line; and (c) equivalent voltage sources.

5.4.3. Test Results and Discussions

To verify the accuracy of the extracted behavioral model, the two test LISNs (LISN B1 and B2) are employed to replace the reference LISN (LISN A) in Figure 5.7, denoted as Test case #1 and #2. As clearly shown in Figure 5.8, they have impedances significantly different from LISN A, and therefore provide different working conditions ($\mathbf{Z}_{LISN-B1,B2}^{2\times2}$). The predicted values are computed by integrating the behavioral model of the PLC system, which is extracted based on the reference case, into the test cases. Specifically, the line currents $\mathbf{I}_{LISN-B1,B2}$ are predicted by:

$$\mathbf{I}_{LISN-B1,B2} = \left(\mathbf{Z}_{LISN-B1,B2}^{2\times2} + \mathbf{Z}_{Tx} + \mathbf{Z}_{Tx}\mathbf{Z}_{Rx}^{-1}\mathbf{Z}_{LISN-B1,B2}^{2\times2}\right)^{-1}\mathbf{V}_{Th-A} \qquad (5.13)$$

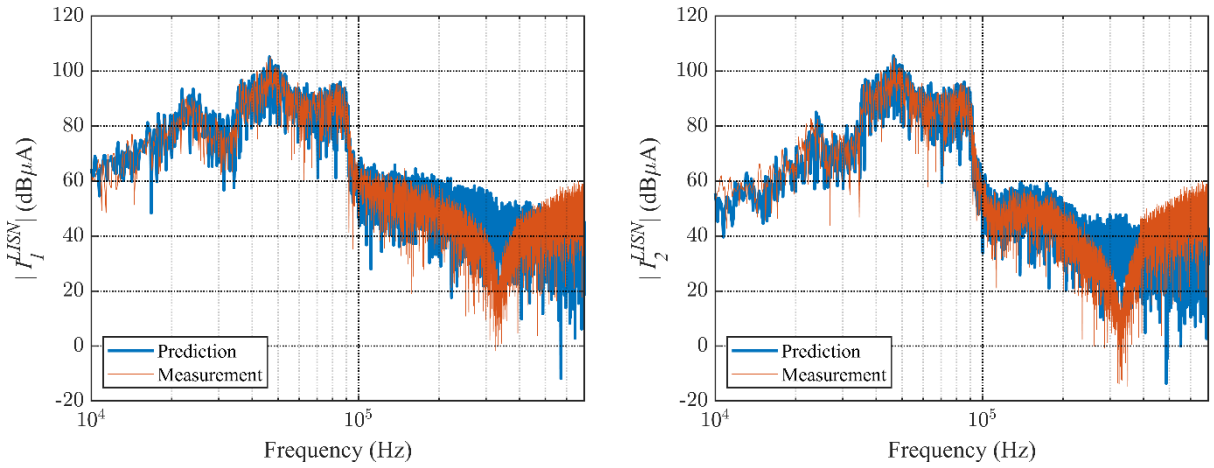

(a) (b)

Figure 5.14: Comparison between the currents I_1^{LISN} and I_2^{LISN} obtained from the prediction model and the measurement of test case #1 (with LISN B1). In the prediction model, the PLC Tx is represented by the improved behavioral model extracted based on the procedure shown in Sec. 5.3.

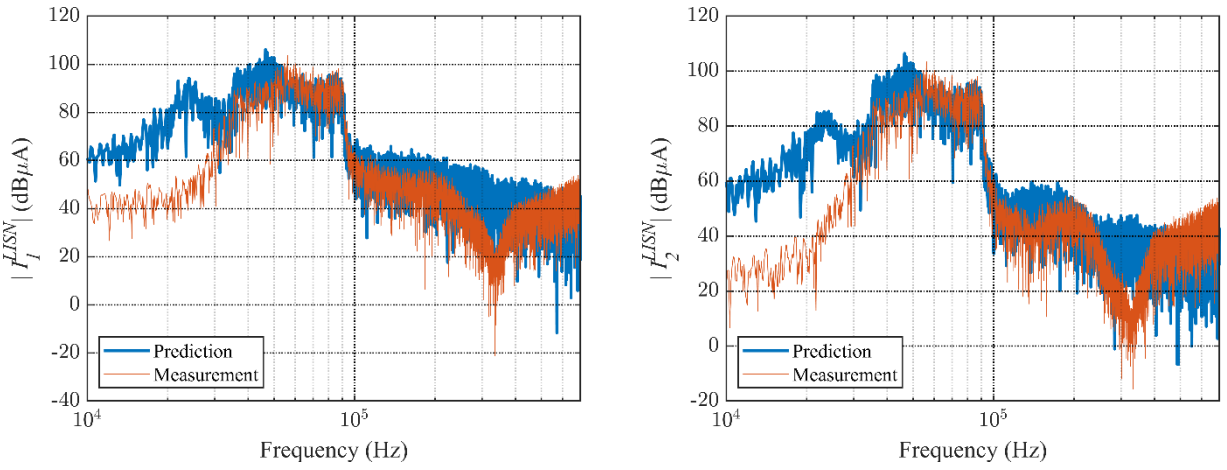

Figure 5.15: Comparison between the currents I_1^{LISN} and I_2^{LISN} obtained from the prediction model and the measurement of test case #2 (with LISN B2). In the prediction model, the PLC Tx is represented by the improved behavioral model extracted based on the procedure shown in Sec. 5.3.

Figure 5.13 shows the line currents obtained from the prediction and the measurement of test case #1. The measured and predicted currents show good consistency below 100 kHz, while some discrepancies are present above 100 kHz. This might be due to the fact that the characteristics of the reference LISN A and the verification LISN (in this case LISN B1) have the same impedance below 100 kHz, while their impedance is different at higher frequencies. This can be noticed by comparing Figure 5.8(a) and 5.8(b). Therefore, to estimate the accuracy of the model below 100 kHz, test case #2 is considered. The results are presented in Figure 5.14, which shows that this behavioral model cannot accurately predict the emissions also below 100 kHz when the working condition changes. These results indicate that the Thevenin equivalent circuit introduced in Section 5.3 is not a proper model for PLC modems since the modems are nonlinear in nature due to their embedded control systems. Indeed, it is easy to explain the results reported in Figure 5.14 considering that the PLC system is designed to inject a controlled signal into the grid, so that its output voltage is related to its output current through suitable control loops. Therefore, an accurate behavioral model of the PLC modems is still required, which will be discussed in the next section.

5.5. Improved Behavioral Model of PLC Tx

As discussed in Section 5.4, the modelling approach proposed in Section 5.3 for the considered PLC systems is not effective. This can be ascribed to the closed-loop control included in the PLC system, which is in contrast with the linearity hypothesis required for the validity of Thevenin equivalent circuits. If this interpretation is correct, it is then possible to model the PLC Tx by substitution theorem, using only a couple of ideal voltage sources. This model should consequently be valid at least in the frequency range in which the internal control algorithms work properly, and in a reasonable range of system impedances. PLC Rx and LISN models are unchanged. Unlike the previous modelling approach, this approach to PLC Tx modelling is supported considering the effect of the PLC control system, which is designed to provide a consistent communication signal regardless of the system impedances.

As a consequence, the circuit reported in Figure 5.6 should be revised as reported in Figure 5.15

.

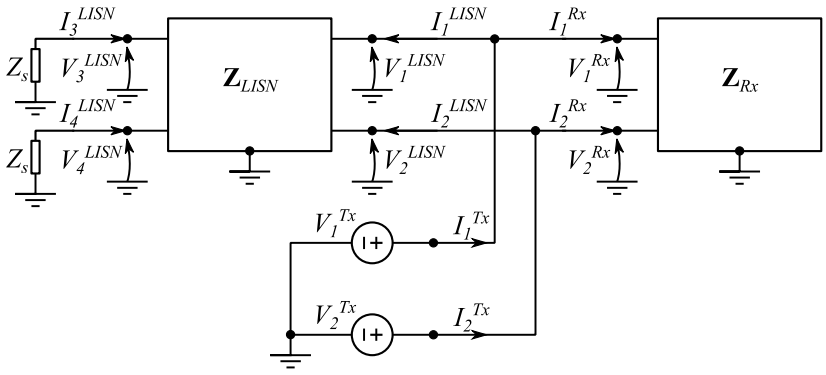

Figure 5.16: Reference circuit for calculation of PLC Tx equivalent voltage sources.

Since the PLC Tx is modelled as a couple of ideal voltage sources, the voltages at the LISNs power ports are equal to the PLC Tx equivalent voltage sources. As a consequence, the voltage sources are obtained directly from measures in the LISN-A setup, namely:

$$\mathbf{V}_{Tx} = \mathbf{V}_{LISN-A}^{2\times 2} \tag{5.14}$$

The frequency responses of the voltage sources are plotted in Figure 5.16.

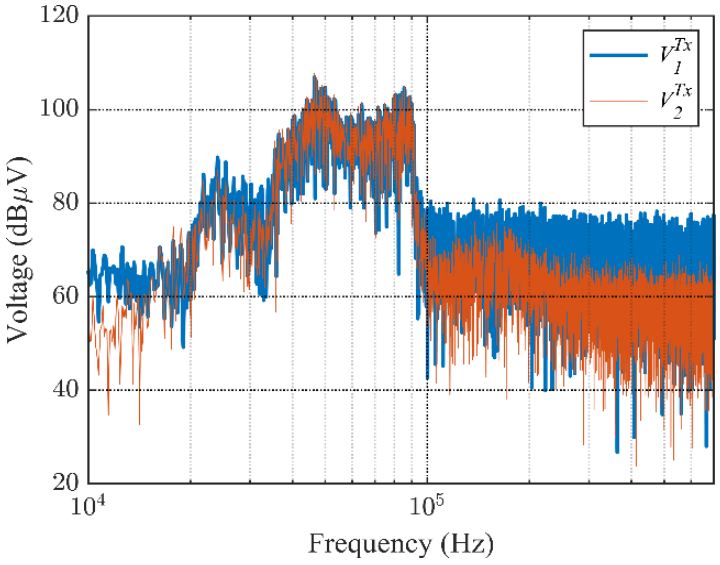

Figure 5.17: Equivalent voltages sources of the improved behavioral model of PLC Tx.

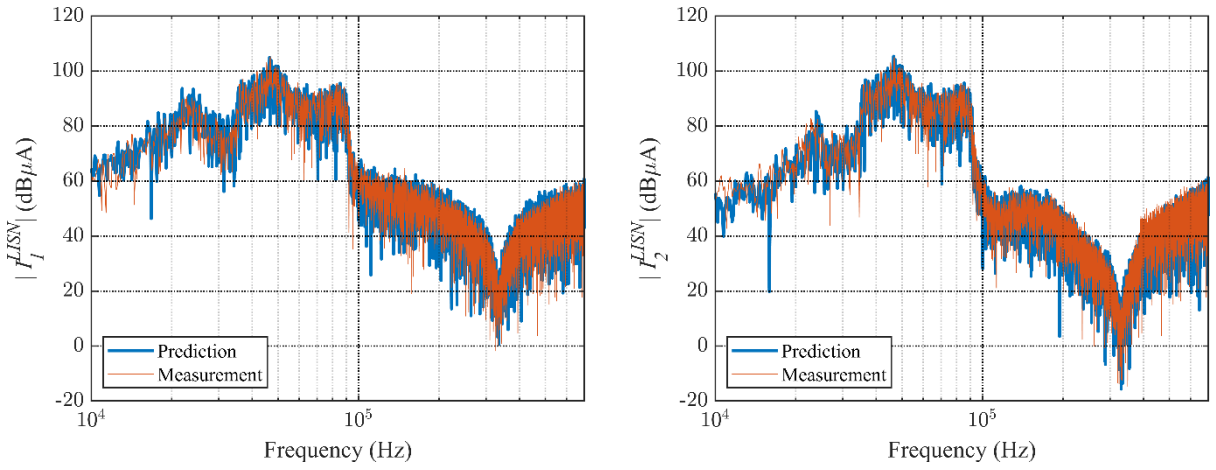

(a) (b)

Figure 5.18: Comparison between the predicted and measured currents I_1^{LISN} and I_2^{LISN} in test case #1 (with LISN B1). In the prediction model, the PLC Tx is represented by the improved behavioral model extracted based on the procedure shown in Sec. 5.5.

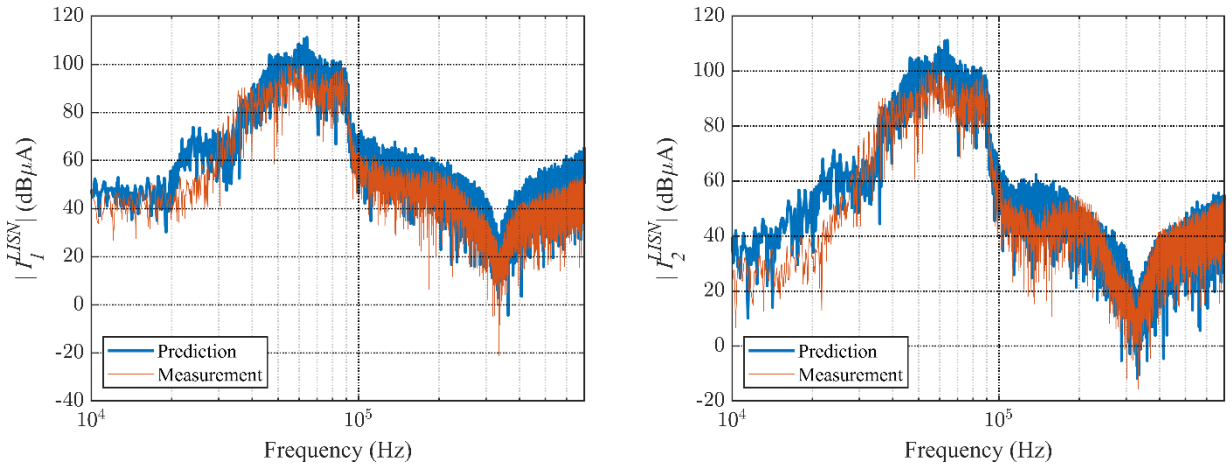

(a) (b)

Figure 5.19: Comparison between the predicted and measured currents I_1^{LISN} and I_2^{LISN} in test case #2 (with LISN B2). In the prediction model, the PLC Tx is represented by the improved behavioral model extracted based on the procedure shown in Sec. 5.5.

5.6. Final Experimental Validation

The model verification is again based on current predictions. In particular, the model is considered verified if the predicted currents obtained from:

$$\mathbf{I}_{LISN-B} = \mathbf{Z}_{LISN-B}^{2\times 2\,-1}\mathbf{V}_{Tx} \qquad (5.15)$$

match the corresponding measures in the LISN-B setup. Concerning test case #1, the predicted currents based on the improved model based on substitution theorem are compared with the measurement results in Figure 5.17. This improved behavioral model can predict the line currents very well up to 500 kHz, which is the maximum frequency band width of the NB G3-PLC. Of course, as explained in Section 5.4.2, since the measured currents with LISN A and LISN B1 are the same below 100 kHz, another verification test (test case #2) with LISN B2 is carried out. The results are shown in Figure 5.18. The

measured and predicted line currents also show a very good agreement up to 500 kHz including the range below 100 kHz. This is a big improvement compared to the predictions from traditional behavioral model (see: Figure 5.15). Therefore, approximating the G3-PLC Tx as two voltage sources is by far the better option. These results are consistent with the idea behind the use of the pure voltage source to model the PLC Tx system. Indeed, the G3-PLC modems provide a spectrum with constant amplitude in the frequency range between 35-91 kHz according to the standard ITU-T G.9901. Additionally, the control system inside them and the robust modulation schemes (OFDM) in this PLC protocol allows to provide a constant spectrum up to 500 kHz. At higher frequency, the effect of the PLC control system will progressively fade, resulting in an uncontrolled LTI system. This is in line with behavioral modelling of power converters [74], which has been successfully applied in a frequency range significantly higher (one decade at least) than the one in which the converter control system is designed to operate.

5.7. Conclusion

In this chapter, an experimental test campaign aimed at providing a suitable black-box model for the G3-PLC system is presented. With the final goal of using the black-box model of the G3-PLC modems in the EMI analysis of complex networks, a set of black-box modelling approaches was compared, and a suitable model was proposed. The modeling aimed to have a separate model of both transmitting PLC and receiving PLC modems so that the model can be easily integrated in any complex networks. Therefore, firstly the black-box modeling approach based on Norton Thevenin equivalent circuit, has been investigated by considering the G3-PLC modem as an intentional noise source. This modelling approach requires the system under analysis to be linear and time invariant, which is not true for G3-PLC system due to their internal control systems. Experimental results proved that representing the G3-PLC modem as a Norton Thevenin equivalent result in inaccurate prediction of EMI noise.

An alternative modelling approach of the G3-PLC system based on the substitution theorem was then proposed, where the PLC Tx was approximated by a couple of independent voltage sources. This modeling approach accurately represented the PLC modems in the frequency band of the G3-PLC. This model is also in line with the ITU-T G.9901 standard, that specifies the amplitude of the spectrum in which the G3-PLC modem uses constant amplitude at the frequency band of interest (below 500 kHz) in the worst operating conditions. In future works, the model of the PLC modems will be used to assess the cross interference between communication systems and different noise sources in complex power system networks such as SG.

CHAPTER 6

Conclusions and Main Contributions

6.1. Conclusions

In this thesis, electromagnetic coexistence between power and data lines in PLC system has been investigated. In particular, the electromagnetic interference between power electronics converters and narrow band PLC systems have been studied comprehensively. Since accurate modelling of electromagnetic noise sources is required to predict the EMI between power and data lines, the first part of the thesis work focused on modelling of power electronics converters. In this regard, both white-box and black-box modelling techniques were investigated in detail considering their application in predicting EMI emissions in complex networks, such as LV distribution networks, and their respective application limitations. Indeed, the white-box modelling approach been implemented to study CE propagation from the LV network to the main grid with the help of PSpice MATLAB co-simulation where different noise sources are modelled in PSpice considering parasitic elements and MATLAB SIMULINK was used to implement control schemes for synchronization. The work started from detail modelling of the LV network components such as transmission lines, inverter, load, transformer and shunt capacitor. The effects of the PFC capacitors, circuit breakers, transmission lines and power factor of the loads on CE propagation have been investigated thoroughly. On the other hand, the black-box modelling approach been applied to a three-phase inverter connected with a PV panel, and the procedures and the possible limitations of this modelling approach have been investigated.

Next to this, the thesis focused on finding alternative solutions to reduce the CE of power converters by using RPWM schemes. The thesis summarized the details of the implementation of different RPWM techniques both in simulation software and practical experiments as well as the comparison of those RPWM techniques in terms of CE reduction. Besides, the main parameters which affect the effectiveness of the specific RPWM techniques have been investigated. It was proven that the spreading factor plays a significant role in the reduction of the CE of randomly modulated power converters.

Further, the thesis investigated possible coexistence issues between randomly modulated power converters and coexisting PLC systems using both simulation tools and laboratory experiments. In this regard, the simulation activity was carried out to study the effects of using RPWM to control the switching activity of power electronics converters in power systems involving PLC for advanced meter reading. Additionally, the effects of connecting the PLC modems to the power line in different configurations have been investigated. The simulation results have been supported by laboratory experiments aimed at examining the interference between RPWM modulated SiC based DC-DC converter and G3-PLC systems, where the performance of the G3-PLC has been investigated with controlling different parameters of RPWM scheme driving power converter (switching frequency, spreading factor and RNUR. Indeed, different RPWM schemes have been compared to draw general conclusions on the effectiveness of RPWM in assuring coexistence.

Eventually, the thesis discussed the activity carried out to find suitable black-box model for the G3-PLC system. With the final goal of using the black-box model of the G3-PLC modems in the EMI analysis of complex networks, a suitable black-box model for the G3-PLC modem was proposed. The modeling aimed to have a separate model of both transmitting PLC and receiving PLC modems. Of course, the proposed model can be used in future activities in EMI and coexistence issue assessment of smart grids.

In the following, the research activity results discussed within this thesis are summarized.

- The Modelling of EMI noises sources with the help of different software such as PSpice SIMULINK cosimulation has been discussed. This cosimulation feature provides the simulation environment where different circuits can be modelled in PSpice considering parasitics and different controlling schemes can be implemented by using SIMULINK. This enables us to make nearly practical EM modelling and simulations.
- Black-Box modelling approach is very beneficial in EM simulation specially in providing a simplified model of electric devices. However, this modelling approach is applicable only for linear time invariant systems and for frequency-domain simulation.
- In EMI analysis of power system networks such LV systems, it is tremendously important to consider the effects of parasitic elements of different power system components such as power converters, transformers, PFC capacitors, circuit breakers, busbars and transmission lines. Besides, it is extremely important to take account the connection of PFC capacitors while making EMI simulations. Indeed, the parasitic elements and the connection of PFC capacitors have been found significantly affecting the propagation of CE from the LV network to the main grid.
- Among the EMI mitigation techniques, the use of RPWM in reducing the CEs of power converters is important especially in application where size and weight are a great concern. RPWM techniques allow to mitigate CE from the source and are relatively cheaper and easier option compared to other mitigation techniques, for instance EMI filter. In fact, most of the DC-DC converters use these techniques to pass the EMC compliance tests. Of course, there are application limitation associated with coexisting communication systems such as PLC system where the benefit of using RPWM is questionable.
- RPWM based converters can be considered as a potential trait to current smart grids. In fact, RPWM based converters can be more detrimental to the communication system in smart grids such as PLC systems compared to conventional PWM based power converters. Of course, this can be avoided by choosing different/non-over-lapping frequency bands for the converters and or the PLC systems. Besides, there are also RPWM techniques which are relatively more compatible with PLC systems such as RPPM. However, further investigation as well as standards are required in this regard since most of the switching frequencies of power converters fall in the frequency bands of NB PLC systems which are mostly deployed in smart grid applications.
- Eventually, EMI models of PLC systems are important to predict and study CE propagation in smart grid applications. Since modelling the PLC system using detailed network elements is very challenging and almost impossible, an approximate model using black-box modelling approach has been investigated. The proposed model can be integrated in any smart grid network and can be used to study the CE propagation throughout the network as well as to study the interference between noise sources and PLC systems. As future extension of the activity, the interference between the power converters and PLC systems in smart grids will be investigated by using the black-box modeling approach.

6.2. Main Contributions

This thesis is prepared by Early-Stage Researcher (ESR 5) from the European Training Network of PhD researchers on Innovative EMI analysis and Power Applications (ETOPIA) project. The ETOPIA project has received funding from the European Union's Horizon 2020 research and innovation program under the Marie Skłodowska-Curie grant agreement No. 812753. With the main objective to train new EMC researchers with a closer interaction of electrical power and power electronics with information technology and communications equipment, six universities (University of Twente, University of Craiova, Politecnico di Milano, Leibniz University, University of Zielona Gora and University of Nottingham) and more than 20 partner organizations have been participated in ETOPIA project.

There were 8 Work Packages (WP) in the ETOPIA project, which helps for the successful and efficient project execution according to work plan, and maintenance of relations between partners and ESRs. Indeed, the author of this thesis (here in after ESR 5) has been working on the project titled "Advanced communication and modulation techniques to assure coexistence of power and data" under WP7, EM coexistence, with the following project objectives.

- To provide a methodology for ensuring the coexistence of communications within converter dense ac and dc power systems.
- Experimental characterization and modelling of the EMI environment in applications characterized by the presence of power converters, such as smart sub-stations, islanded micro-grids, ships, electric and hybrid vehicles.
- Coexistence of ac and dc lines. Characterization by simulation and measurement of the interference induced on data lines.
- Identification of hardware and software (communication techniques) solution to assure coexistence with control lines and communication systems. Investigation on the feasibility of applying the powerline communications technology in these contexts.
- Identification and/or development of suitable modulation schemes, based on random and/or spread spectrum techniques, to mitigate conducted, and therefore radiated, emissions generated by power converters.

Therefore, ESR 5 has been performing different activities to achieve the goals/objectives set by the ETOPIA project. This included the main research activities such as courses, simulations, and experiments, as well as collaboration with Universities and Industrial partners through secondments. The secondments as well as research collaboration works are summarized in Table 6.1.

Table 6.1: Summary of academic and industrial secondments covered by ESR 05.

Seconded to	**Start date**	**End date**	**Duration months**	**Goals of secondment**
RSE	01/04 /2020	31/12 /2021	4	▪ Black-Box modelling of power converters. ▪ Modelling and CE prediction of an LV network.
University of Zielona Góra	01/05 /2020	17/12 /2021	0.17	▪ Studied the interference between Randomly Modulated converters and PLC system both in simulation and experimental activities
University of Craiova	13/05 /2021	27/11 /2022	1	▪ Comparison of conventional (FFT based OFDM) Vs Wavelet based OFDM for PLC application in Smart Grid and, ▪ Collaborated on the co-existence issue of power and data lines in PLC system

ABB	01/07 /2022	31/07 /2022	0.5	▪ Performed Near Field immunity test in close proximity in the ABB lab. ▪ Collaborated on the design and simulation of Horn antenna for Near RF field immunity test

6.2.1. Research Contributions

In the following, the main research contributions are summarized.

- White-box and black-box EMI models of power electronics converters together with their limitations as well as their application in predicting EMI in different power system networks has been provided.
- This thesis provided the detailed analysis of an alternative EMI mitigation technique called Random Pulse Width Modulation. In this regard, both simulation models (including the procedures) as well as experimental findings have been provided.
- This thesis outlined the main challenges of smart grids associated with the coexisting power converters resorted to different modulation techniques and the PLC systems. Indeed, both simulation models and experimental findings have been provided. The results from this thesis can be used as a starting point to prepare standards for the future with regards to randomly modulated power converters used in smart grids.
- Finally, a novel EMI model of G3-PLC system has been provided. This model can be integrated to any power system networks and can help to predict EMI and study the coexistence issues.

6.2.2. Publications

Published Journal papers:

J1. **A. H. Beshir,** S. Negri; L. Wan, F. Grassi, X. Wu, X. Liu, G. Spadacini and S.A. Pignari, “Behavioural Model of the G3- Powerline Communication Modems for low frequency EMI analysis,” Energies, vol.16, pp.3336, 2023. https://doi.org/10.3390/en16083336

J2. **A. H**. **Beshir,** W. El Sayed, L. Wan, F. Grassi, P. S. Crovetti, X. Liu, X. Wu, A. Madi, R. Smolenski, and S.A. Pignari, “Influence of Random Modulated Power Converter on G3 Power Line Communication,” Appl. Sci. vol.12, pp.5550, 2022,. https://doi.org/10.3390/app12115550

J3. **A. H. Beshir**, L. Wan, F. Grassi, P. S. Crovetti, X. Liu, X. Wu, W. El Sayed, G. Spadacini and S.A. Pignari, “Electromagnetic Interference of Power Converter with Random Modulation on the Power Line Communication System,” Electronics, vol.10, pp.2979, 2021. https://doi.org/10.3390/electronics10232979

J4. L. Wan, **A. H. Beshir,** X. Wu, X. Liu, F. Grassi, G. Spadacini, S. A. Pignari, "Black-box Modeling of Converters in Renewable Energy Systems for EMC Assessment: Overview and Discussion of Available Models", Chinese Journal of Electrical Engineering, vol.8, no.2, pp.13-28, 2022.

J5. L. Wan, **A. H. Beshir**, X. Wu, X. Liu, F. Grassi, G. Spadacini, S. A. Pignari, M. Zanoni, L. Tenti, and R. Chiumeo, “Black-Box Modelling of Low-Switching-Frequency Power Inverters for EMC Analyses in Renewable Power Systems,” Energies, vol. 14, no. 12, p. 3413, Jun. 2021.

Published Conference papers:

C1. **A. H. Beshir**, Waseem El Sayed, Amr Madi, Lu Wan, Flavia Grassi, Paolo S Crovetti, Xinglong Wu, Xiaokang Liu, Robert Smolenski, Sergio A Pignari, "Effects of the Switching Frequency of Random Modulated Power Converter on the G3 Power Line Communication System," 2022 International Symposium on Electromagnetic Compatibility – EMC Europe, 2022, pp. 778-782, doi: 10.1109/EMCEurope51680.2022.9901074.

C2. **A. H. Beshir**, L. Wan, H. Loschi, D. Nascimento, F. Grassi, R. Smolenski, G. Spadacini, S. A. Pignari, "PSpice-Simulink Co-Simulation of the Conducted Emissions of a DC-DC Converter with Random Modulation," 2020 6th Global Electromagnetic Compatibility Conference (GEMCCON), 2020, pp. 1-4.

C3. **A. H. Beshir**, W.E. Sayed, L. Wan, F. Grassi, P.S. Crovetti, " Effects of Random Modulation on Powerline Communication system," presented at the APEMC 2021, Sept. 27-30, Bali, Indonesia.

C4. L. Wan, **A. H. Beshir**, Xinglong Wu, Xiaokang Liu, Flavia Grassi, Giordano Spadacini, Sergio A Pignari. "Un-terminated Black-Box EMI Models of Power Converters Driven by Random Modulation Strategies," 2022 International Symposium on Electromagnetic Compatibility–EMC Europe, 2022, pp. 758-763, doi: 10.1109/EMCEurope51680.2022.9901160.

C5. A. Madi, W. Elsayed, D. Nascimento, **A. H. Beshir**, P. Lezynski and R. Smolenski, "Influence of Chaotic spreading factor modulation based Random Modulation on G3-PLC system," 2022 International Symposium on Electromagnetic Compatibility – EMC Europe, 2022, pp. 770-773, doi: 10.1109/EMCEurope51680.2022.9901316.

C6. A. Madi, N. Moonen, W. Elsayed, **A. H. Beshir**, P. Lezynski and R. Smolenski, "Solving the grid overvoltage caused by connected PV systems: DSTATCOM based on MMC," *2022 IEEE International Symposium on Electromagnetic Compatibility & Signal/Power Integrity (EMCSI)*, 2022, pp. 221-225, doi: 10.1109/EMCSI39492.2022.9889562.

C7. L. Wan, **A. H. Beshir**, Xinglong Wu, Xiaokang Liu, Flavia Grassi, Giordano Spadacini, Sergio A. Pignari, "Cable Effects on Noise Propagation in Distribution Networks with Renewable Sources," 2022 20th International Conference on Harmonics & Quality of Power (ICHQP), 2022, pp. 1-6, doi: 10.1109/ICHQP53011.2022.9808610.

C8 L. Wan, **A. H. Beshir**, X. Wu, X. Liu, F. Grassi, G., Spadacini, S.A. Pignari, "Assessment of Validity Conditions for Black-Box EMI Modelling of DC/DC Converter", presented at the EMC+SIPI 2021, Jul.26-Aug. 20, 2021, Glasgow, UK.

C9. D. Nascimento, R. Smolenski, H. Loschi, F. Grassi, L. Wan, **A. H. Beshir**, "Electromagnetic Fields on 3-Phase Induction Motor Using Finite Element Analysis," presented at the EMC+SIPI 2021, Jul.26-Aug. 20, 2021, Glasgow, UK.

C10. L. Wan, A. Khilnani, **A. H. Beshir**, F. Grassi, G. Spadacini, S.A. Pignari, M. Sumner, D. Thomas, " Limitations in Applying the Existing LISN Topologies for Low Frequency Conducted Emission Measurements and Possible Solution," presented at the APEMC 2021, Sept. 27-30, Bali, Indonesia.

C11. A. Khilnani, L. Wan, M. Sumner, D. Thomas, **A. H. Beshir** and F. Grassi, "Conducted Emissions Measurements in DC Grids: Issues in Applying Existing LISN Topologies and Possible Solutions," 2021 IEEE 15th International Conference on Compatibility, Power Electronics and Power Engineering (CPE-POWERENG), 2021, pp. 1-6, doi: 10.1109/CPE-POWERENG50821.2021.9501169.

C12. L. Wan, **A. H. Beshir**, F. Grassi, G. Spadacini and S. A. Pignari, "SPICE Simulation of Modal Impedances in Automotive Powertrains under Different Operating Conditions," 2020 International Symposium on Electromagnetic Compatibility - EMC EUROPE, 2020, pp. 1-5.

Submitted manuscripts (under review):

J1. Waseem EL Sayed, Amr Madi, Robert Smolenski, Piotr Lezynski, Paolo Crovetti, **Abduselam Hamid Beshir**, Niek Moonen, and Frank Leferink . Performance of G3-PLC Channel in the Presence of Spread-Spectrum Modulated Electromagnetic Interference. IEEE Transactions on Electromagnetic Compatibility.

APPENDIX A1

Table A1.1: The Load profile of the LV network.

	P (kW)	cos_fi	A (kVA)	Q (kvar)	In (A)
U1	50	0,8	62	37	90
U2	65	0,85	76	40	110
U3A	30	0,9	33	14	48
U3B	20	0,8	25	15	36

Table A1.2: The details of the PFC capacitors of the LV network.

	cos_fi	S_id (kvar)	Q_id (kvar)	Delta Q (kvar)	C_th (µF)	C (µF)
C1	0,9	55	24	-13	3x88,1	3x99
C2	0,9	72	31	-8,8	3x58	3x66
C3A	0,9	33	14	0,0	0	
C3B	0,9	22	9,7	-5,3	3x35	3x33

Table A1.3: The transmission lines and the busbar profile of the LV network.

	Length (m)	Topology	Area (mm2)	Iz' (A)	r (mΩ/m)	x (mΩ/m)	Neutral conductor area (mm2)
L1	80	3x Single Core Cables with Sheath Cu	50	150	0,47	0,1	25
L2	70	3x Single Core Cables with Sheath Cu	70	184	0,33	0,1	35
L3A	20	3x Single Core Cables with Sheath Cu	25	100	0,89	0,1	16
L3B	30	3x Single Core Cables with Sheath Cu	25	100	0,89	0,1	16
L3	80	Three-core cables with neutral conductor Cu	50	141	0,49	0,1	
L0	3	Single Core Cables with Sheath Cu	3x70 per phase	3x184	0,33	0,1	3x35
S0	3	KSA400ED4306 Canalis - Straight element - 400 A (From Schneider catalog)		400	0,2	0,14	

Table A1.4: Transformer profile.

	An (Kva)	Indice Orario	Vp (kV)	Vs (V)	i_0 (%)	v_cc (%)	p_cu (%)	p_0 (%)
T0	250	Dyn11	20	400	1	4	1.04	0.21

Table A1.5: The description of the main grid (MV grid).

	Pcc (MVA)	R (LV side)	X (LV side)
MV network	500	0,000048	0,00031

Table A1.6: Description of the circuit breakers used in the LV network.

	Icc_3F (kA)	**Chosen switch (Schneider catalog)**	**Nominal Current (A)**
I0	8,879	Compact switch NSX400F - 400 A - 4 poli - S/ release	400
I1	4,439	Magnetic Switch NG125a 4P C 125A 16kA	125
I2	5,627	Magnetic Switch NG125a 4P C 125A 16kA	125
I3A	3,436	Magnetic Switch NG125a 4P C 80A 16kA	80
I3B	3,060	Magnetic Switch NG125a 4P C 80A 16kA	80
I3	4,490	Magnetic Switch NG125a 4P C 125A 16kA	125

Table A1.7: Parameters of the inverter model in Figure 2.4(b).

Parameter	**Value**	**Description**
Lw	10nH	External wire inductance
CEL	1.500mF	Nominal capacitance
LEL	30nH	Internal series inductance
REL	40 mΩ	Internal series resistance
Rd	1kΩ	Discharging resistance
Rwa	3.9 mΩ	Stray resistance
Lwa	0.36μH	Stray inductance
Cs	0.33μF	Nominal capacitor
Ls	30nH	Internal series inductance
Rs	30mΩ	Internal series resistance
LC	40nH	Collector stray inductance
LE	40nH	Emitter stray inductance
Chs	280pF	Stray capacitor between IGBT and heatsink

APPENDIX A2

A2.1. Generation of RPWM signals for the simulation activities

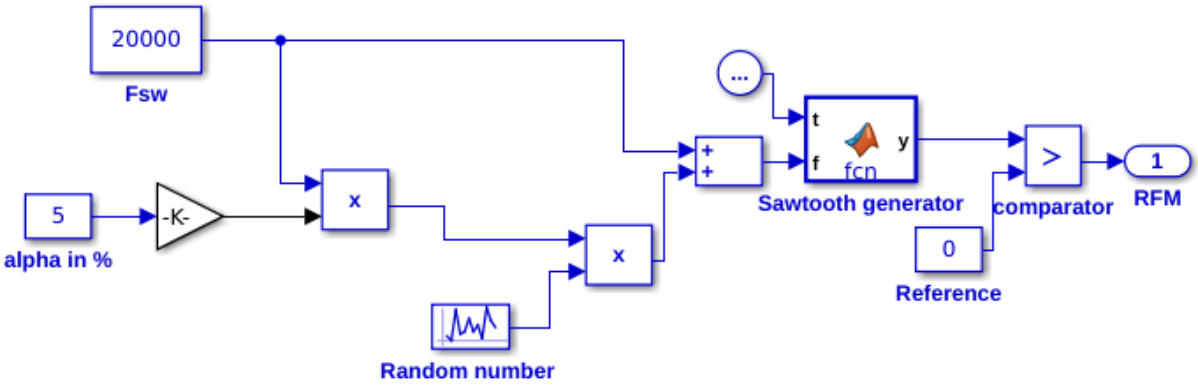

Figure A2.1: SIMULINK implementation of RFM for simulation activity carried out in Chapter 3, (Section 3.2).

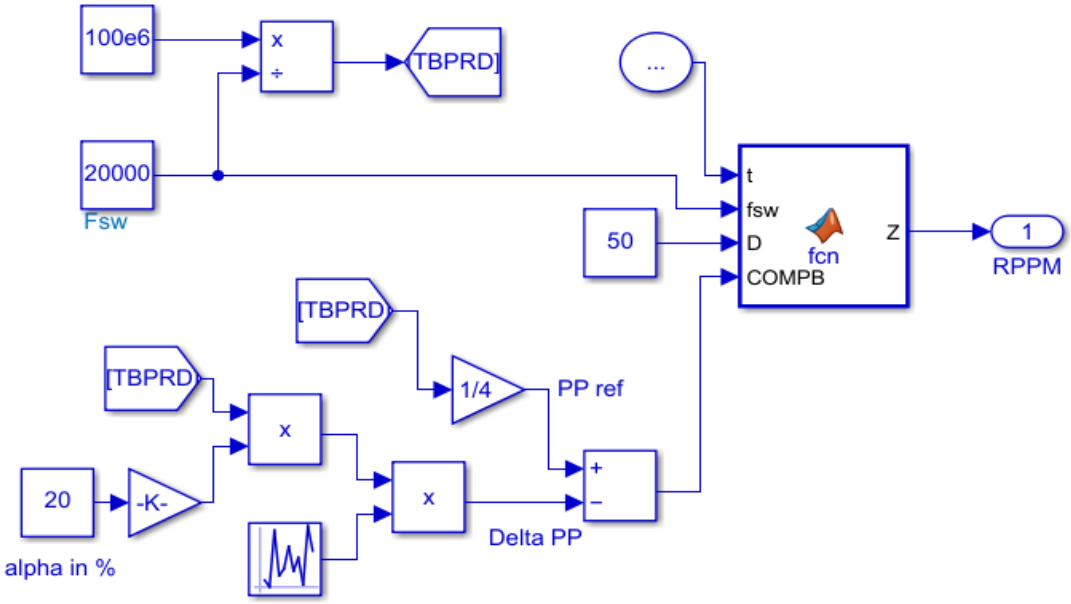

Figure A2.2: SIMULINK implementation of RPPM for simulation activity carried out in Chapter 3, (Section 3.2).

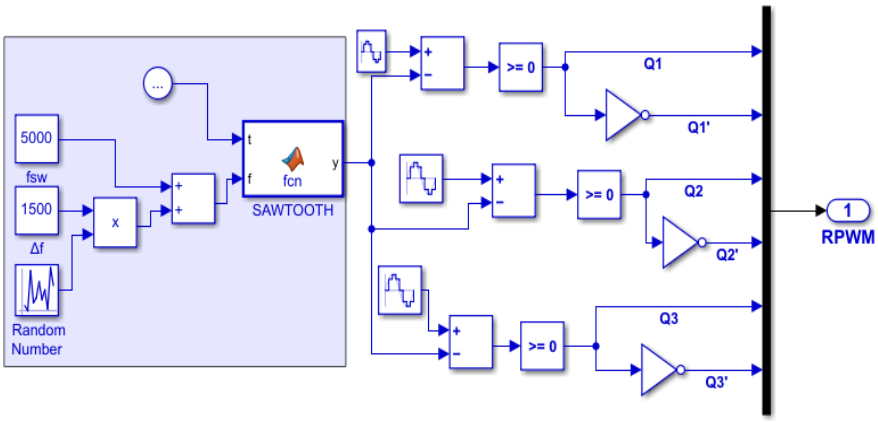

Figure A2.3: SIMULINK implementation of RFM for three-phase inverter.

A2.2. Generation of RPWM signals for Lab activities

RPWM can be generated using C2000 TI microcontroller and MATLAB SIMUINK. For conventional PWM, the ePWM module in SIMULINK can be programmed as follows and the details can be inferred from [72, 73].

$$\text{TBPRD} = \text{TPWM}/_{2\text{TBCLK}} \qquad \text{(A2.1)}$$

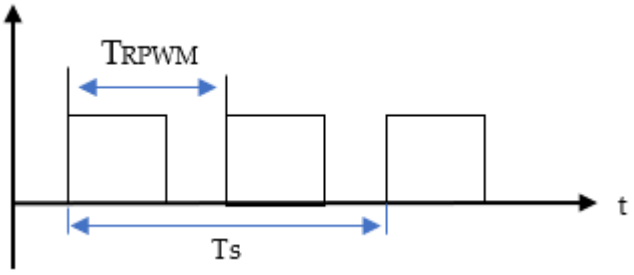

Figure A2.4: The RPWM signal.

$$\text{and CMPA} = (1 - \text{D}) \times \text{TBPRD} \qquad \text{(A2.2)}$$

where: TBCLK is the Time Base Clock; TBPRD is Time-Base Period; TPWM - Period of the PWM; CMPA and CMPB are the reference compare A and B values.

For RFM, the procedure followed for PWM generation can be applied with a small modification to the TBPRD. In this case the TBPRD is randomly changing to get variable switching frequency. Hence, the procedures discussed in Section 3.2.2.1 can be applied and implemented as shown in Figure A2.2.

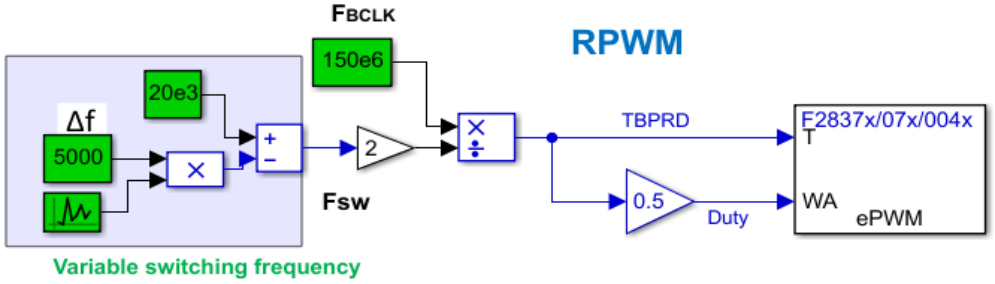

Figure A2.5: Schematics to generate RFM signal using SIMULINK and TMS320F28379D micro controller.

However, the implementation of RPPM is a bit more complex. In this case, controlling the CMPA and CMPB reference values according to (A2.3) and (A2.4) is required.

$$\text{CMPB'} = \text{CMPB} + \Delta\text{CMPB} \times \text{RAND} \qquad \text{(A2.3)}$$

and

$$\text{CMPA} = 2 \times \text{TBPRD} - \text{CMPB'} - (\text{D} \times 2 \times \text{TBPRD}) \qquad \text{(A2.4)}$$

where RAND is pseudo-random number between 1 and -1, CMPB' is the random CMPB value, D is the duty cycle and ΔCMPB is the change in CMPB reference. The randomization factor α or spreading factor can be expressed as:

$$\alpha = {}^{\Delta\text{CMPB}}/_{\text{TBPRD}} \qquad \text{(A2.5)}$$

Note that UP/Down counter should be selected with CMPB UP is 'Set' and CMPA DOWN is 'Clear' for this specific RPPM set up. The random PWM starts when the counter counts up and reaches to CMPB reference and stops when the counter counts down and reaches to CMPA value. The SIMULINK model implemented for the RPPM considered in this thesis is shown in Figure A2.6.

The Uniform Random Number block generates uniformly distributed random numbers over an interval between 1 & -1. The time interval between samples is the sampling time (Ts).

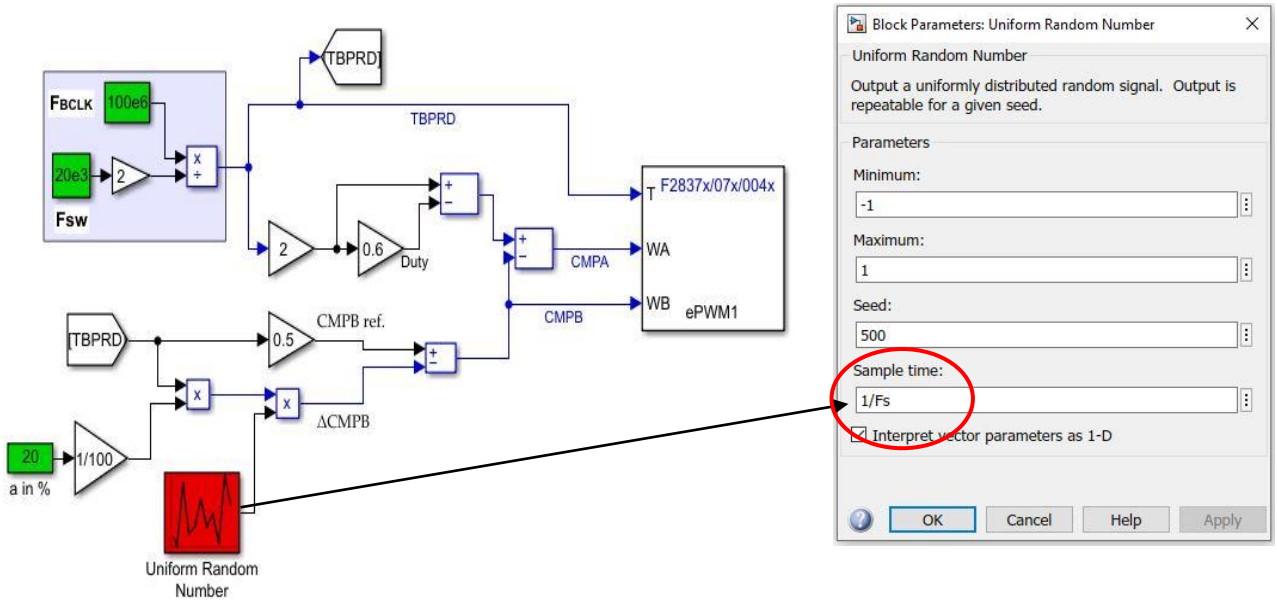

Figure A2.6: Schematics to generate RPPM signal using SIMULINK and TMS320F28379D micro controller.

Random Number Repetition (RNR) is the number of periods of the RPWM within the same random number. RNP can be expressed as:

$$\text{RNR} = \frac{\text{Ts}}{\text{TRPWM}} \qquad \text{(A2.6)}$$

where, Ts is the sampling time of the random number generator SIMULINK block (see Figure A2.6) and TRPWM is the period of the RPWM signal. For example, in Figure A2, the pulse position changes after two consecutive periods of the RPWM signal (RNR = 2). In general, the higher RNR, the lower pulse position variation.

The Random Number Update Rate (RNUR) is the rate of the switching period over one sampling time, Ts and can be expressed as:

$$\mathrm{RNUR} = \frac{\mathrm{TRPWM}}{\mathrm{Ts}} \qquad \text{(A2.7)}$$

To get pulse position variation of the RPWM signal, the sampling time, Ts should be greater than or equal to the period of the RPWM. Therefore, the value of RNUR is ≤1. In general, the higher the RNUR, the more pulse position variation repetition of the RPWM signal. RNUR can also be expressed in percentage as:

$$\mathrm{RNUR} = \frac{\mathrm{TRPWM}}{\mathrm{Ts}} \times 100 \qquad \text{(A2.8}$$

Bibliography

1. L. Lampe, A.M. Tonello, and T.G. Swart, *Power line communications principles, standards, and applications from multimedia to smart grid*. 2nd ed., Wiley & Sons, 2016.
2. A. Pittolo, *Characterization and modeling of power line communication channels*, Università Degli Studi di Udine, PhD thesis, 2016.
3. A. Papaioannou and F.N. Pavlidou, "Evaluation of Power Line Communication Equipment in Home Networks," *in IEEE Systems Journal*, vol. 3, no. 3, pp. 288-294, Sept. 2009, doi: 10.1109/JSYST.2009.2023202.
4. I. C. Papaleonidopoulos, C. N. Capsalis, C. G. Karagiannopoulos and N. J. Theodorou, "Statistical analysis and simulation of indoor single-phase low voltage power-line communication channels on the basis of multipath propagation," *in IEEE Transactions on Consumer Electronics*, vol. 49, no. 1, pp. 89-99, Feb. 2003, doi: 10.1109/TCE.2003.1205460.
5. J. W. Lechleider, "High bit rate digital subscriber lines: a review of HDSL progress," *in IEEE Journal on Selected Areas in Communications*, vol. 9, no. 6, pp. 769-784, Aug. 1991, doi: 10.1109/49.93088.
6. O. Strobel and J. Lubkoll, "Fiber-optic communication an overview," *20th International Crimean Conference "Microwave & Telecommunication Technology"*, Sevastopol, Ukraine, 2010, pp.16-20, doi: 10.1109/ CRMICO. 2010. 5632426. Wifi
7. "IEEE Standard for Information Technology, Telecommunications and Information Exchange Between Systems Local and Metropolitan Area Networks, Specific Requirements, Part 11: Wireless LAN Medium Access Control (MAC) and Physical Layer (PHY) Specifications," in IEEE Std 802.11-2007 (Revision of IEEE Std 802.11-1999) vol., no., pp.1-1076, 12 June 2007, doi: 10.1109/IEEESTD.2007.373646.
8. Z. Wang, W. Ge, C. Wang and C. Zeng, "The applications of networking of consumption data acquisition system by combining broadband powerline communication and wireless communication," IEEE PES Innovative Smart Grid Technologies, Tianjin, 2012, pp. 1-4, doi: 10.1109/ISGT-Asia.2012.6303277.
9. H. Latchman, S. Katar, L. Yonge and A. Amarsingh, "High speed multimedia and smart energy PLC applications based on adaptations of HomePlug AV," 2013 IEEE 17th International Symposium on Power Line Communications and Its Applications, Johannesburg, South Africa, 2013, pp. 143-148, doi: 10.1109/ISPLC.2013.6525840.
10. D. Wang, Y. Song and X. Wang, "Channel modeling of broadband powerline communications," *2017 IEEE 9th International Conference on Communication Software and Networks (ICCSN)*, Guangzhou, China, 2017, pp. 427-430, doi: 10.1109/ICCSN.2017.8230149.
11. M. Yigit, V. C. Gungor, G. Tuna, M. Rangoussi, E. Fadel, Power line communication technologies for smart grid applications: A review of advances and challenges, Computer Networks, Volume 70, 2014, Pages 366-383, ISSN 1389-1286, https://doi.org/10.1016/j.comnet.2014.06.005.
12. S. Galli, A. Scaglione, and Z. Wang, "For the Grid and Through the Grid: The Role of Power Line Communications in the Smart Grid," *in Proceedings of the IEEE*, vol. 99, no. 6, pp. 998-1027, June 2011, doi: 10.1109/JPROC.2011.2109670.
13. S. C. Pereira, A. S. Caporali and I. R. S. Casella, "Power line communication technology in industrial networks," *2015 IEEE International Symposium on Power Line Communications and Its Applications (ISPLC)*, Austin, TX, USA, 2015, pp. 216-221, doi: 10.1109/ISPLC.2015.7147617.
14. K. R. Sohn, S. H. Yang, J. H. Jeong, K. S. Han and J. S. Moon, "Experiments of In-Vehicle Inductive High-Voltage Power Line Communication," *2019 Eleventh International Conference on Ubiquitous and Future Networks (ICUFN)*, Zagreb, Croatia, 2019, pp. 601-603, doi: 10.1109/ICUFN.2019.8805918.
15. C. Lewandowski, S. Gröning, J. Schmutzler and C. Wietfeld, "Interference analyses of Electric Vehicle charging using PLC on the Control Pilot," *2012 IEEE International Symposium on Power Line Communications and Its Applications*, Beijing, China, 2012, pp. 350-355, doi: 10.1109/ISPLC.2012.6201296.
16. N. R. James, A. Eldhose and D. D. Krishna, "PLC modem for home automation over three phase powerline," *2013 Fourth International Conference on Computing, Communications and Networking Technologies (ICCCNT)*, Tiruchengode, India, 2013, pp. 1-4, doi: 10.1109/ICCCNT.2013.6726836.
17. W. d. S. Costa, W. G. V. d. Santos, H. R. d. O. Rocha, M. E. V. Segatto and J. A. L. Silva, "Power Line Communication based SmartPlug Prototype for Power Consumption Monitoring in Smart Homes," *in IEEE Latin America Transactions*, vol. 19, no. 11, pp. 1849-1857, Nov. 2021, doi: 10.1109/TLA.2021.9475618.
18. G. Lopez, J. Matanza, D. De La Vega; M. Castro, A. Arrinda, J. I. Moreno and A. Sendin, "The role of power line communications in the smart grid revisited: Applications challenges and research initiatives," *IEEE Access*, vol.7, pp.117346–117368,2019.
19. C. Lavenu, C. Chauvenet, P. Treffiletti, M. Varesio and K. Hueske, "Standardization Challenges, Opportunities and Recent Evolutions for the G3-PLC Technology," *Energies*, vol.14, pp.1937, 2021.
20. N. U. Pérez, I. Angulo, D. De la Vega, T. Arzuaga, I. Fernández and A. Arrinda, "Smart Grid Applications for

a Practical Implementation of IP over Narrowband Power Line Communications," *Energies*, vol.10, pp.1782. 2017, https://doi.org/10.3390/en10111782.

21. M. S. Khan, T. Ahmed, I. Aziz, F.B. Alam, M.S.U. Bhuiya, M.J. Alam, R. Chakma, S.S. Mahtab, "PLC Based Energy Efficient Home Automation System with Smart Task Scheduling," *In Proceedings of the 2019 IEEE Sustainable Power and Energy Conference (iSPEC)*, Beijing, China, 21–23 November 2019; pp. 35–38.
22. S. Barmada, M. Raugi, M. Tucci, Y. Maryanka, O. Amrani, "PLC systems for electric vehicles and Smart Grid applications," *In Proceedings of the 2013 IEEE 17th International Symposium on Power Line Communications and Its Applications, Johannesburg*, South Africa, 24–27 March 2013; pp. 23–28.
23. F. Grassi, S.A. Pignari, J. Wolf, "Channel Characterization and EMC Assessment of a PLC System for Spacecraft DC Differential Power Buses," *IEEE Trans. Electromagn. Compat.*, vol.53, pp.664–675, 2011.
24. A. Llano, D. De La Vega, I. Angulo, and L. Marron, "Impact of Channel Disturbances on Current Narrowband Power Line Communications and Lessons to Be Learnt for the Future Technologies," in IEEE Access, vol. 7, pp. 83797-83811, 2019, doi: 10.1109/ACCESS.2019.2924806.
25. Y. Kim, J. N. Bae, and J. Y. Kim, "Performance of power line communication systems with noise reduction scheme for smart grid applications," in IEEE Transactions on Consumer Electronics, vol. 57, no. 1, pp. 46-52, February 2011, doi: 10.1109/TCE.2011.5735480.
26. Electromagnetic Interference Between Electrical Equipment/Systems in the Frequency Range Below 150 kHz, Standard CENELEC SC 205A, 2015. Available online: https://standards.iteh.ai/catalog/standards/clc/f2fe2993-4360-4bee-9cce-1cf000ebb2da/clc-tr-50627-2015 (accessed on 1 December 2020).
27. N. U. Pérez, I. Angulo, L. H. Callejo, T. Arzuaga, D. De la Vega; A. Arrinda, "Study of Unwanted Emissions in the CENELEC-A Band Generated by Distributed Energy Resources and Their Influence over Narrow Band Power Line Communications," *Energies*, vol.9, pp.1007, 2016.
28. J. R. Riba, M. M. Eguilaz, S. Bogarra, A. Garcia, "Parameter Identification of DC-DC Converters under Steady-State and Transient Conditions Based on White-Box Models," *Electronics*, vol.7, pp.393, 2018.
29. F. A. Kharanaq, A. Emadi, B. Bilgin, "Modelling of Conducted Emissions for EMI Analysis of Power Converters: State-of-the-Art Review," *IEEE Access*, vol.8, pp.189313–189325,2020.
30. K. K. Tse, H.S.-Chung, S.Y. Huo and H.C. So, "Analysis and spectral characteristics of a Spread-Spectrum technique for conducted EMI suppression," in *IEEE Trans. Power Electron*., vol. 15, no.2, pp. 399-410, Mar. 2000.
31. C. M. Liaw, Y. M. Lin, C. H. Wu and K. I. Hwu, "Analysis, Design, and Implementation of a Random Frequency PWM Inverter," *in IEEE Transactions on Power Electronics*, vol.15, no.5, pp.843-854.Sept. 2000.
32. H. Loschi, P. Lezynski, R. Smolenski, D. Nascimento and W. Sleszynski, "FPGA-Based System for Electromagnetic Interference Evaluation in Random Modulated DC/DC Converters," *Energies*, vol.9, pp.2389, 2020.
33. W. E. Sayed, H. Loschi, R. Smolenski, P. Lezynski, C. L. Lok, "Performance Evaluation of the Effect of Power Converters Modulation on Power line Communication," *In Proceedings of the Sterowaniew Energoelektronicei Napedzie Elektrycznym (SENE)*, Łód´z, Poland, pp.20–22, November 2019.
34. W. E. Sayed, P. Lezynski, R. Smolenski, A. Madi, M. Pazera, A. Kempski, "Deterministic vs. Random Modulated Interference on G3Power Line Communication," Energies, vol.14, pp. 3257, 2021.
35. W. E. Sayed, P. Lezynski, R. Smolenski, N. Moonen, P. Crovetti, D.W.P. Thomas, "The Effect of EMI Generated from Spread Spectrum-Modulated SiC-Based Buck Converter on the G3-PLC Channel," *Electronics,* vol.10, pp.1416, 2021.
36. M. Rucinski, P. J. Chrzan, P. Musznicki, J. L. Schanen, A. Labonne, "Analysis of Electromagnetic Disturbances in DC Networkof Grid Connected Building-Integrated Photovoltaic System,". *In Proceedings of the 2015 9th International Conference on Compatibility and Power Electronics (CPE)*, Costa da Caparica, Portugal, 24–26 June 2015; pp. 332–336.
37. G. Grandi, D. Casadei, U. Reggiani, "Common- and Differential-Mode HF Current Components in AC Motors Supplied by Voltage Source Inverters," *IEEE Trans. Power Electron.*, vol.19, pp.16–24, 2004.
38. IEEE Power and Energy Society IEEE Recommended Practice and Requirements for Harmonic Control in Electric Power Systems. Available online: https://ieeexplore.ieee.org/document/6826459 (accessed on 8 June 2021).
39. S. Shahil, "Step-by-Step Design of an LCL Filter for Three-Phase Grid Interactive Converter". Available online: http://rgdoi.net/10 .13140/RG.2.1.3883.6964 (accessed on 8 June 2021).
40. T. Betz and D. Konig, "Influence of grading capacitors on the breaking capacity of two vacuum interrupters in series," *in IEEE Transactions on Dielectrics and Electrical Insulation*, vol. 6, no. 4, pp. 405-409, Aug. 1999, doi: 10.1109/94.788734.
41. M. Bigdeli, M. Valii, and D. Azizian, "Applying Intelligent Optimization Algorithms for Evaluation of Transformer Black Box Model," *in Soft Computing Applications*, vol. 357, V. E. Balas, L. C. Jain, and B. Kovačević, Eds. Cham: Springer International Publishing, 2016, pp. 1271–1286. doi: 10.1007/978-3-319-

18416-6_102.
42. G. Spadacini, F. Grassi, D. Bellan, S.A. Pignari, F. Marliani, "Prediction of Conducted Emissions in Satellite Power Buses," Available online: https://www.hindawi.com/journals/ijae/2015/601426/ (accessed on 15 February 2021).
43. A. Ales, J. Schanen, D. Moussaoui, J. Roudet, "Impedances Identification of DC/DC Converters for Network EMC Analysis," *IEEE Trans. Power Electron.*, vol.29, pp.6445–6457, 2014.
44. H. Bishnoi, A.C. Baisden, P. Mattavelli, D. Boroyevich, "Analysis of EMI Terminal Modeling of Switched Power Converters," *IEEE Trans. Power Electron*, vol.27, pp.3924–3933, 2012.
45. H. Cheaito, M. Diop, M. Ali, E. Clavel, C. Vollaire, L. Mutel, "Virtual Bulk Current Injection: Modeling EUT for Several Setups and Quantification of CM-to-DM Conversion," *IEEE Trans. Electromagn. Compat.*, vol.59, pp.835–844, 2017.
46. D. A. Frickey, "Conversions between S, Z, Y, H, ABCD, and T Parameters Which Are Valid for Complex Source and Load Impedances," *IEEE Trans. Microw. Theory Tech.*, vol.42, 205–211, 1994.
47. H. Robert, "Extracting Scattering Parameters from SPICE." Available online: https://www.yumpu.com/en/document/read/4047 9516/create-s-parameter-subcircuits-for-microwave-and-rf-applications (accessed on 17 February 2021).
48. A. M. Trzynadlowski, F. Blaabjerg, J. K. Pedersen, R. L. Kirlin and S. Legowski, "Random pulse width modulation techniques for converter-fed drive systems-a review," *in IEEE Transactions on Industry Applications*, vol. 30, no. 5, pp. 1166-1175, Sept.-Oct. 1994, doi: 10.1109/28.315226.
49. M. Reuter, T. Friedl, S. Tenbohlen, and W. Kohler, "Emulation of conducted emissions of an automotive inverter for filter development in HV networks," *Proc. IEEE Int. Symp. on Electromagn. Compat.*, 236–241, Denver, CO, August 5–9, 2013.
50. H. Guo, Z. Li, B. Zhang and Z. Li, "Conduced EMI Suppression by Random Frequency Modulation Techniques," *2009 Int. Conf. Communications, Circuits and Systems*, Milpitas, CA, 2009, pp.693-696
51. C. Qi, X. Chen and Y. Qiu, "Carrier-Based Randomized Pulse Position Modulation of an Indirect Matrix Converter for Attenuating the Harmonic Peaks," *IEEE Trans. Ind. Applications*, vol. 28, no.7, pp.3539-3548, July 2013.
52. M. M. Bech, *Analysis of Random Pulse-Width Modulation Techniques for Power Electronic Converters*, PhD Thesis, Faculty of Engineering & Science, Aalborg University, Denmark, 2000. Available: https://vbn.aau.dk/ws/portalfiles/portal/316407375/michael_m_bech.pdf : (accessed on 15 October 2021).
53. A. M. Stankovic, G. C. Verghese and D. J. Perreault, "Analysis and synthesis of randomized modulation schemes for power converters", *IEEE Trans. Power Electron.*, vol. 10, no. 6, pp. 680-693, Nov. 1995.
54. A. M. Stanković and H. Lev-Hari, "Randomized modulation in power electronic converters", *Proc. IEEE*, vol. 90, no. 5, pp. 782-799, May 2002
55. A. H. Beshir, Design and Development of 20 kW Bidirectional dc-dc Converter Using Silicon Carbide Technology, master's Thesis, Department of EECS, University of Oviedo, Oviedo, Spain, 2019.
56. E. Kabalci, Y. Kabalci, I. Develi, "Modelling and analysis of a power line communication system with QPSK modem for renewable smart grids," *Int. J. Electr. Power Energy Syst.*, vol.34, pp.19–28, 2012.
57. S. Bolognani, L. Peretti, L. Sgarbossa, M. Zigliotto, "Improvements in Power Line Communication Reliability for Electric Drives by Random PWM Techniques," *In Proceedings of the IECON 2006–32nd Annual Conference on IEEE Industrial Electronics*, Paris, France, 6–10 November 2006; pp. 2307–2312.
58 F. Musolino, P.S. Crovetti, "Interference of Spread-Spectrum Modulated Disturbances on Digital Communication Channels," IEEE Access, vol.7, pp.158969–158980, 2019.
59. Datasheet Stock No: 811-1448 RS Pro Red Tri-Rated Cable, PVC. Available online: http://static6.arrow.com/aropdfconversion/92d7c9b42b27b406d3fa7b241b5395b6a3c10155/pgurl_8111448.pdf (accessed on 1 December 2020)
60. A. C. Baisden, D. Boroyevich, F. Wang, "Generalized Terminal Modeling of Electromagnetic Interference," *IEEE Trans. Ind. Appl*., vol.46, 2068–2079, 2010.
61. L. Wan, A. H. Beshir, X. Wu, X. Liu, F. Grassi, G. Spadacini, S.A. Pignari, M. Zanoni, L. Tenti, R. Chiumeo, "Black-Box Modelling of Low-Switching-Frequency Power Inverters for EMC Analyses in Renewable Power Systems," *Energies*, vol.14, pp.3413, 2021
62. T. J. Donnelly, S. D. Pekarek, D. R. Fudge, N. Zarate, "Thévenin Equivalent Circuits for Modeling Common-Mode Behavior in Power Electronic Systems," *IEEE Open Access J. Power Energy*, vol.7, pp.163–172. 2020
63. M. Amara, C. Vollaire, M. Ali, F. Costa, "Black Box EMC Modelling of a Three Phase Inverter," *In Proceedings of the 2018 International Symposium on Electromagnetic Compatibility (EMC EUROPE)*, Amsterdam, The Netherlands, 27–30 August 2018; pp. 642–647.
64. J. A. Del Puerto-Flores, J. L. Naredo, F. Peña-Campos, C. Del-Valle-Soto, L. J. Valdivia, R. Parra-Michel, "Channel Characterization and SC-FDM Modulation for PLC in High-Voltage Power Lines," Future Internet, vol.14, pp.139, 2022.

65. S. Barmada, M. Raugi, M. Tucci, Y. Maryanka, O. Amrani, “PLC systems for electric vehicles and Smart Grid applications,” *In Proceedings of the 2013 IEEE 17th International Symposium on Power Line Communications and Its Applications*, Johannesburg, South Africa, 24–27 March 2013; pp. 23–28.
66. Y. Kami, F. Xiao, K. Murano, “Mode-port-network approach to analyze power-line EMC problems for PLC,” *in Proc. 20th Int. Zurich Symp. Electromagn. Compat.*, Zurich, Switzerland, Jun. 2009, pp. 9–12.
67. F. Grassi, X. Wu, Y. Yang, G. Spadacini and S. A. Pignari, “Modeling of imbalance in differential lines targeted to SPICE simulation,” *Prog. Electromagn. Res. B*, vol. 62, pp. 225–239, 2015.
68. LISN manual: https://www.atecorp.com/atecorp/media/pdfs/hv_an_150.pdf?ext=.pdf(accessed on 18 September 2022).
69. DSOX1204G Oscilloscope datasheet: https://www.keysight.com/us/en/product/DSOX1204G/oscilloscope-70-100-200-mhz-4-analog channels-waveform-generator.html (accessed on 11 March 2023)
70. PL360-EK Quick Start User Guide: https://ww1.microchip.com/downloads/en/DeviceDoc/PL360-EK-Quick-Start User-Guide-DS50002752A.pdf (accessed on 20 September 2022).
71. PL360-EK User Guide: https://www.microchip.com/en-us/product/PL360B (accessed on 20 September 2022).
72. S. B. Santra, K. Bhattacharya, T. R. Chudhury and D. Chatterjee, "Generation of PWM Schemes for Power Electronic Converters," 2018 20th National Power Systems Conference (NPSC), 2018, pp. 1-6, doi: 10.1109/NPSC.2018.8771819.
73. Datasheet TMS320F28379D Texas Instruments, http://www.ti.com/lit/ds/symlink/tms320f28374d.pdf.
74. L. Wan, A. H. Beshir, X. Wu, X. Liu, F. Grassi, G. Spadacini, S.A. Pignari, “Black-box Modeling of Converters in Renewable Energy Systems for EMC Assessment: Overview and Discussion of Available Models,” *Chinese Journal of Electrical Engineering*, vol.8, no.2, pp.13-28, 2022.